UNIVERSITY OF CALIFORNIA SAN DIEGO

The Locus Coeruleus: In vivo Characterization with Magnetic Resonance Imaging and Associations with Alzheimer's Disease-Related Markers

A Dissertation submitted in partial satisfaction of the requirements
for the degree Doctor of Philosophy

in

Neurosciences

by

Seraphina Kay Solders

Committee in charge:

Professor Mark Bondi, Co-Chair
Professor Lawrence Frank, Co-Chair
Professor Andrea Chiba
Professor Lisa Delano-Wood
Professor David Salmon

2023

The Dissertation of Seraphina Kay Solders is approved, and it is acceptable in quality and form for publication on microfilm and electronically.

University of California San Diego

2023

DEDICATION

This dissertation is dedicated to my parents: to my dad, who recognized my curiosity early on and was the first person to encourage me to become a scientist; and to my mom, who has always set the example for her children that we can do hard things.

TABLE OF CONTENTS

LIST OF FIGURES

LIST OF TABLES

LIST OF ABBREVIATIONS

AD	Alzheimer's Disease
CN	Cognitively normal
CSF	Cerebrospinal fluid
DRS	Dementia Rating Scale
dMRI	Diffusion MRI
EMI	Eigenmode imaging
EP	Equilibrium probability
GO-ESP	Geometric-Optics based Entropy Spectrum Pathways
HCP	Human Connectome Project
LC	Locus coeruleus
MCI	Mild cognitive impairment
MMSE	Mini Mental State Examination
MNI	Montreal Neurological Institute
MRI	Magnetic resonance imaging
ROI	Region of interest
SWD	Spherical wave decomposition
SYMREG	Symplectomorphic registration with phase space regularization
TEC	Transentorhinal cortex
WM	White matter

ACKNOWLEDGMENTS

First and foremost, thanks to my advisors Larry Frank and Mark Bondi for their mentorship and for giving me the interdisciplinary education I was craving. Thanks to my NGP peers - grad school is tough, and I'm grateful to be in a program with students who are committed to creating such supportive spaces. I also want to acknowledge the Lady Birds, my friendtors who have given me community, encouragement, laughs, and have elevated me in academic spaces: Alex Weigand, Allie Clark, Shanna Cooper, Kelsey Thomas, and Lisa Graves. I'm grateful for everyone I've gotten to work with through the GAPSWell Associates program – our discussions about well-being, self-compassion, and mindfulness have helped me take care of myself throughout grad school, and I'll carry them throughout life. Finally, I must acknowledge my cat, Callie, who listens to me whether she wants to or not.

Chapter 1, in full, is a reprint of the material as it appears in Magnetic Resonance in Medicine 2022. Solders, S.K.; Galinsky, V.L.; Clark, A.L.; Sorg, S.F.; Weigand, A.J.; Bondi, M.W.; Frank, L.R. The dissertation author was the primary investigator and author of this paper.

Chapter 2, in full, is currently being prepared for submission for publication of the material. Solders, S.K.; Galinsky, V.L; Bondi, M.W.; Frank, L.R. "Tau and amyloid moderate the relationship between locus coeruleus-transentorhinal cortex equilibrium probability and cognition"

Chapter 3, in full, is currently being prepared for submission for publication of the material. Solders, S.K.; Weigand, A.J.; Macomber, A.; Thayer, R.E.; Elman, J.A.; Granholm, E.L.; Frank, L.R.; Bondi, M.W. "Tau moderates the relationship between locus coeruleus MR signal and cognition".

VITA

2017 Bachelor of Arts in Biology and Psychology with a minor in Interdisciplinary Studies, San Diego State University

2023 Doctor of Philosophy in Neurosciences, University of California San Diego

PUBLICATIONS

Solders, S.K.; Galinsky, V.L.; Clark, A.L.; Sorg, S.F.; Weigand, A.J.; Bondi, M.W.; Frank, L.R. (2021). Diffusion MRI tractography of the locus coeruleus-transentorhinal cortex connections using GO-ESP. *Magnetic Resonance in Medicine 87*(4): 1816-1831. https://doi.org/10.1002/mrm.29088

Clark, A.L.; Solders, S.K.; Thomas, K.R.; Bangen, K.J. (2021). White Matter Microstructure is Associated with Serum Clusterin and Everyday Functioning in a Sample of Nondemented Older Adults. *Current Alzheimer Research 18*(14): 1118-1126. doi: 10.2174/1567205019666211227102350. PMID: 34961443.

Bangen, K.J.; Thomas, K.R.; Weigand, A.J.; Edmonds, E.C.; Clark, A.L.; Solders, S.K.; Delano-Wood, L.; Galasko, D.; Bondi, M.W. (2021). Elevated Plasma Neurofilament Light Predicts a Faster Rate of Cognitive Decline over 5 Years in Participants with Objectively-Defined Subtle Cognitive Difficulties and MCI. ˆ*The Journal of the Alzheimer's Association 17*(10): 1756-1762. doi: 10.1002/alz.12324

Clark, A.L.; Weigand, A.J.; Thomas, K.R.; Solders, S.K.; Delano-Wood, L.; Bondi, M.W.; Bernier, R.A.; Sundermann, E.E.; Banks, S.J.; Bangen, K.J. (2021). Elevated Inflammatory Markers and Arterial Stiffening Exacerbate Tau but not Amyloid Pathology in Older Adults with MCI. *Journal of Alzheimer's Disease 80*(4):1451-1463. doi: 10.3233/JAD-201382.

Eill, A.; Jahedi, A.; Gao, Y.; Kohli, J.S.; Fong, C.H.; Solders, S.; Carper, R.A.; Valafar, F.; Bailey, B.A.; Müller, R.A. (2019). Functional connectivities are more informative than anatomical variables in diagnostic classification of autism. *Brain Connectivity 9*(8):604-612. doi: 10.1089/brain.2019.0689

Solders, S.K.; Carper, R.A.; Müller, R.A. (2017). White matter compromise in autism? Differentiating motion confounds from true differences in diffusion tensor imaging. *Autism Research 10*(10)1606-1620. doi: 10.1002/aur.1807

Carper RA, Solders S, Treiber JM, Fishman I, Müller R-A (2015). Corticospinal tract anatomy and functional connectivity of primary motor cortex in autism spectrum disorder. *Journal of the American Academy of Child and Adolescent Psychiatry*. 54(10): 859-867.

Nair, A.; Carper, R.A.; Abbott, A.E.; Chen, C.P.; Solders, S.; Nakutin, S.; Datko, M.C.; Fishman, I.; Müller, R.A. (2015). Regional specificity of aberrant thalamocortical connectivity in autism. *Human Brain Mapping 36*(11): 4497–4511. doi: 10.1002/hbm.22938

FIELD OF STUDY

Major Field: Neurosciences

Studies in diffusion magnetic resonance imaging methods applied to aging and detection of risk factors for Alzheimer's disease

Professors Lawrence R. Frank and Mark W. Bondi

ABSTRACT OF THE DISSERTATION

The Locus Coeruleus: In vivo Characterization with Magnetic Resonance Imaging and Associations with Alzheimer's Disease-Related Markers

by

Seraphina Kay Solders

Doctor of Philosophy in Neurosciences

University of California San Diego, 2023

Professor Mark Bondi, Co-Chair
Professor Lawrence Frank, Co-Chair

Alzheimer's disease (AD) is a debilitating, slowly progressive neurodegenerative disorder affecting over 50 million people globally, a figure expected to increase to 152 million by 2050. Not only is there a long prodromal period wherein individuals show early signs and risk factors for the disease, which are often mistaken as effects of normal aging, but insidious pathological processes are thought to begin taking place in the brain decades before

individuals show severe cognitive impairments. Suitably, recent research efforts have focused on detecting signs of AD earlier in life to identify the disease preclinically and before irreversible damage occurs. However, knowing *what* to focus on in this preclinical period is proving to be a considerable challenge. The locus coeruleus (LC) is a small brainstem nucleus critical for healthy brain functioning that has been implicated in the pathogenesis of AD, and recent advances in neuroimaging allow for in vivo examination. This dissertation aims to characterize the LC in vivo using magnetic resonance imaging (MRI), neuropsychological testing, and biomarker assessment, with the goal of bettering our understanding of prodromal AD and AD risk. In Chapter 1 I detail our work optimizing a novel diffusion MRI analysis tool to establish a reliable method for reconstructing an LC projection pathway to the transentorhinal cortex, a region heavily affected by AD pathology. In Chapter 2, I explore how connectivity within this pathway relates to cognition in the context of tau and amyloid biomarkers. Finally, in Chapter 3 I use an LC-sensitive anatomical MRI scan to measure relative LC signal, potentially a marker of nuclear integrity, and examine its associations with cognition in the context of tau and amyloid. Importantly, I show that the relationship between these MRI markers and cognition depends on tau and amyloid status, implicating a more complex relationship between macroscopic imaging measures and cognitive outcomes. This work has implications for preclinical AD research as well as clinical neuroimaging research aiming to uncover in vivo disease markers in general.

1. Diffusion MRI Tractography of the Locus Coeruleus-Transentorhinal Cortex Connections Using GO-ESP

Abstract

Purpose: The locus coeruleus (LC) is implicated as an early site of protein pathogenesis in Alzheimer's disease (AD). Tau pathology is hypothesized to propagate in a prion-like manner along the LC-transentorhinal cortex (TEC) white matter (WM) pathway, leading to atrophy of the entorhinal cortex and adjacent cortical regions in a progressive and stereotypical manner. However, WM damage along the LC-TEC pathway may be an earlier observable change that can improve detection of preclinical AD. Methods: Diffusion-weighted magnetic resonance imaging (dMRI) allows reconstruction of WM pathways in vivo, offering promising potential to examine this pathway and enhance our understanding of neural mechanisms underlying the preclinical phase of AD. However, standard dMRI analysis tools have generally been unable to reliably reconstruct this pathway. We apply a novel method, Geometric-Optics Based Entropy Spectrum Pathways (GO-ESP) and produce a new measure of connectivity: the equilibrium probability (EP). Results: We demonstrated reliable reconstruction of LC-TEC pathways in 50 cognitively normal older adults and showed a negative association between LC-TEC EP and CSF tau. Using Human Connectome Project data, we demonstrated replicability of the method across acquisition schemes and scanners. Finally, we compared our findings with the only other existing LC-TEC tractography template, and replicated their pathway as well as investigated the source of these discrepant findings. Conclusions: AD-related tau pathology may be detectable within GO-ESP-identified LC-TEC pathways. Further, there may be multiple possible routes from LC to TEC, raising important questions for future research on the LC-TEC connectome and its role in AD pathogenesis.

Introduction

The locus coeruleus (LC) is a small brainstem nucleus containing norepinephrine-synthesizing neurons that send diffuse projections throughout the central nervous system. LC neurons provide the sole source of norepinephrine—a neurotransmitter critical in arousal and neurocognitive functioning—to the neocortex, hippocampus, cerebellum, and most of the thalamus (1,2). It has been well-established that degeneration of LC neurons is a ubiquitous feature of Alzheimer's disease (AD)(3-6), a debilitating, slowly progressive neurodegenerative disorder that affects more than 50 million people globally (a figure expected to increase to 152 million by 2050)(7). Further, recent histochemistry (8-10) and unbiased stereology (11,12) studies have suggested that nonfibrillar abnormal tau in the LC may be one of the earliest detectable signs of AD-like neuropathology.

In particular, the white matter (WM) connecting the LC to the transentorhinal cortex (TEC) has gained interest as a potential early predilection pathway of pathologic protein transmission and degeneration in AD (9,13). Indeed, Braak recently modified his original neurofibrillary tangle staging system, which posited that AD tau pathology begins in the medial temporal cortex (14), to instead suggest that the pathologic process may begin in the LC (9). Subsequently, tau pre-tangles are thought to propagate along the LC WM pathway to the TEC in a prion-like manner to initiate the stereotypical spread of tau pathology in AD, damaging neuronal tissue and resulting in reduced connectivity (9). Importantly, tau pathology in LC axonal projections do not appear to result in immediate cell death; rather, LC neurons are known to survive until the latest stages of the disease, albeit with reduced functionality (see Braak and Del Tredici (15) for a review on this topic). Thus, changes to the LC-TEC pathway may be observable before gray matter tissue loss in either LC or TEC, highlighting the important

potential of the integrity of this pathway as an early, sensitive, and specific biomarker of preclinical AD. Establishing a method to examine the microstructural connectivity of this pathway in vivo would provide an opportunity to enhance our understanding of the role of the LC in AD pathogenesis, and potentially lead to the discovery of novel markers of AD risk that could aid in diagnostic assessments and inform our understanding of the preclinical period of the disease.

Diffusion-weighted magnetic resonance imaging (dMRI), a powerful tool for characterizing the structural connectome of the brain in both healthy and disease states, offers promise to fulfill this goal. This technique allows for non-invasive and quantitative assessment of in vivo local tissue microstructure. In the case of cerebral WM, for example, dMRI can be used to estimate WM fiber coherence (the degree to which axons are co-aligned). Further, by using estimates of fiber orientations, dMRI can reconstruct WM fiber pathways via a process called tractography.

Notably, standard dMRI analysis methods have had difficulty with successful reconstruction of WM pathways in regions with complex fiber orientations, such as the brainstem. For this reason, it has been especially challenging to use dMRI to assess the connectivity of the LC-TEC pathway in humans. This difficulty is demonstrated by the fact that a reconstruction of this pathway has only very recently been reported for the first time (two reports from the same senior investigator) (16,17). Even so, these reconstruction approaches understandably employed tight constraints in the form of groupwise consistency or assumed anatomical priors. Since there is currently no agreed upon ground-truth evidence for the spatial trajectory of this pathway in the human brain, particular care must be taken in applying methods with explicit (or implicit) constraints that may bias the construction of fiber pathways.

Reducing such bias was one of the motivating factors in our development of a general principled probabilistic approach to simultaneously estimate both local diffusion characteristics (e.g., anisotropy) and long-range structural connectivity that capitalizes on prior information within the data itself. This method combines geometrical optics and the theory of entropy spectrum pathways (ESP) (18) using a probabilistic formulation, and is called Geometric-Optics Based Entropy Spectrum Pathways (GO-ESP) (19).

In this work, we demonstrate a unique approach to reconstructing the LC-TEC fiber pathways by using a much more general, flexible, and less biased characterization of the underlying diffusion data. In this study we applied GO-ESP to a sample of 50 dMRI scans from cognitively normal older adults to obtain a reliable and spatially consistent reconstruction of a LC-TEC WM pathway and examined relationships between connectivity in this pathway and CSF measures of amyloid-beta and tau. We also took advantage of high-resolution data from the Human Connectome Project (HCP) and sought replicability across acquisition schemes by applying GO-ESP to a sample of 5 datasets from the MGH HCP Adult Diffusion release (20). Finally, we compared our findings with those of Xia and Shi (16) and Sun et al., (17) who present an alternative spatial trajectory of the LC-TEC pathway. We interpret this observed discrepancy to suggest the presence of multiple possible routes from the LC to the TEC and raise important questions to be answered in future research on the LC-TEC connectome and its putative role in AD pathogenesis.

Theory

Entropy Spectrum Pathways

GO-ESP takes a novel approach to estimate intravoxel diffusion profiles and intervoxel connectivity, based fundamentally on probability theory and statistical mechanics. This process

requires that the description of the data be as general and complete as possible. Toward this goal, rather than calculating a 3D displacement probability density distribution in each voxel, which is expensive in terms of data acquisition, we use spherical wave decomposition (SWD) (21) to decompose the signal in each voxel into the sum of spherical harmonics and spherical Bessel functions, rewriting the spin density function in terms of this SWD.

This approach provides a description of the intravoxel diffusion in terms of a clearly defined expansion order which we can use to fit a model of diffusion most optimally. The next problem is how to incorporate the intra- and intervoxel information. Critically, GO-ESP does not estimate the diffusion profile in each voxel independently as if the voxels were structurally isolated from one another; rather, the fundamental quantity that is estimated is the transition probability (TP) between voxels, which is influenced not only by the intravoxel diffusion properties, but also by the intervoxel relationships. This is accomplished using the theory of ESP. (18)

ESP expands upon the concept of a random walk – a process by which a randomly moving object (or walker) moves away from its starting position. This can also be thought of as a path made of a series of random steps on a lattice. In a generic random walk, a step from one point in any direction is equiprobable. However, consider the situation where some points on the lattice are less accessible than others (perhaps due to structural barriers) – a biased random walk. In this case, a step from one point to any other is not equiprobable but is based on some probability distribution influenced by prior information about the relationship between points. GO-ESP expands this concept to dMRI by using a type of biased random walk called the maximum entropy random walk. In this case, our "points" are dMRI voxels, and the prior information about the relationship between these voxels (i.e., which voxels are more accessible

and more likely to be physically connected) takes the form of a coupling matrix which characterizes the intervoxel interactions (in this work, these interactions are computed as the inner product of the full diffusion tensors). Once the coupling matrix is known, the probability of stepping from one voxel to another (the TP) can be calculated. Thus, the TP depends not only on the diffusion profile within each voxel, but the similarity of the diffusion profiles between voxels.

The TPs describe the probabilities of various pathways within the data, or trajectories that a random walker may follow. Over time, biased random walkers will tend to localize in more accessible regions, and this final distribution provides the novel dependent measure of GO-ESP - the equilibrium probability (EP). In other words, regions of higher EP represent locations that are more accessible – there are a greater number of ways that these regions can be reached (higher entropy).

Tractography using geometric optics guided by ESP

Tractography is the process of reconstructing WM tracts from dMRI data. In practice, a set of curves are generated that are mere proxies for actual WM tracts. Nevertheless, we refer to these curves as "tracts", with this understanding in mind.

As mentioned previously, the local diffusion profiles and long-range connectivity are mathematically coupled through the entropy; this is done by modeling the evolution of probabilities with the Fokker-Planck equation where the path entropy plays the role of an external potential that influences the evolution of probabilities (18). This is accomplished by recharacterizing the spatial-temporal characteristics of the probability density in terms of the conservation of probability:

$$\partial_t P + \nabla J_I = 0$$

Where the flux, J_I, consists of diffusive ($J_d = -D\nabla P$) and convective ($J_c = -LP\nabla S$) components. S is the entropy, where $S(x) = k \ln W(x)$, with x representing spatial location, and $W(x)$ representing the density of states. L is the product of k and D, where k is the Onsanger coefficient and D is the diffusion tensor. By combining these relationships, we can represent the relationship between the local and long-range structure:

$$\partial_t P + \nabla \cdot (LP\nabla S) = \nabla \cdot D\nabla P$$

This Fokker-Planck equation describes information flow in terms of both diffusion and convection, and a geometric optics-like approach is taken to perform ray tracing through the convective modes. This ray tracing takes the place of traditional tract propagation. (19)

Eigenmode Imaging

After calculating EP maps, tractography is performed at the level of the whole-brain (Figure 1) or individual pathways (Figure 2), depending on the distribution of seeds, which is decided by the user. Either way, the result is a set of tracts. GO-ESP takes an additional, novel step to calculate pathways of high probability based on these tracts - a technique we call EigenMode Imaging (EMI). Briefly, this method involves calculating the eigensystem of the connectivity matrix constructed from the tracts. The resulting eigenvectors represent the spatial distribution of probability corresponding to the most likely pathways within the entire set of all tracts in a volume of interest. Intuitively, if fiber tracts connecting two endpoints A and B are nearly adjacent throughout their trajectories and therefore form a tight bundle between these points, the resulting eigenvector will be the volume that surrounds the bundle trajectory. For example, in the idealized case that the fibers were packed tightly into a perfect flexible cylinder that curved from point A to point B, the eigenmode would just be that cylindrical volume or 'tube'. These probability pathways are called tract (or connectivity) eigenmodes and are ranked

in decreasing order according to their associated eigenvalues. The eigenvector associated with the largest eigenvalue (the principal eigenvector) corresponds to the most probable probability pathway. While multiple eigenmodes provide interesting information about the structure at different spatial scales in the brain (i.e. potential substructures revealing significant connectivity information), in the present paper we are concerned only with the principal eigenvector, since it represents the major communication pathway between two regions.

The computation of tract eigenmodes involves the following steps. The tracts generated from the GO-ESP tractography process are used to generate the connectivity matrix which is of dimensions that are the square of the dimensions of the diffusion dataset. The connectivity matrix records the number of connections from every voxel i to every voxel j where i and j are of dimensions N = nx*ny*nz. This matrix is symmetric, so only N*N/2 elements are needed to store it in full dense form. Even so, the matrix is very large, so we use a sparse representation to store it in the so-called Yale sparse format. The eigenvector/eigenvalue decomposition of the matrix is then performed using the ARPACK package (22) that employs the Arnoldi algorithm which can efficiently calculate a subset of eigenvectors. The decomposition of the tractography connectivity matrix into connectivity eigenmodes elucidates and ranks neural connections at multiple spatial scales from the highly complex tractography in a well-defined quantitative, and reproducible procedure.

A visualization of whole-brain tractography and subsequent principle EMI can be seen in Figure 1. An example reconstruction of a specific and well-studied pathway, the inferior longitudinal fasciculus, and its resulting principle EMI can be seen in Figure 2.

Methods

Participants

This study included data from 53 cognitively normal older adults as part of an ongoing study of quantitative neuroimaging metrics of LC connectivity in AD pathogenesis and progression. This study was approved by the University of California, San Diego (UCSD) Institutional Review Board, with written informed consent obtained on all participants.

MRI acquisition

Scans were performed on a 3 Tesla GE Discovery MR750 scanner at the UCSD Center for Functional MRI using a 32-channel head coil (Nova Medical Inc, Wilmington MA).

Whole-brain dMRI scans were collected using a novel Extended Hybrid Sense EPI acquisition (23); data were simultaneously acquired with both polarities of the phase encoding gradient to perform TOPUP gradient and eddy current distortion correction, which was done in offline specialized reconstruction routines that implemented the FMRIB Software Library's (FSL) Eddy and TOPUP tools (24-26) directly within the image reconstruction (23). Multiple diffusion-weighted shells were collected at b-values of 1000, 2000, and 3000s/m^2 with the number of directions being 30, 45, and 60, respectively. The data acquisition parameters were: slice thickness=2mm, FOV=20cm, TE=119ms, TR=4.0s, matrix size=100x100x72. Using a SENSE factor of 4, the imaging time was approximately 13 minutes. This is a standard dMRI gradient sampling scheme. Therefore, findings generated from this study are a result of the analysis, not the acquisition, and should be replicable across datasets.

CSF biomarkers

A subset of our participants (n = 20) underwent lumbar punctures as part of participation in the UCSD Alzheimer's Disease Research Center with standardization of procedures,

preanalytical preparation, and storage of CSF and plasma as previously described (27), and in accordance with recommended best practices (28). In brief, CSF (15–25 mL) was collected by routine lumbar puncture early in the morning after overnight fasting. Samples were processed, aliquoted into 500 μL fractions in polypropylene microtubes, snap frozen, and stored at −80°C until assayed. All samples were analyzed locally using the automated Lumipulse platform using assays developed with established monoclonal antibodies (Fujirebio Inc) (29). The majority of lumbar punctures were conducted within one year of the MRI visit (n = 11), although we included data collected within two (n = 2), three (n = 5), and four (n = 2) years of the visit given research showing the stability of CSF biomarkers over several years (30) in an effort to maximize our sample size. CSF measures of Aβ40, Aβ42, total tau, and phosphorylated tau (p-tau) were obtained.

Preprocessing and quality assessment

FSL (v.6.025) was used to correct for inter-volume head motion (eddy; b-vectors adjusted for correction) (26) and remove skull and other non-brain tissue (BET) (31). Data were resampled to a $1mm^3$ resolution using our novel registration tool, Symplectomorphic Registration with Phase Space Regularization (SYMREG) (32).

Quality control consisted of visual inspection for slice-wise signal dropout, image noise, and shifts of head placement between diffusion volumes. Scans were excluded if they had single slices of signal dropout affecting 10 or more diffusion directions, multiple slices of signal dropout on 5 or more diffusion directions, color banding evident in the RGB display of the primary eigenvector image, visible nods or head shakes between diffusion directions, or visible image noise.

GO-ESP diffusion estimation and tractography

For each subject, GO-ESP was used to calculate EP maps, and FSL's dtifit (33) was used to calculate FA maps for comparison to a more commonly used metric. To reconstruct the LC-TEC WM connections, we used GO-ESP to generate tracts intersecting two regions of interest (ROIs): a publicly available LC map (34), and the anterior division of the parahippocampal gyrus, meant to approximate the transentorhinal cortex (TEC), extracted from the Harvard-Oxford cortical structural atlas in FSL (HarvardOxford-cort-maxprob-thr50-1mm). Only the most anterior lateral portion of the anterior parahippocampal gyrus ROI was used to maintain specificity of generated tracts (Figure 3, middle panel). As both ROIs were created in standard Montreal Neurological Institute (MNI) coordinate space, SYMREG (32) was used to register each participant's EP map to the "MNI152_T1_1mm_brain" map from the template in FSL. These registrations were used to transform the ROIs from MNI coordinate space into each subject's native diffusion space, in which tractography was performed.

Tractography was performed in two ways. Seeds were first distributed within a boxed region encapsulating the portion of the brain most likely to contain the LC-TEC pathway, excluding only the top part of the cerebral cortex and the brain below the ROIs; this was done instead of distributing seeds throughout the entire brain for efficiency (xyz coordinates in MNI space 0-200, 0-200, 0-142; Figure 3, top panel). Only tracts that intersected both ROIs were kept (Figure 3, middle panel). We refer to this strategy as "widely-distributed" seeding. Next, to increase the spatial consistency of output between subjects, we took the principle eigenmode of a representative LC-TEC pathway reconstruction using widely-distributed seeds, and binarized and dilated this region to obtain a mask that could be used as a more "spatially-weighted" seeding region (Figure 3, bottom panel). In this approach, seeds are still distributed throughout the boxed

region described above, but placement is weighted more heavily within the "spatially-weighted" mask. As before, only tracts that intersected both ROIs were kept. For both analyses, two million starting seeds were randomly distributed throughout the seed regions, and tracking was only permitted to pass through regions where the EP was at least 0.5 (this value corresponds reliably with the location of WM). For efficiency and consistency, we have restricted our analyses to the principle eigenmode of the resulting connectivity matrix for all datasets.

To generate masks for visualization and statistical analyses, we applied a threshold to the tract EMIs. The EMIs generated from tractography are automatically normalized so that the sum of all included voxels is equal to one, where higher values correspond with a higher probability. To exclude voxels with the lowest probability of belonging to the pathway, we kept only those highest value voxels whose intensities sum to 0.9. This technique ensures a level of within-subject anatomical consistency. These thresholded EMIs were binarized and used for the statistical analyses as well as visualization in Figs. 5 and 8.

Statistical analysis

For each participant, we computed the average of left and right LC-TEC pathway EP and FA. To examine associations between average bilateral LC-TEC EP and FA with CSF measures of amyloid (Aβ42/Aβ40), total tau, and p-tau, we performed Pearson's partial correlations controlling for age.

Replication in HCP datasets

To examine replicability across datasets with different acquisition parameters, we repeated our analysis technique on a sample of 5 randomly selected dMRI datasets from the HCP, which provides multi-shell dMRI at an isotropic resolution of 1.5mm (35,36). We used data from the MGH HCP Adult Diffusion release of 35 young adults (20). These data were

collected on a customized MGH Siemens 3 Tesla Connectome scanner, which has 300 mT/m maximum gradient strength for diffusion imaging. Multiple diffusion-weighted shells were collected at b-values of 1000, 2000, 3000, 5000, and 10000s/mm^2 with the number of directions being 64, 64, 128, 128, 128, respectively. The data acquisition parameters were: slice thickness=1.5mm, FOV=210x210mm, TR/TE=8800/57ms, matrix size=140x140. The total acquisition time was approximately 89 minutes.

The downloaded HCP data were already minimally preprocessed using tools from Freesurfer V5.3.0 (37) and FSL V5.0 (25). Scans were corrected for gradient nonlinearity, bulk head motion (38), and eddy current distortions (b-vectors adjusted for correction) (26). The only additional preprocessing steps we performed were removal of non-brain tissue using FSL's BET (31) and resampling to a 1mm^3 resolution using SYMREG (32) to be consistent with our processing scheme. We then applied tractography as before, using the spatially-weighted seeding strategy described above (Figure 3, bottom).

Comparison with previous LC-TEC tractography reports

Because a previous reconstruction of the LC-TEC pathway has been reported (16,17) and differs in spatial trajectory from ours (see results; we refer to this as the "medial" pathway to distinguish from the GO-ESP generated pathway), the last stage of our analysis was an exploratory investigation into the source of this discrepancy. Sun et al. (17) employed different diffusion estimation and tractography algorithms (state-of-the-art spherical deconvolution and FOD-based probabilistic tractography) (39), as well as a different, two-stage seeding approach. They first used an amygdala mask as a target ROI to track from the LC, along with a dilated thalamus inclusion ROI and a ventral tegmental area (VTA) exclusion ROI. They then used this output as a mask to track toward the TEC, again using the thalamus inclusion and VTA

exclusion ROIs. Thus, we aimed to investigate whether the spatial discrepancy was due to differences in the dMRI algorithms and/or seeding strategies.

To accomplish this, we first applied our spatially-weighted seeding approach, but used the LC-TEC probabilistic atlas generated from Sun et al. (17) as a seeding mask rather than the LC-TEC mask from our own data. Next, we applied their seeding strategy in GO-ESP. Then, we compared GO-ESP with spherical deconvolution and FOD-probabilistic tractography in MRtrix3 (40), first replicating the approach of Sun et al. (17), and then tracking simply from LC to TEC without additional ROI constraints. Finally, we explored whether we could use GO-ESP to extract the medial pathway within our data, first by examining lower-ranked eigenmodes within our previously-generated tractography output, and then by experimenting with different seeding strategies.

To compare the potential ability to detect AD-related pathology within this medial pathway versus the GO-ESP generated pathway, we registered the medial pathway provided in the publicly available atlas (17) to each subject's native diffusion space, extracted the average EP within this region, and performed additional correlations with CSF biomarkers.

Results

Sample characteristics

The initial pool of data consisted of 53 dMRI scans from cognitively normal older adults. Three scans were excluded during quality inspection. The remaining 50 participants were predominantly women (n=38), with an average age of 73.92 years (range: 62-85, standard deviation = 6.02). Our sample had an average of 15.96 years of education (range: 12-20, standard deviation = 2.11), and was mostly white (n = 44) and non-Hispanic/Latino (n = 45) (See Supporting Information Table S1).

Reconstruction of LC-TEC tracts

Diffusion estimation and tractography were performed using both seeding strategies described above ("widely-distributed" and "spatially-weighted"). Of these, 49 were initially successful (see Figure 4 for example from a representative subject using the spatially-weighted seeding strategy); one participant had failed tractography on the right side. Further inspection revealed a cranial nerve that appeared very bright on the EP map and appeared to connect the brainstem with the medial temporal lobe, resulting in tracts that incorrectly crossed over before the temporal lobe connects with the midbrain. This nerve was manually removed from the EP map, and the tractography was re-run successfully.

Slice-wise maps demonstrating inter-subject spatial consistency of the principle LC-TEC EMIs generated from GO-ESP are shown in Figure 5. The thresholded EMIs for all participants were registered to standard MNI space, binarized, and summed to create the inter-subject spatial consistency maps (Figure 5). Importantly, no threshold was set for the number of participants having overlapping output in a given voxel, so these maps do not represent a best-case scenario but reveal the full extent of EMI output across participants. While the overall spatial trajectories of the pathways generated using the two seeding strategies were very similar, using a more spatially-weighted seeding strategy resulted in more anatomical consistency between subjects (Figure 5).

Associations between LC-TEC Pathway EP and CSF Biomarkers

Twenty of our participants had CSF biomarker data available. Averages and ranges of CSF biomarker data can be found in Supporting Information Table S1. Average bilateral LC-TEC EP was significantly negatively associated with CSF p-tau ($r = -0.538$, $p = 0.018$), and was positively, but not significantly, associated with Aβ42/Aβ40 ($r = 0.416$, $p = 0.076$). Average

bilateral LC-TEC FA was significantly negatively correlated with CSF total tau ($r = -0.645$, $p = 0.003$) and p-tau ($r = -0.479$, $p = 0.038$), but not Aβ42/Aβ40 ($r = 0.037$, $p = 0.882$). Average EP within the bilateral medial pathway was not associated with any CSF biomarkers (Figure 6).

Replication in HCP datasets

Diffusion estimation and tractography were performed using an identical processing pipeline as above for 5 sample HCP subjects, using the spatially-weighted seeding strategy that provided the most consistent output in our data. The reconstructions were anatomically consistent among all subjects (Figure 7). Further, the spatial trajectory of these reconstructions resembled the output generated from our data (Figure 4). Figures 4 and 7 provide three-dimensional representations of the spatial trajectory of the LC-TEC pathway as shown in the slice-wise group frequency maps in Figure 5. Together, these results demonstrate consistency between both individual datasets, as well as between different participant characteristics (i.e., age), acquisition schemes, and MRI machines (GE vs. Siemens).

Comparison with previous LC-TEC tractography reports

Because reconstruction of the LC-TEC pathway has been reported previously (16,17), we investigated the spatial similarity of these previous results to our own. Strikingly, our results differ significantly in terms of spatial trajectory. While the LC-TEC map generated by Xia and Shi (16) and Sun et al. (17) stays medial and proximal to the thalamus before turning into the TEC, our LC-TEC map makes the turn from the brainstem into the TEC much sooner (Figure 8). This notable difference prompted us to investigate whether this discrepancy was due to differences in analysis algorithms and/or seeding strategies.

First, we used GO-ESP and applied our spatially-weighted seeding approach, but used the LC-TEC probabilistic atlas generated from Sun et al. (17) as a seeding mask rather than the LC-

TEC mask from our own data. Interestingly, the resulting EMIs resembled the pathway we consistently see with our approach rather than the medial pathway (Figure 9A). Next, we used GO-ESP but applied the seeding strategy from Sun et al. (17). Again, the resulting EMIs resembled that of our own findings rather than the medial pathway (Figure 9B). Next, we replicated the approach of Sun et al. (17) and used the spherical deconvolution and FOD tractography tools in MRtrix3, along with their two-stage seeding approach, and unsurprisingly replicated their medial pathway (Figure 9C). Interestingly, when we used MRtrix3 to track from the LC seed ROI with only the TEC as an inclusion ROI, the resulting pathway resembled the medial tract from Sun et al. (17) (Figure 9D). Taken together, these comparative results suggest that the difference in spatial trajectory between our pathway and that of Sun et al. (17) looked to be due to the different dMRI analysis algorithms rather than choice of ROIs and seeding strategies.

Finally, we explored whether we could extract the medial pathway using GO-ESP. We examined some of the lower-ranked eigenmodes from our tractography results, wherein we markedly observed a similar pathway from output generated using the widely-distributed seeding strategy in one HCP subject (Figure 10A). However, this finding appeared to be sporadic, so we next tried different seeding approaches to more reliably extract the medial path. First, we used the most anterior-medial portion of an amygdala ROI as an additional seeding region. This consistently resulted in EMIs closer to the midline, but still not quite resembling that of Sun et al. (17) (Figure 10B). We then tried using 2-dimensional disc-shaped ROIs right along the midline, encompassing the most anterior-medial portion of the LC-TEC atlas generated by Sun et al. (17). This consistently resulted in EMIs more closely resembling the medial pathway (Figure 10C).

Discussion

Diffusion-weighted MRI is the best available tool for in vivo examination of WM pathways in the human brain. Despite significant progress in dMRI acquisition and analysis techniques, there remain significant limitations in standard analysis methodologies that ultimately limit its clinical utility. The application to tractography in the LC-TEC complex discussed in this paper, a crucial pathway for its putative role in the initiation and progression of AD pathologic changes, highlights the central issue: the difficulty in accurately reconstructing pathways passing through regions with complex fiber orientation distributions. GO-ESP was developed with a motivation to improve upon some of these difficulties, and takes a novel mathematical approach to the problem based fundamentally on probability theory (18,19). We have applied this technique to reconstruct the LC-TEC pathway in a sample of cognitively normal older adults, and a subsample with varying degrees of underlying AD biomarkers, to provide feasibility of in vivo examination of this important tract in the pathophysiology of AD.

Interestingly, our results show moderate to large negative associations between both LC-TEC pathway EP and FA with CSF measures of p-tau protein accumulation. This relationship is consistent with the assumption that higher CSF tau signifies neurodegeneration, as it is thought that tau-mediated neurofibrillary tangles leak out of dying neurons and diffuse into the CSF. We did not see significant associations between LC-TEC pathway EP or FA with CSF amyloid, although the effect size for the positive association between EP and amyloid was moderate, while that for the FA-amyloid relationship was weak. Thus far, these findings suggest that FA and EP may have similar ability to detect microstructural tau pathology, although EP might have additional sensitivity to detect amyloid pathology. Of course, further investigations with much larger sample sizes are needed to support these hypotheses. Notably, EP computation depends on

parameters such as length sensitivity, so it is possible that the calculation can be further optimized to be more sensitive to particular pathology, a worthy avenue of future research. Further, while our results apply only to cognitively normal older individuals, given the evidence for feasibility of LC-TEC tracking in our study and other studies, future investigations will assess the integrity of this pathway in the context of AD, including associations with cognitive decline or other AD biomarkers. Such findings would have implications for an improved understanding of the earliest pathologic changes in AD and may highlight future treatment targets to prevent the spread of pathology prior to the clinical manifestation of dementia.

As noted above, only one other group has published a tractography reconstruction of the LC-TEC pathway in two different reports (16,17). Xia and Shi (16) reconstructed the right LC-TEC pathway which required ad hoc tract-filtering depending on group-wise consistency, which, while helping to generate more consistent and anatomically feasible tracts in this case, has the potential to compromise the ability to capture individual or between-group differences in WM structure and may overall reduce the sensitivity of the analysis. In addition, Sun et al. (17) used a tract-filtering algorithm based on topographic regularity (41), which produced spatially consistent output between datasets without making assumptions about inter-individual consistency, but employed strict anatomical priors in order to obtain a clean and reliable reconstruction. GO-ESP makes minimal assumptions about the data and no assumptions about the fiber structure.

Interestingly, our results differed in terms of spatial trajectory. We performed several iterations of testing to demonstrate that this discrepancy arose from inherent differences in the choice of dMRI analysis algorithms rather than from the choice of ROIs and seeding strategies (Figure 9). Indeed, even when using minimal seeding and inclusion ROIs (only LC and TEC)

with the state-of-the-art MRtrix3 tools, we still obtained a pathway resembling that of Sun et al. (17), whereas using the more restrictive seeding strategy (LC, amygdala, thalamus, VTA, and TEC) with GO-ESP still resulted in a more lateral pathway (Figure 5).

A major limitation of all of these studies, including our own, is that the true anatomy of the human LC-TEC pathway is not well described as post-mortem mapping of the posited projections from brainstem LC nuclei have proven quite difficult. While the pathway has been characterized using anatomical tracing methods in rodents (42,43), we have no evidence from which to base the spatial trajectory of this pathway in humans. Braak and Del Tredici (15) further note that the LC-TEC pathway takes its greatest form only in higher primates, so rodent anatomical work specifying the LC-TEC pathway trajectory may have a paucity of connectivity and be relatively unhelpful. Sun et al. (17) state in their report that they are currently collecting high-resolution dMRI of post-mortem human brain tissue and plan to compare with expert delineations on slices of the same tissue to assess the accuracy of the reconstruction. This will be a critical next step to determine what anatomical constraints may or may not be appropriate for accurate reconstruction of the LC-TEC pathway(s). Thus, without a ground truth knowledge of the true anatomy of LC-TEC connections, we posit that both of these pathways could potentially be true. Indeed, it is possible that the two pathways represent alternative routes from the LC to the TEC, as having all projections from the LC to the TEC pass through the amygdala could be problematic from a functional standpoint. In the interim, we believe the option of imposing the fewest assumptions and constraints onto the analyses is a more conservative strategy, and our conservative approach offers an alternative option for an LC-TEC pathway. Indeed, the fact that we are able to detect associations between EP and AD-related CSF biomarkers within the GO-ESP generated pathway and not the medial pathway supports the efficacy of our approach.

In summary, GO-ESP and EMI provide a unique opportunity to obtain more general, less biased descriptions of putative neural fiber tracts from data acquired using standard dMRI acquisition schemes by coupling local diffusion and long-range connectivity information. Using these tools, we have demonstrated consistent tractography of a pathway within a highly complex neuroanatomical region where the limitations of standard analysis methods become the most apparent. This work was carried out in the context of a wider research focus on AD, as the LC-TEC pathway has been implicated as an early region of disease-related pathologic transmission (9). Indeed, we have shown that AD-related pathology may be detectable within GO-ESP derived LC-TEC WM pathways. This study serves as a proof-of-concept that we can reliably reconstruct this pathway, and paves the way for future efforts to apply these techniques to a clinical sample with the goals of exploring how microstructural characteristics of the LC-TEC pathway differ along the aging-AD continuum and how they relate to other markers of AD pathology.

Acknowledgements

The authors thank Thomas Lesperance, M.S., at CSCI for his work on the graphical user interface and visualization of results, and Aaron Jacobson, M.A., at CFMRI for assistance in the collection of the data. Finally, we especially thank all those who participated in the study. This work was supported by the National Science Foundation (NSF) Graduate Research Fellowship Program under Grant Nos. DGE-2038238 (SKS) and DGE-1650112 (AJW), and NSF grant ACI-1550405 (LRF and VLG). Any opinions, findings, and conclusions or recommendations expressed in this material are those of the author(s) and do not necessarily reflect the views of the NSF. This work was also supported by NIH awards R01AG054049 (LRF, MWB, and VLG), R01AR070830 (LRF and VLG), and R01HD088437 (LRF), and University of California MPRI

award MRP17454755 (LRF and VLG). Data were provided [in part] by the Human Connectome Project, MGH-USC Consortium (Principal Investigators: Bruce R. Rosen, Arthur W. Toga and Van Wedeen; U01MH093765) funded by the NIH Blueprint Initiative for Neuroscience Research grant; the National Institutes of Health grant P41EB015896; and the Instrumentation Grants S10RR023043, 1S10RR023401, 1S10RR019307. HCP data are disseminated by the ConnectomeDB database from the HCP neuroinformatics infrastructure.

Chapter 1, in full, is a reprint of the material as it appears in Magnetic Resonance in Medicine 2022. Solders, S.K.; Galinsky, V.L.; Clark, A.L.; Sorg, S.F.; Weigand, A.J.; Bondi, M.W.; Frank, L.R. The dissertation author was the primary investigator and author of this paper.

Figures

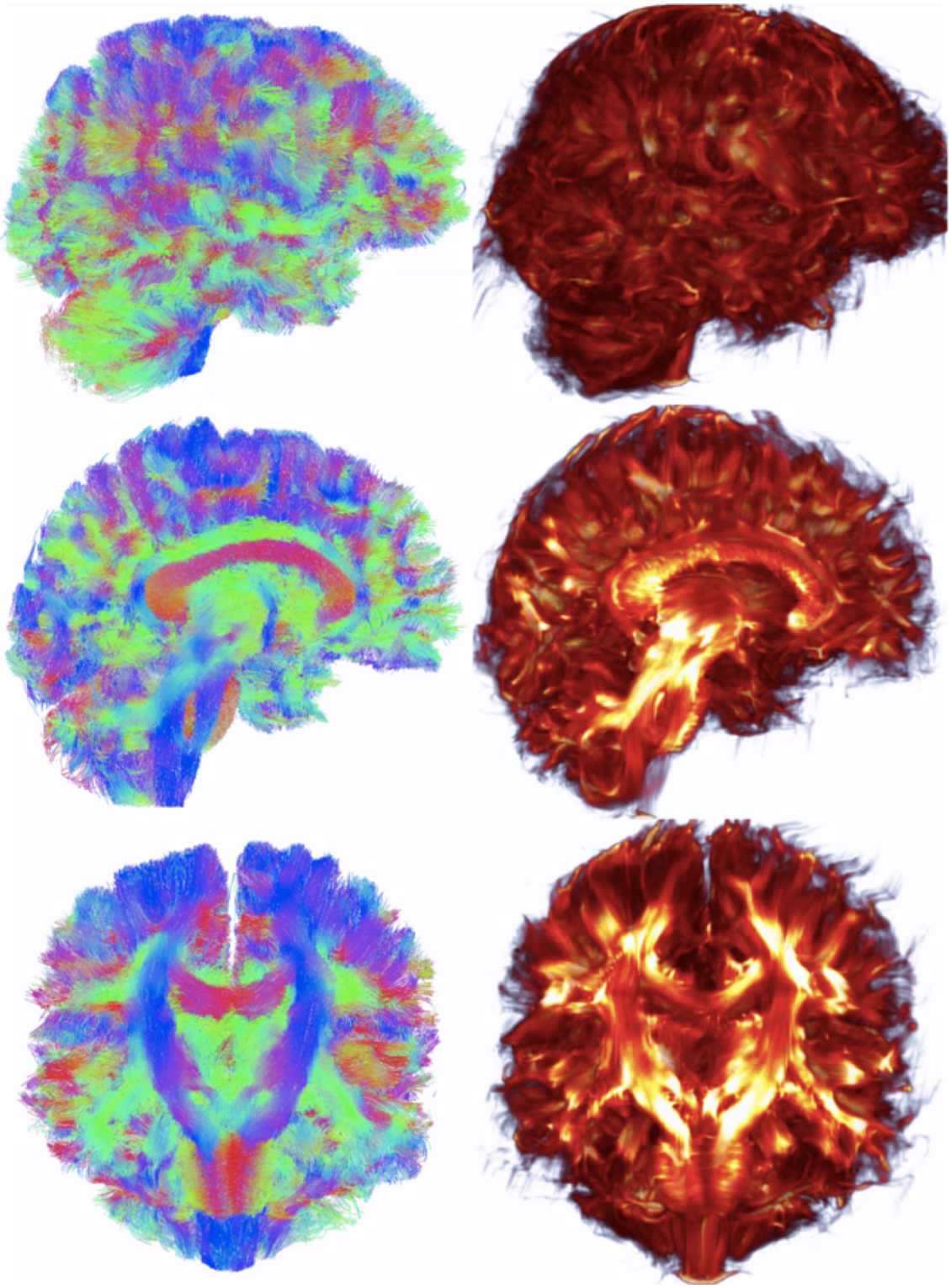

Figure 1.1: Whole-brain tract. vs. eigenmode images. Left, Wholebraian tractography tract results. Right, Eigenmode of connectivity matrix. Top, View from right side of brain. Middle, Mi-sagittal sections. Bottom, Coronal Sections.

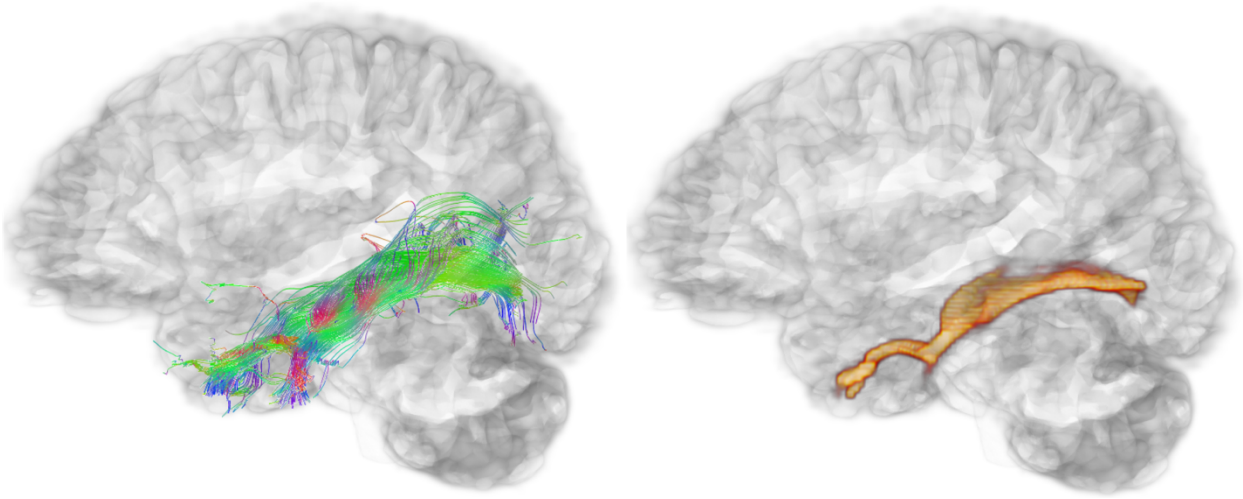

Figure 1.2: Pathway-specific tract vs. eigenmode images. View from the left side of the brain showing the left inferior longitudinal.

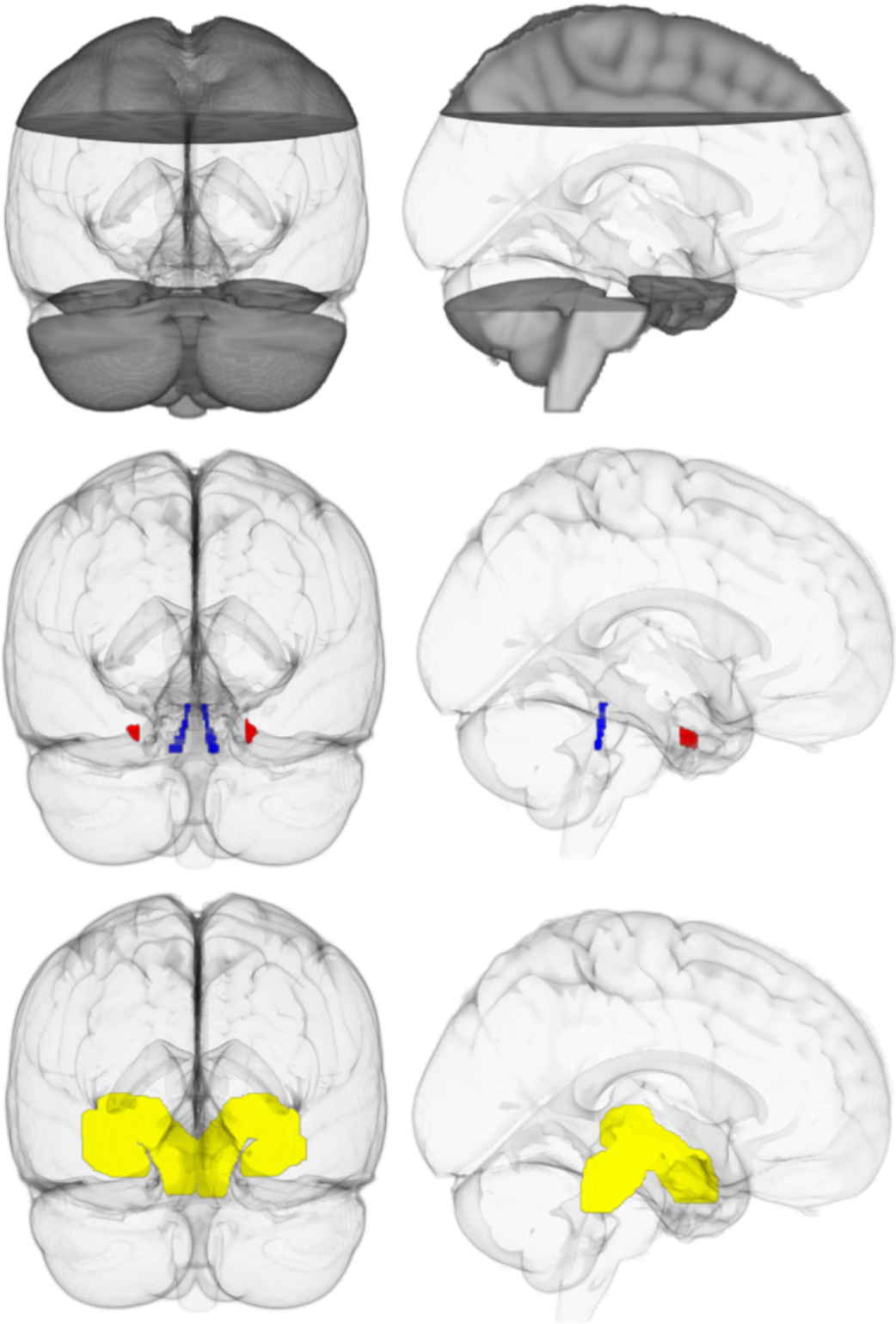

Figure 1.3: Regions of interest. Top, Clear region indicates the "widely distributed" seed region. Middle, Inclusion regions in MNI space. Locus coeruleus (blue) and transentorhinal cortex (red). Bottom, Spatially weighted seed regions (yellow). Left, View from back of brain. Right, View from right side of brain.

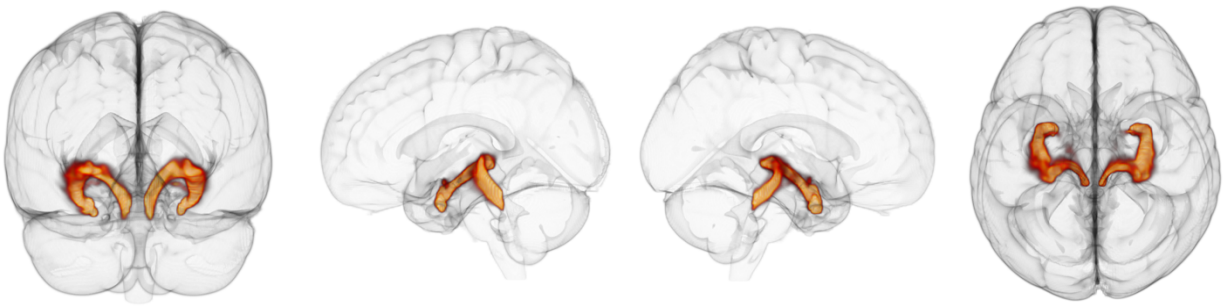

Figure 1.4: Representative LC-TEC pathway reconstruction using the spatially-weighted seeding strategy. 3D output of principle eigenmode of the LC-TEC tractography connectivity matrix from a representative subject. Left: view from back of brain. Middle left: View of left side of brain. Middle right: View of right side of brain. Right: view from top of brain.

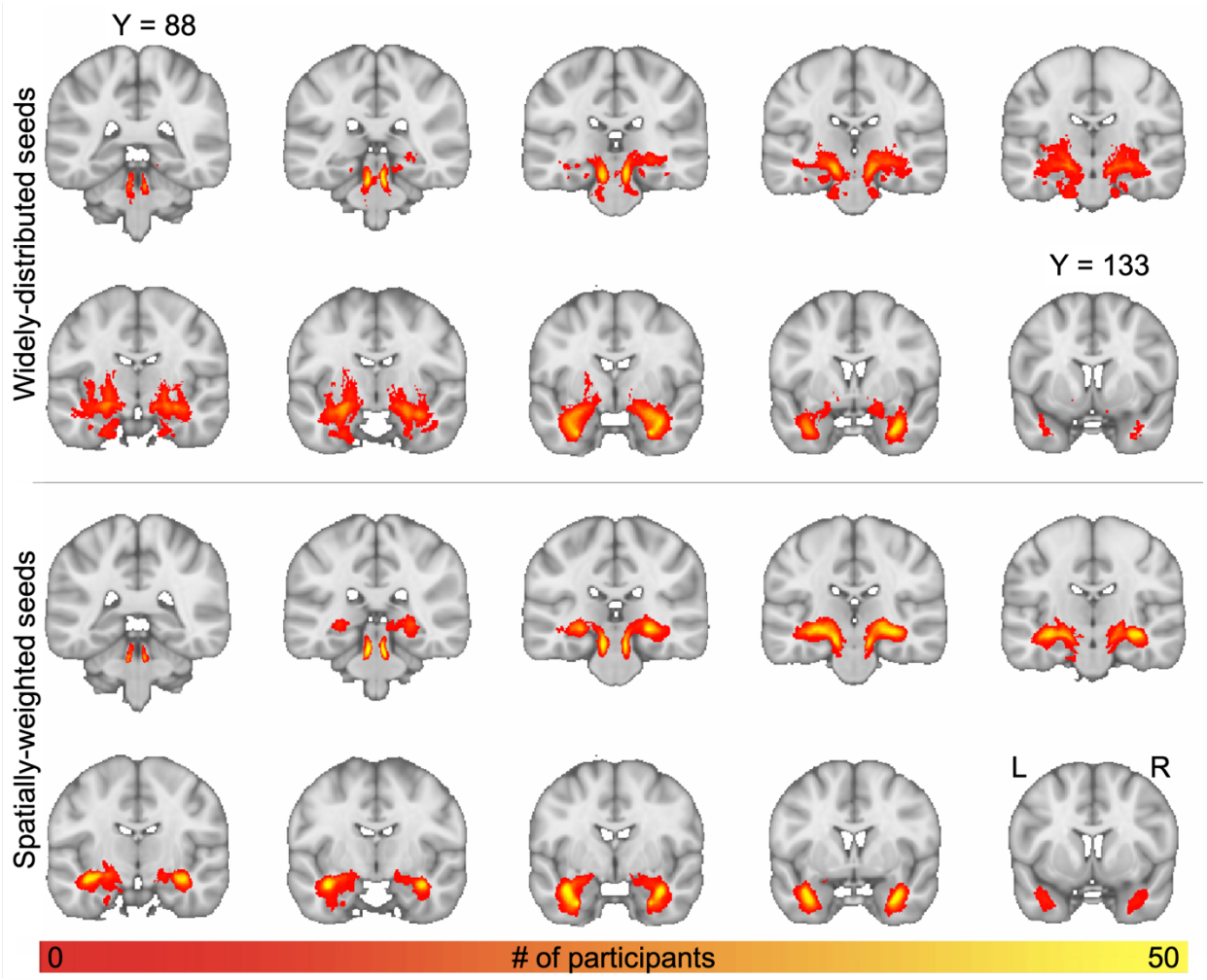

Figure 1.5: Groupwise spatial frequency map of LC-TEC pathway reconstruction. Top: output generated using widely distributed seeds; bottom: output generated using spatially-weighted seeds. Individual participants' thresholded principle EMIs were registered to MNI space, binarized, and summed. The intensity represents the number of subjects that had output in each respective voxel.

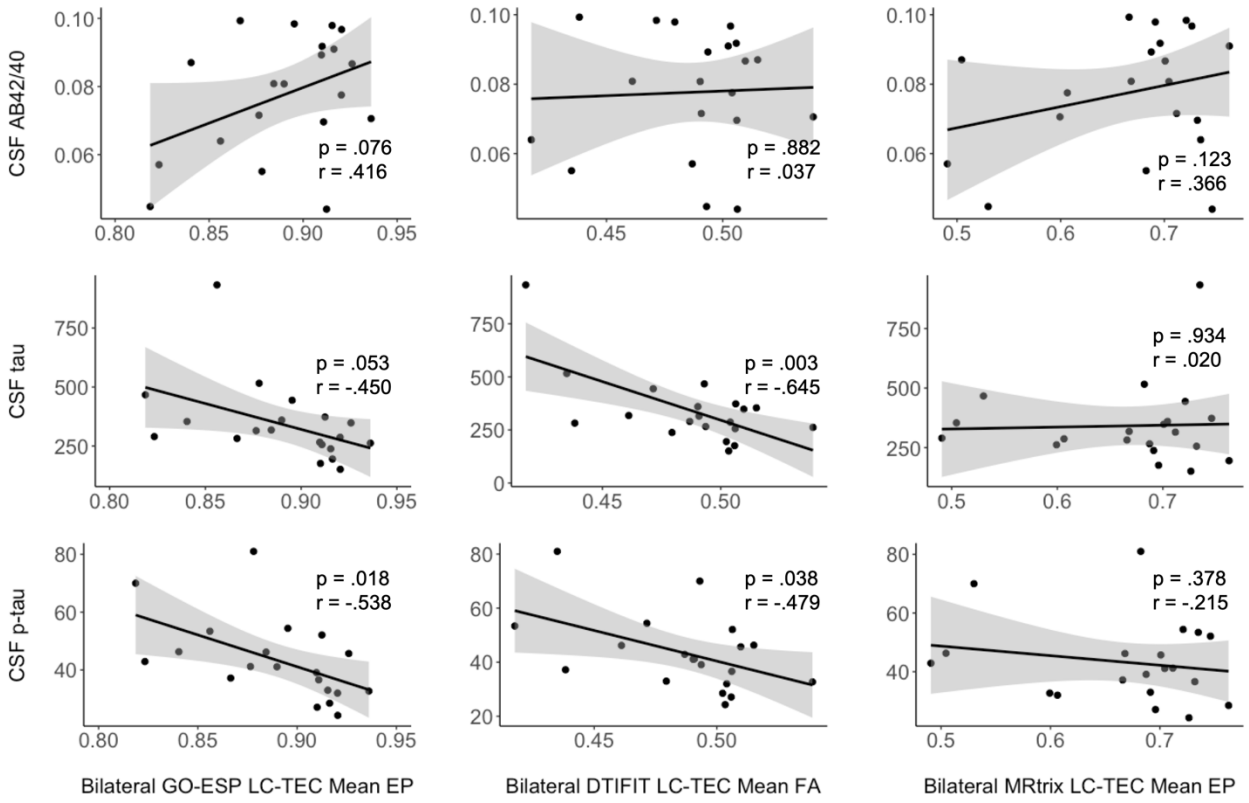

Figure 1.6: Associations between LC-TEC connectivity metrics and CSF biomarkers. Pearson's partial correlations were used, controlling for age. Average bilateral LC-TEC EP is significantly negatively correlated with CSF p-tau (r = -0.538, p = 0.018; bottom left). Average bilateral LC-TEC FA is significantly negatively correlated with CSF total tau (r = -0.645, p = 0.003; middle middle) and p-tau (r = -0.479, p = 0.038; bottom middle). Average bilateral medial path EP is not significantly correlated with any CSF biomarkers.

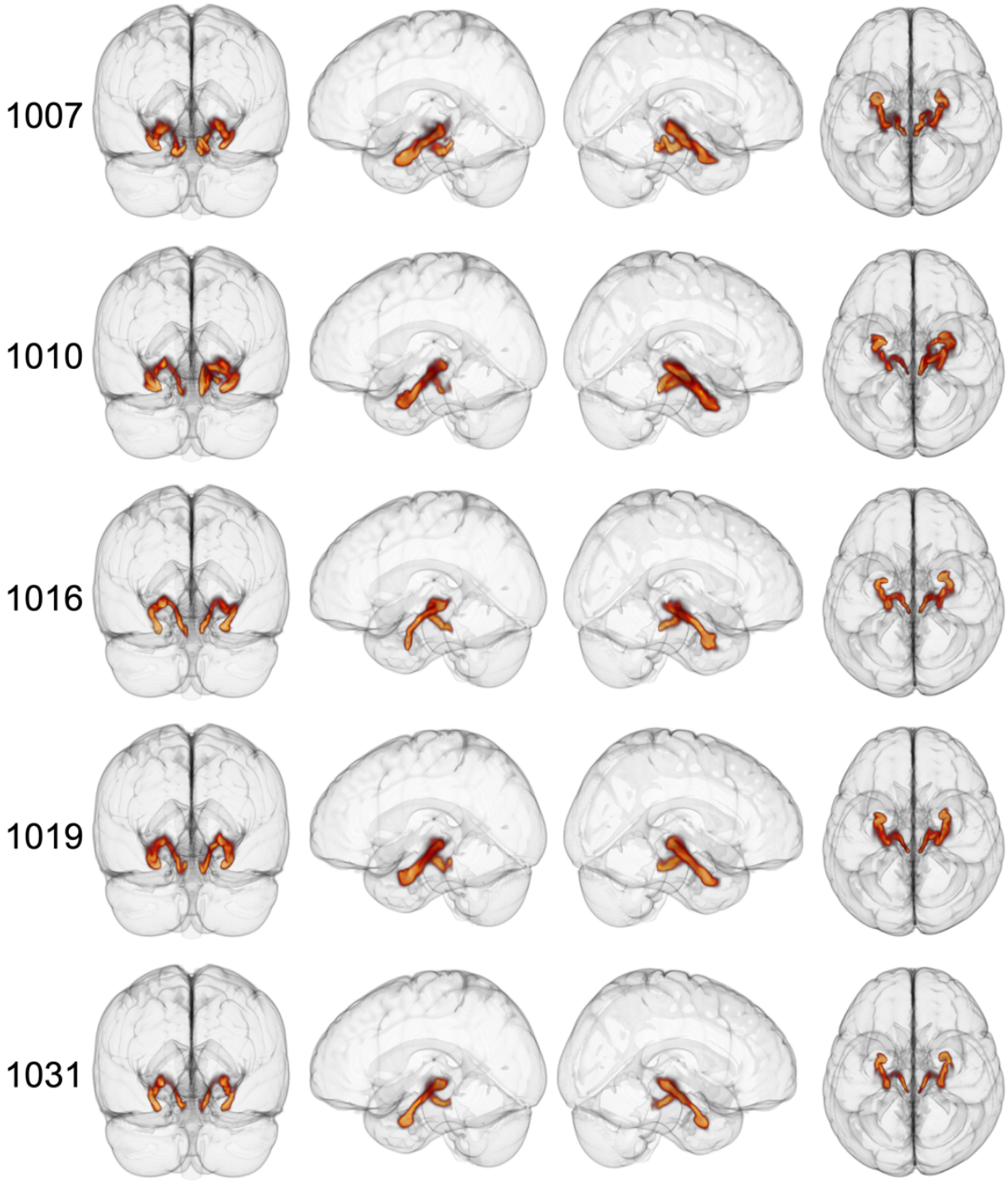

Figure 1.7: 3D LC-TEC principle EMIs for 5 HCP participants using the spatially-weighted seeding strategy. Left: view from back of brain. Middle left: View of left side of brain. Middle right: View of right side of brain. Right: view from top of brain.

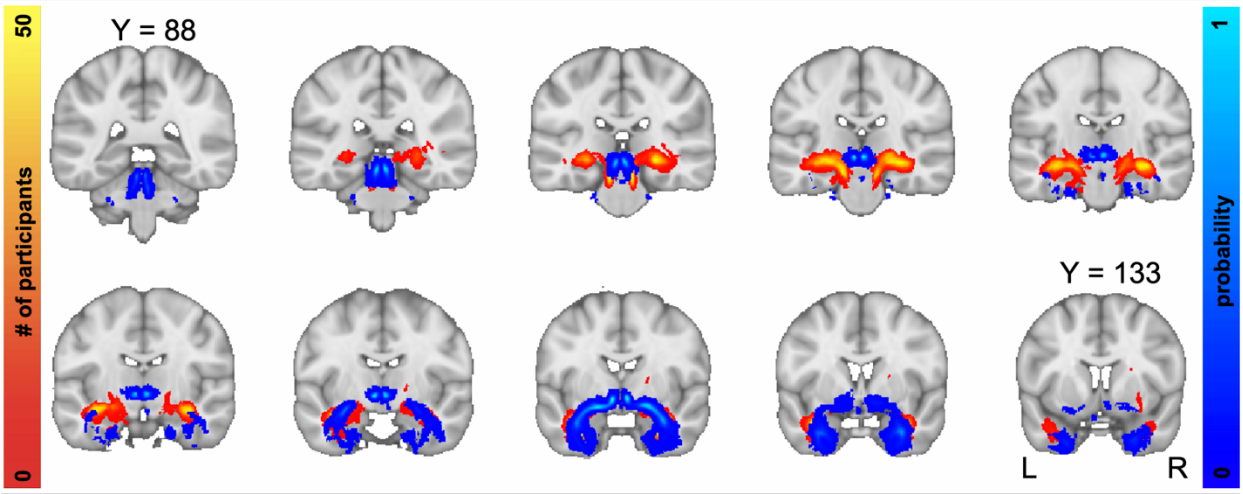

Figure 1.8: Comparison of our results using the spatially-weighted seeding strategy (in red) with LC-TEC pathway probabilistic atlas from Sun et al. (2020) (in blue).

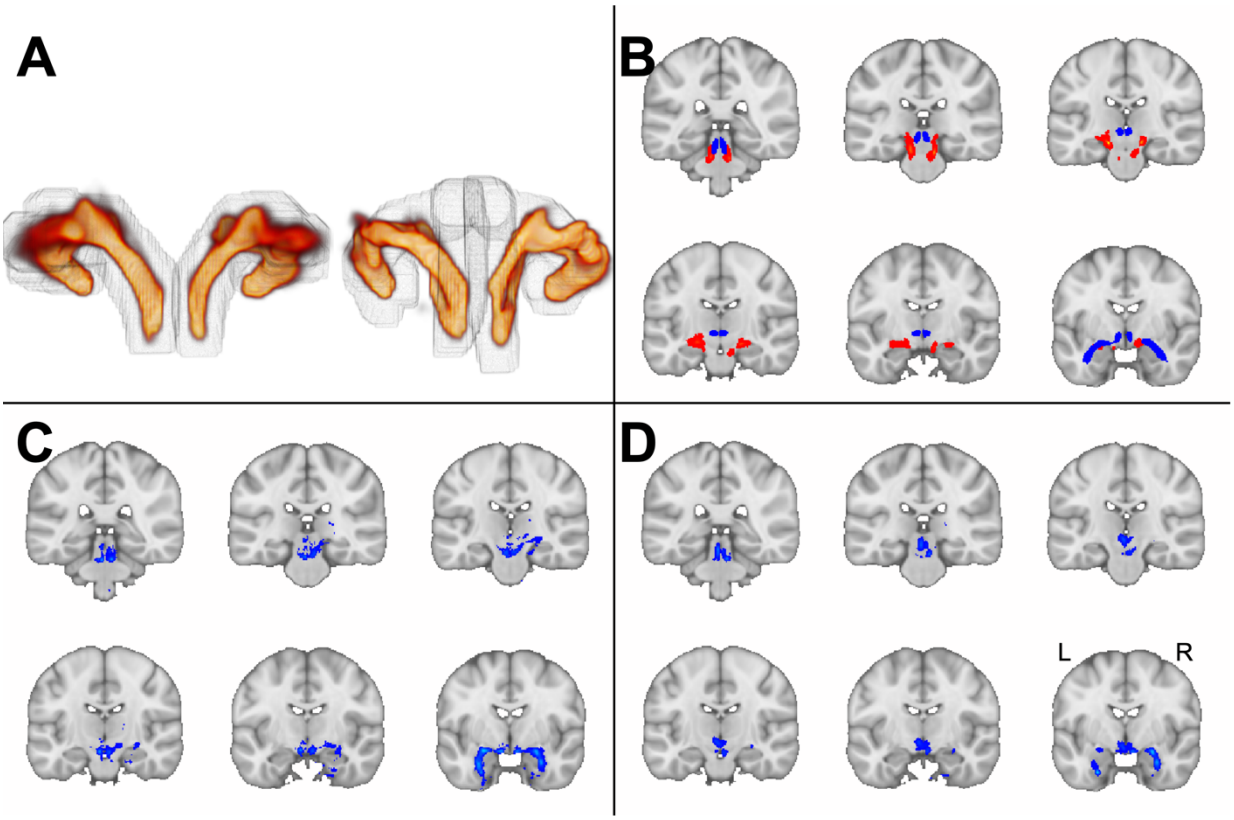

Figure 1.9: Comparison of GO-ESP with state-of-the-art approach. A: 3D view of GO-ESP generated pathways from the back of brain. Left: principle EMI generated using our spatially-weighted seeding region (grey outline). Right: principle EMI generated using dilated mask of medial pathway from Sun et al. (2020) as seeding region (grey outline). B: Red: principle EMI generated from GO-ESP using LC, amygdala, and dilated thalamus as inclusion regions and VTA as an exclusion region. Blue: medial track from Sun et al. (2020). C: Replication of medial pathway in MRtrix using seeding approach from Sun et al. (2020). D: Generation of medial pathway in MRtrix seeding from LC and using the TEC as the only inclusion region.

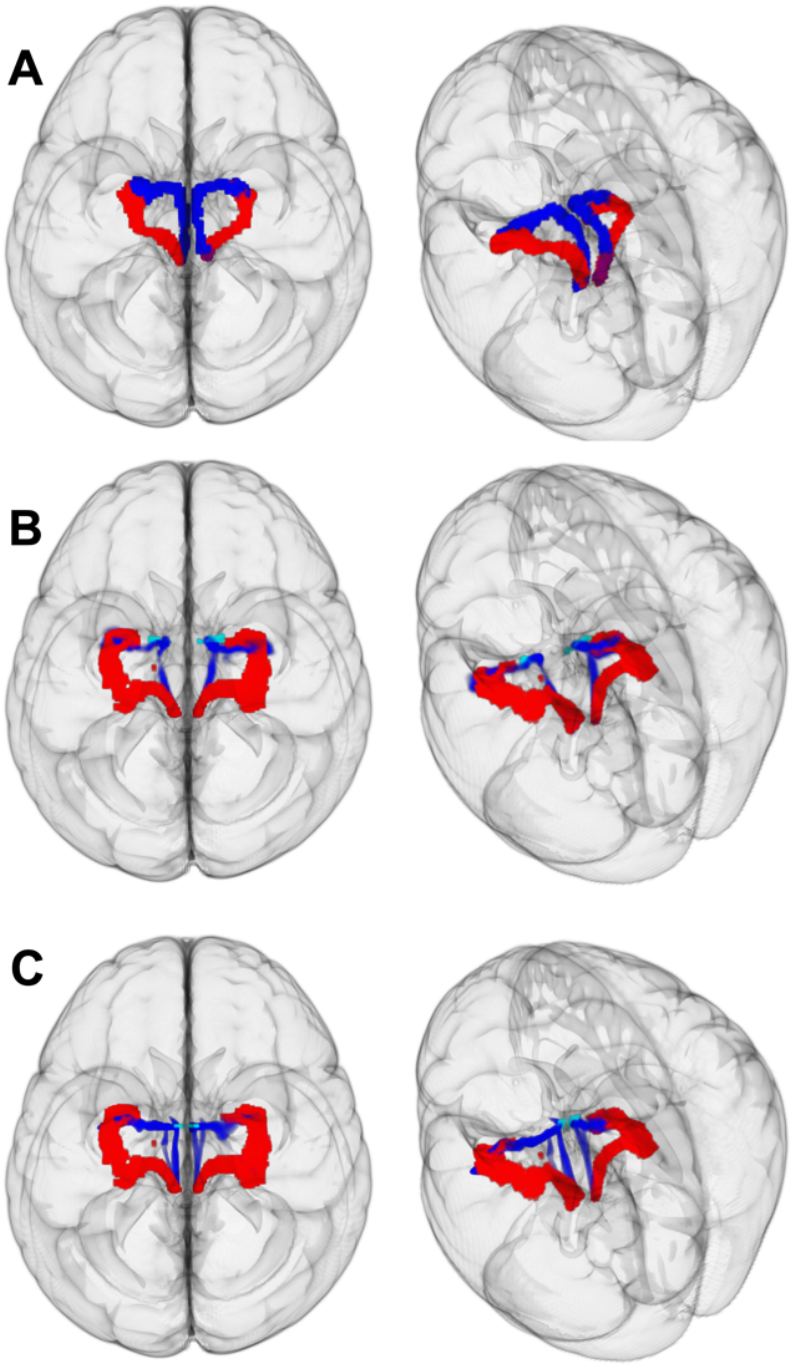

Figure 1.10: Extracting "medial" pathway using GO-ESP in HCP subjects. Left: View from top of brain. Right: View from top left angle. A: extraction of both pathways with widely-distributed seeding strategy. Red: principle EMI. Blue: 3rd EMI for left hemisphere, and 2nd EMI for the right hemisphere. B: Red: principle GO-ESP generated EMI. Blue: principle GO-ESP generated EMI using anterior-medial amygdala (light blue) as additional seeding region. C: Red: principle GO-ESP generated EMI. Blue: principle GO-ESP generated EMI using a medial disc ROI (light blue) encompassing the anterior-medial portion of pathway from Sun et al. (2020).

Tables

Table 1.1: Supporting Information Table S1. Sample characteristics. Demographic, cognitive, and CSF biomarker measurements.

	Mean ± SD	Range
Age (years)	73.92 ± 6.02	62-85
Education (years)	15.96 ± 2.11	12-20
MMSE total raw score	28.9 ± 1.3	25-30
DRS total raw score	139.6 ± 3.29	131-144
CSF Aβ42/40	0.08 ± 0.02	0.04-0.10
CSF tau	373.19 ± 218.42	151.00-1006.00
CST p-tau	43.60 ± 13.81	24.30-81.00
	n	
Sex	n = 37 women	
Ethnicity	n = 5 Hispanic/Latino	
Race	n = 2 African American, n = 1 Asian, n = 1 American Indian/Alaska Native, n = 2 more than one, n = 44 White	

References

1. Foote, S. L., Bloom, F. E., & Aston-Jones, G. (1983). Nucleus locus ceruleus: new evidence of anatomical and physiological specificity. *Physiol Rev*, *63*(3), 844-914. https://doi.org/10.1152/physrev.1983.63.3.844

2. Nagai, T., Satoh, K., Imamoto, K., & Maeda, T. (1981). Divergent projections of catecholamine neurons of the locus coeruleus as revealed by fluorescent retrograde double labeling technique. *Neurosci Lett*, *23*(2), 117-123. https://doi.org/10.1016/0304-3940(81)90027-6

3. Bondareff, W., Mountjoy, C., & Roth, M. (1982). Loss of neurons of origin of the adrenergic projection to cerebral cortex (nucleus locus ceruleus) in senile dementia. *Neurology*, *32*(2), 164-168. https://doi.org/https://doi.org/10.1212/wnl.32.2.164

4. Mann, D., Yates, P., & Hawkes, J. (1982). The noradrenergic system in Alzheimer and multi-infarct dementias. *Journal of Neurology Neurosurgery and Psychiatry*, *45*(2), 113-119. https://doi.org/https://doi.org/10.1136/jnnp.45.2.113

5. Mann, D. M., Yates, P. O., & Marcyniuk, B. (1984). A comparison of changes in the nucleus basalis and locus caeruleus in Alzheimer's disease. *J Neurol Neurosurg Psychiatry*, *47*(2), 201-203. https://doi.org/10.1136/jnnp.47.2.201

6. Tomlinson, B., Irving, D., & Blessed, G. (1981). Cell loss in the locus coeruleus in senile dementia of Alzheimer type. *Journal of the Neurological Sciences*, *49*(3), 419-428. https://doi.org/10.1016/0022-510x(81)90031-9

7. International, A. s. D. (2019). *World Alzheimer's Report 2019: Attitudes to Dementia* (Alzheimer's Disease International: London, Issue.

8. Andrés-Benito, P., Fernández-Dueñas, V., Carmona, M., Escobar, L., Torrejón-Escribano, B., Aso, E., Ciruela, F., & Ferrer, I. (2017). Locus coeruleus at asymptomatic early and middle Braak stages of neurofibrillary tangle pathology. *Neuropathology and Applied Neurobiology*, *43*(5), 373-392. https://doi.org/10.1111/nan.12386

9. Braak, H., Thal, D., Ghebremedhin, E., & Tredici, K. (2011). Stages of the pathologic process in Alzheimer disease: age categories from 1 to 100 years. *Journal of Neuropathology and Experimental Neurology*, *70*(11), 960-969. https://doi.org/10.1097/NEN.0b013e318232a379

10. Grudzien, A., Shaw, P., Weintraub, S., Bigio, E., Mash, D., & Mesulam, M. (2007). Locus coeruleus neurofibrillary degeneration in aging, mild cognitive impairment and early Alzheimer's disease. *Neurobiology of Aging*, *28*(3), 327-335. https://doi.org/10.1016/j.neurobiolaging.2006.02.007

11. Ehrenberg, A., Nguy, A., Theofilas, P., Dunlop, S., Suemoto, C., Di Lorenzo Alho, A., Leite, R., Diehl Rodriguez, R., Mejia, M., Rüb, U., Farfel, J., de Lucena Ferretti-Rebustini, R., Nascimento, C., Nitrini, R., Pasquallucci, C., Jacob-Filho, W., Miller, B., Seeley, W., Heinsen, H., & Grinberg, L. (2017). Quantifying the accretion of hyperphosphorylated tau in the locus coeruleus and dorsal raphe nucleus: the pathological building blocks of early Alzheimer's disease. *Neuropathology and Applied Neurobiology*, *43*(5), 393-408. https://doi.org/10.1111/nan.12387

12. Theofilas, P., Ehrenberg, A., Dunlop, S., Di Lorenzo Alho, A., Nguy, A., Leite, R., Rodriguez, R., Mejia, M., Suemoto, C., Ferretti-Rebustini, R., Polichiso, L., Nascimento, C., Seeley, W., Nitrini, R., Pasquallucci, C., Filho, W., Rueb, U., Neuhaus, J., Heinsen, H., & Grinberg, L. (2017). Locus coeruleus volume and cell population changes during Alzheimer's disease progression: A stereological study in human postmortem brains with potential implication for early-stage biomarker discovery. *Alzheimer's & Dementia*, *13*(3), 236-246. https://doi.org/10.1016/j.jalz.2016.06.2362

13. Braak, H., & Del Tredici, K. (2012). Where, when, and in what form does sporadic Alzheimer's disease begin? *Curr Opin Neurol*, *25*(6), 708-714. https://doi.org/10.1097/WCO.0b013e32835a3432

14. Braak, H., & Braak, E. (1991). Neuropathological stageing of Alzheimer-related changes. *Acta Neuropathol*, *82*(4), 239-259. https://doi.org/10.1007/BF00308809

15. Braak, H., & Del Tredici, K. (2015). The preclinical phase of the pathological process underlying sporadic Alzheimer's disease. *Brain*, *138*(Pt 10), 2814-2833. https://doi.org/10.1093/brain/awv236

16. Xia, Y., & Shi, Y. (2020). Groupwise track filtering via iterative message passing and pruning. *NeuroImage*, *221*, 117147. https://doi.org/10.1016/j.neuroimage.2020.117147

17. Sun, W., Tang, Y., Qiao, Y., Ge, X., Mather, M., Ringman, J. M., Shi, Y., & for Alzheimer's Disease Neuroimaging, I. (2020). A probabilistic atlas of locus coeruleus pathways to transentorhinal cortex for connectome imaging in Alzheimer's disease. *NeuroImage*, *223*, 117301. https://doi.org/10.1016/j.neuroimage.2020.117301

18. Frank, L. R., & Galinsky, V. L. (2014). Information pathways in a disordered lattice. *Phys Rev E Stat Nonlin Soft Matter Phys*, *89*(3), 032142. https://doi.org/10.1103/PhysRevE.89.032142

19. Galinsky, V., & Frank, L. (2015). Simultaneous multi-scale diffusion estimation and tractography guided by entropy spectrum pathways. *IEEE Transactions on Medical Imaging*, *34*(5), 1177-1193. https://doi.org/10.1109/TMI.2014.2380812

20. Fan, Q., Witzel, T., Nummenmaa, A., Van Dijk, K. R. A., Van Horn, J. D., Drews, M. K., Somerville, L. H., Sheridan, M. A., Santillana, R. M., Snyder, J., Hedden, T., Shaw, E. E., Hollinshead, M. O., Renvall, V., Zanzonico, R., Keil, B., Cauley, S., Polimeni, J. R., Tisdall, D., Buckner, R. L., Wedeen, V. J., Wald, L. L., Toga, A. W., & Rosen, B. R. (2016). MGH-USC Human Connectome Project datasets with ultra-high b-value diffusion MRI. *NeuroImage*, *124*(Pt B), 1108-1114. https://doi.org/10.1016/j.neuroimage.2015.08.075

21. Galinsky, V. L., & Frank, L. R. (2014). Automated segmentation and shape characterization of volumetric data. *NeuroImage*, *92*, 156-168. https://doi.org/10.1016/j.neuroimage.2014.01.053

22. Lehoucq, R., Sorensen, D., & Yang, C. (1998). ARPACK Users' Guide. *Society for Industrial and Applied Mathematics*. https://doi.org/10.1137/1.9780898719628

23. Zahneisen, B., Aksoy, M., Maclaren, J., Wuerslin, C., & Bammer, R. (2017). Extended hybrid-space SENSE for EPI: Off-resonance and eddy current corrected joint interleaved blip-up/down reconstruction. *NeuroImage*, *153*, 97-108. https://doi.org/10.1016/j.neuroimage.2017.03.052

24. Andersson, J. L., Skare, S., & Ashburner, J. (2003). How to correct susceptibility distortions in spin-echo echo-planar images: application to diffusion tensor imaging. *NeuroImage*, *20*(2), 870-888. https://doi.org/10.1016/S1053-8119(03)00336-7

25. Smith, S. M., Jenkinson, M., Woolrich, M. W., Beckmann, C. F., Behrens, T. E., Johansen-Berg, H., Bannister, P. R., De Luca, M., Drobnjak, I., Flitney, D. E., Niazy, R. K., Saunders, J., Vickers, J., Zhang, Y., De Stefano, N., Brady, J. M., & Matthews, P. M. (2004). Advances in functional and structural MR image analysis and implementation as FSL. *NeuroImage*, *23 Suppl 1*, S208-219. https://doi.org/10.1016/j.neuroimage.2004.07.051

26. Andersson, J. L. R., & Sotiropoulos, S. N. (2016). An integrated approach to correction for off-resonance effects and subject movement in diffusion MR imaging. *NeuroImage*, *125*, 1063-1078. https://doi.org/https://doi.org/10.1016/j.neuroimage.2015.10.019

27. Xiao, M., Xu, D., Craig, M., Pelkey, K., Chien, C., Shi, Y., Zhang, J., Resnick, S., Pletnikova, O., Salmon, D., Brewer, J., Edland, S., Wegiel, J., Tycko, B., Savonenko, A., Reeves, R., Troncoso, J., McBain, C., Galasko, D., & Worley, P. (2017). NPTX2 and cognitive dysfunction in Alzheimer's Disease. *eLife*, *6*. https://doi.org/10.7554/eLife.23798

28. Vanderstichele, H., Bibl, M., Engelborghs, S., Bastard, N. L., Lewczuk, P., Molinuevo, J. L., Parnetti, L., Perret-Liaudet, A., Shaw, L. M., Teunissen, C., Wouters, D., & Blennow, K. (2012). Standardization of preanalytical aspects of cerebrospinal fluid biomarker testing for Alzheimer's disease diagnosis: a consensus paper from the Alzheimer's Biomarkers Standardization Initiative. *Alzheimer's & Dementia*, *8*(1), 65-73. https://doi.org/10.1016/j.jalz.2011.07.004

29. Kaplow, J., Vandijck, M., Gray, J., Kanekiyo, M., Huyck, E., Traynham, C., Esquivel, R., Fagan, A., & Luthman, J. (2020). Concordance of Lumipulse cerebrospinal fluid t-tau/Aβ42 ratio with amyloid PET status. *Alzheimer's & Dementia*, *16*(1), 144-152. https://doi.org/10.1002/alz.12000

30. Lleó, A., Alcolea, D., Martínez-Lage, P., Scheltens, P., Parnetti, L., Poirier, J., Simonsen, A. H., Verbeek, M. M., Rosa-Neto, P., Slot, R. E. R., Tainta, M., Izaguirre, A., Reijs, B. L. R., Farotti, L., Tsolaki, M., Vandenbergue, R., Freund-Levi, Y., Verhey, F. R. J., Clarimón, J., Fortea, J., Frolich, L., Santana, I., Molinuevo, J. L., Lehmann, S., Visser, P. J., Teunissen, C. E., Zetterberg, H., & Blennow, K. (2019). Longitudinal cerebrospinal fluid biomarker trajectories along the Alzheimer's disease continuum in the BIOMARKAPD study. *Alzhemer's & Dementia*, *15*(6), 742-753. https://doi.org/10.1016/j.jalz.2019.01.015

31. Smith, S. M. (2002). Fast robust automated brain extraction. *Human Brain Mapping*, *17*(3), 143-155. https://doi.org/https://doi.org/10.1002/hbm.10062

32. Galinsky, V. L., & Frank, L. R. (2019). Symplectomorphic registration with phase space regularization by entropy spectrum pathways. *Magnetic Resonance in Medicine*, *81*(2), 1335-1352. https://doi.org/https://doi.org/10.1002/mrm.27402

33. Jenkinson, M., Beckmann, C. F., Behrens, T. E. J., Woolrich, M. W., & Smith, S. M. (2012). FSL. *NeuroImage*, *62*(2), 782-790. https://doi.org/10.1016/j.neuroimage.2011.09.015

34. Keren, N. I., Lozar, C. T., Harris, K. C., Morgan, P. S., & Eckert, M. A. (2009). In vivo mapping of the human locus coeruleus. *NeuroImage*, *47*(4), 1261-1267. https://doi.org/10.1016/j.neuroimage.2009.06.012

35. Setsompop, K., Kimmlingen, R., Eberlein, E., Witzel, T., Cohen-Adad, J., McNab, J. A., Keil, B., Tisdall, M. D., Hoecht, P., Dietz, P., Cauley, S. F., Tountcheva, V., Matschl, V., Lenz, V. H., Heberlein, K., Potthast, A., Thein, H., Van Horn, J., Toga, A., Schmitt, F., Lehne, D., Rosen, B. R., Wedeen, V., & Wald, L. L. (2013). Pushing the limits of in vivo diffusion MRI for the Human Connectome Project. *NeuroImage*, *80*, 220-233. https://doi.org/10.1016/j.neuroimage.2013.05.078

36. McNab, J. A., Edlow, B. L., Witzel, T., Huang, S. Y., Bhat, H., Heberlein, K., Feiweier, T., Liu, K., Keil, B., Cohen-Adad, J., Tisdall, M. D., Folkerth, R. D., Kinney, H. C., & Wald, L. L. (2013). The Human Connectome Project and beyond: initial applications of 300 mT/m gradients. *NeuroImage*, *80*, 234-245. https://doi.org/10.1016/j.neuroimage.2013.05.074

37. Fischl, B. (2012). FreeSurfer. *NeuroImage*, *62*(2), 774-781. https://doi.org/10.1016/j.neuroimage.2012.01.021

38. Greve, D. N., & Fischl, B. (2009). Accurate and robust brain image alignment using boundary-based registration. *NeuroImage*, *48*(1), 63-72. https://doi.org/10.1016/j.neuroimage.2009.06.060

39. Tran, G., & Shi, Y. (2015). Fiber Orientation and Compartment Parameter Estimation From Multi-Shell Diffusion Imaging. *IEEE Trans Med Imaging*, *34*(11), 2320-2332. https://doi.org/10.1109/TMI.2015.2430850

40. Tournier, J. D., Smith, R., Raffelt, D., Tabbara, R., Dhollander, T., Pietsch, M., Christiaens, D., Jeurissen, B., Yeh, C. H., & Connelly, A. (2019). MRtrix3: A fast, flexible and open software framework for medical image processing and visualisation. *NeuroImage*, *202*, 116137. https://doi.org/10.1016/j.neuroimage.2019.116137

41. Wang, J., Aydogan, D. B., Varma, R., Toga, A. W., & Shi, Y. (2018). Modeling topographic regularity in structural brain connectivity with application to tractogram filtering. *NeuroImage*, *183*, 87-98. https://doi.org/10.1016/j.neuroimage.2018.07.068

42. Aston-Jones, G. (2004). CHAPTER 11 - Locus Coeruleus, A5 and A7 Noradrenergic Cell Groups. In G. Paxinos (Ed.), *The Rat Nervous System* (3rd ed., pp. 259-294). Academic Press. https://doi.org/https://doi.org/10.1016/B978-012547638-6/50012-2

43. Kebschull, J. M., Garcia da Silva, P., Reid, A. P., Peikon, I. D., Albeanu, D. F., & Zador, A. M. (2016). High-Throughput Mapping of Single-Neuron Projections by Sequencing of Barcoded RNA. *Neuron*, *91*(5), 975-987. https://doi.org/10.1016/j.neuron.2016.07.036

2. Tau and amyloid moderate the relationship between locus coeruleus-transentorhinal cortex equilibrium probability and cognition

Abstract

The locus coeruleus (LC) is an early site of tau pathogenesis in Alzheimer's disease (AD), yet LC neurons are known to survive with reduced functionality until the latest stages of the disease. Therefore, examining microstructural patterns along LC fiber pathways may offer novel insight into the preclinical period of AD, thereby improving our ability to detect those at greater risk. In this study we use diffusion magnetic resonance imaging to reconstruct a fiber pathway connecting the LC to the transentorhinal cortex in a sample of older adults with and without mild cognitive impairment. We examine the relationship between a novel measure of tract connectivity, equilibrium probability (EP), and cognition in the context of cerebrospinal fluid biomarkers of p-tau and Aβ42/40. Surprisingly, we find that participants with mild cognitive impairment have elevated tract EP compared to their cognitively normal counterparts. Further, we find that across all participants the relationship between tract EP and cognition is moderated by p-tau and Aβ42/40, whereby the association between EP and cognition becomes more negative at greater levels of putative tau and amyloid neuropathology. Our findings suggest that EP is not simply a measure of connectivity, and contributions to the signal may change with increasing levels of amyloid and tau pathology.

Introduction

Alzheimer's Disease (AD) is a debilitating, slowly progressive neurodegenerative disorder affecting over 50 million people globally. With the exponential growth of the older adult population, this figure is expected to increase to 152 million by 2050 (1). This disease not only inflicts profound burdens of impairment on those affected (including patients and the emotional burdens on families, friends, and caregivers); the AD epidemic also carries significant

economic and public health consequences. Thus, there is an urgent need to better understand the early period of the disease so that we can identify those at risk of developing AD and improve our chances of successful intervention.

The noradrenergic system, which plays a critical role in shaping brain dynamics that support various cognitive functions, is increasingly appreciated as a key player in the progression of AD. The primary source of noradrenaline in the brain is the locus coeruleus (LC), a small brainstem nucleus comprised of about 50,000-60,000 neurons in the adult human that nonetheless has massively branching projections reaching throughout the neuraxis. While it has been known for decades that degeneration of neurons within the LC is a ubiquitous feature of AD (2-4), recent histochemistry (5-7) and unbiased stereology (8,9) studies have suggested that nonfibrillar abnormal tau in the LC may be one of the earliest detectable signs of AD-like neuropathology. This finding may account for some of the early behavioral impairments observed in AD patients involving the sleep-wake cycle, agitation, attention, appetite, anxiety, and depression (10-12).

There has been a wave of recent studies examining in vivo magnetic resonance imaging (MRI) measures of putative LC "integrity" assessed using relative signal contrast within the LC (e.g. (13-21)). However, LC neurons are known to survive, albeit with limited functionality, until the latest stage of the disease (22). Therefore, while examining information from voxels comprising the LC nucleus itself is an important avenue of exploration, it is possible that examining microstructural changes along LC pathways may provide more sensitive information earlier in the AD prodrome. Braak recently modified his original neurofibrillary tangle staging system to suggest that the pathogenic process begins with the formation of pre-tangle material deep within the brainstem, including the LC, where it then spreads via specific projections to the

transentorhinal cortex (TEC) (6). Therefore, it is important to study not only the changes taking place within the LC itself, but also its projections to the medial temporal cortex and TEC, where neurofibrillary tangle pathology proceeds as commonly understood (23).

We recently developed a method for reconstructing the LC-TEC pathway from in vivo diffusion MRI (dMRI) data reliably and consistently (24), using a novel mathematical approach for characterizing diffusion MRI data called Geometric Optics-Based Entropy Spectrum Pathways (GO-ESP) (25). This work was carried out in a sample of cognitively normal (CN) older adults. In the present study, we extend our previous work by applying the approach developed in (24) to a sample of older adults with and without mild cognitive impairment (MCI), thought to represent a prodromal stage between normal aging and dementia (26). We reconstruct an LC-TEC pathway, extract a measure of tract connectivity, and examine associations between connectivity and cognition in the context of other AD risk markers derived from cerebrospinal fluid (CSF; p-tau and Aβ42/40). We hypothesized that tract connectivity would be reduced in those with MCI compared to CN adults, and that this difference would be especially apparent in the portion of the tract more distal from the LC. This hypothesis is based on previous findings in APOE-deficient mice showing that synaptic disturbances in an LC tract were more apparent in terminals that were farther away from the cell body (27). We also hypothesized that across participants, reduced connectivity would be associated with increased AD risk as measured by cognitive and biomarker positivity. In particular, we expected to see stronger associations in models incorporating tau in comparison to amyloid, since the LC is specifically implicated in AD-related tau pathogenesis (5-9).

Methods

Participants

Participants were recruited primarily from the University of California, San Diego (UCSD) Alzheimer's Disease Research Center, which is funded by the National Institute on Aging to conduct longitudinal studies on older adults. Additional participants were recruited from the community in San Diego, California. Referrals came from participants enrolled in past studies, flyers, Veteran's Affairs Neuropsychological Assessment Unit, and Research Match where they are screened for eligibility. This study was approved by the UCSD Institutional Review Board, and written informed consent was obtained from all participants upon enrollment.

A total of 109 participants (age range: 62-85 years, average age of 74.46 years, 58% women) were recruited, and 24 were excluded from all analyses: 1 subject was unable to receive a diagnosis due to incomplete neuropsychological data; 1 participant was unable to complete MRI scanning due to a stent that was not reported during phone screening; 1 participant had an incidental finding on MRI; 3 participants had errors in MRI acquisition that resulted in unusable data or data that were unable to be reconstructed; 1 participant had an artifact that made their data unusable; and 6 were excluded due to excessive head motion during MRI scanning. Further, our data collection was restricted due to the COVID-19 pandemic, and we only enrolled 11 participants with AD, 2 of which were unable to complete scanning due to anxiety upon entering the scanner bore. We therefore excluded them from analyses due to lack of statistical power in such a small sample. Our final example consisted of 85 participants.

Cognitive testing & diagnostic classification of MCI

Participants completed a comprehensive neuropsychological test battery including sensitive measures of memory (California Verbal Learning Test-II, WMS-R Visual

Reproduction Test with delayed recall and recognition, WMS-R Logical Memory with delayed recall and recognition, Benson Complex Figure Copy), attention (WAIS-R Digit Span), language (Multilingual Naming Test, and Letter and Category Fluency Tests), problem solving and executive function (modified Wisconsin Card Sort Test, Trail-Making Test Parts A and B, Digit Symbol Substitution Test, Fluency Switching and Color-Word Interference subtests of the Delis-Kaplan Executive Functioning System [DKEFS]), constructional and visuospatial abilities (WASI-II Block Design Test, Clock Drawing Test, D-KEFS Visual Scanning), and global cognition (Mattis Dementia Rating Scale [DRS], Mini-Mental State Examination [MMSE]).

We define MCI as having scores below one standard deviation of the norms on two or more tests within one or more cognitive domains, according to Jak/Bondi actuarial neuropsychological test methods (28,29). This actuarial approach was developed to improve rigor and sensitivity of MCI classifications and has been shown to assign diagnoses that are less prone to false positive errors and more related to AD biomarkers (30-32).

The final sample after all exclusion criteria were applied included 62 CN older adults, 15 with amnestic MCI (defined as having impairment in memory; 9 multi-domain, 6 single-domain), and 8 with non-amnestic MCI (defined as having impairment only in non-memory domains; 4 single-domain, 4 multi-domain). Single-domain non-amnestic MCI participants were included in the CN group due to the instability of the diagnosis (28). Thus, our final groups consisted of 66 CN and 19 MCI participants.

To examine associations between tract connectivity and cognition, cognitive composites were created by averaging z-scores from raw data for attention (Digit Symbol total, Digit Span forward total, Trails A seconds), executive function (Digit Span backward total, Trails B seconds, and DKEFS Color-Word Inhibition Switching seconds), verbal learning (CVLT List A

1-5 total and Logical Memory 1), and verbal memory (CVLT Long Free Recall and Logical Memory 2).

CSF biomarker assessment

A subset of our participants (n = 59) underwent lumbar punctures as part of participation in the UCSD Alzheimer's Disease Research Center. Procedures, preanalytical preparation, and storage of CSF were carried out as previously described (33) in accordance with recommended best practices (34). In brief, 15–25 mL of CSF was collected by lumbar puncture early in the morning after overnight fasting. Samples were processed, aliquoted into 500 μL fractions in polypropylene microtubes, snap frozen, and stored at −80°C until assayed. All samples were analyzed locally using the automated Lumipulse platform using assays developed with established monoclonal antibodies (Fujirebio Inc) (35). The majority of lumbar punctures were conducted within one year of the MRI visit (n = 20), although we included data collected within two (n = 15), three (n = 4), and four (n = 8) years of the visit given research showing the stability of CSF biomarkers over several years (36) in an effort to maximize our sample size. Twelve samples were excluded from analyses for being collected over 4 years from MRI scanning and cognitive testing, resulting in a final sample of 47 CSF measurements. CSF measures of Aβ40, Aβ42, total tau, and phosphorylated tau (p-tau) were obtained. We used p-tau for analyses as previous research has suggested p-tau to be a more specific biomarker for AD (37) whereas total tau may be a marker of neurodegeneration in general (38). Further, we used the Aβ42/40 ratio which has been shown to perform better at identifying AD patients compared to AB42 alone (39).

MRI acquisition

Scans were performed on a 3 Tesla GE Discovery MR750 scanner at the UCSD Center for Functional MRI using a 32-channel head coil (Nova Medical Inc, Wilmington MA). Whole-brain diffusion MRI scans were collected using a novel Extended Hybrid Sense EPI acquisition (40); data were simultaneously acquired with both polarities of the phase encoding gradient to perform TOPUP gradient and eddy current distortion correction, which was done in offline specialized reconstruction routines that implemented the FMRIB Software Library's (FSL) Eddy and TOPUP tools (41-43) directly within the image reconstruction (40). Multiple diffusion-weighted shells were collected at b-values of 1000, 2000, and 3000s/m^2 with the number of directions being 30, 45, and 60, respectively, and 6 b0s. The data acquisition parameters were: slice thickness=2mm, FOV=20cm, TE=93ms, TR=2.7s, matrix size=100x100x72. Using a SENSE factor of 4, the imaging time was approximately 13 minutes. This is a standard diffusion MRI gradient sampling scheme. Therefore, findings generated from this study are a result of the analysis, not the acquisition, and should be replicable across datasets.

MRI preprocessing and quality assessment

FSL (v.6.0) (42) was used to correct for inter-volume head motion (eddy; b-vectors adjusted for correction) (43) and remove skull and other non-brain tissue (BET) (44). Data were resampled to a 1mm3 resolution using Symplectomorphic Registration with Phase Space Regularization (SYMREG) (45).

Quality control consisted of visual inspection for slice-wise signal dropout, image noise, and shifts of head placement between diffusion volumes, as well as quantitative measurement of in-scanner head motion (from eddy). Scans with greater quantitative measures of head motion

corresponded with visual confirmation of slice-wise signal dropout in volumes collected during head movement. Six scans with total average head motion over 0.7 mm were excluded.

Diffusion Estimation and Tractography

Diffusion MRI post-processing was performed using GO-ESP, a novel diffusion estimation and tractography approach which simultaneously estimates local diffusion and long-range connectivity patterns using the theory of **E**ntropy **S**pectrum **P**athways and a **G**eometric **O**ptics-like approach for tracing out tracts as proxies for white matter pathways (25,46). ESP builds off the concept of a maximum entropy random walk, calculating transition probabilities between voxels using a coupling matrix (in this work, the coupling matrix defines inter-voxel interactions as the inner product of the full diffusion tensor). The transition probabilities describe the probabilities of various pathways within the data, and the final distribution of these probabilities over long time results in our dependent measure of interest – the equilibrium probability (EP). Because the calculation of EP considers the global structure of the dMRI data, it is more robust to local regions of spurious signal dropout due to complex underlying fiber orientation geometry and may be more a measure of connectivity than anisotropy. While many parameters go into the calculation of the EP (46), one parameter of interest is the coupling power – the exponent that the coupling matrix is raised to. We find that varying this parameter and taking the average EP across different coupling values results in a more normally distributed EP variable across datasets, thus we took the average EP generated using coupling values of 3, 4, and 6, and used this as our measure of tract connectivity.

To reconstruct an LC-TEC pathway, we used GO-ESP to generate tracts intersecting two regions of interest (ROIs): a publicly available LC map (47), and the anterior division of the parahippocampal gyrus, meant to approximate the TEC, extracted from the Harvard-Oxford

cortical structural atlas in FSL (HarvardOxford-cort-maxprob-thr50-1mm). Only the most anterior lateral portion of the anterior parahippocampal gyrus ROI was used to maintain specificity of generated tracts (Figure 1, middle panel). As both ROIs were created in standard Montreal Neurological Institute (MNI) coordinate space, SYMREG (45) was used to register each participant's EP map to the "MNI152_T1_1mm_brain" map from the template in FSL. These registrations were used to reverse transform the ROIs from MNI coordinate space into each subject's native diffusion space, in which tractography was performed.

Tractography was performed as previously described (24). In a representative subject, seeds were first distributed throughout the brain excluding only the top part of the cerebral cortex and the brain below the ROIs (this was done for computational efficiency; xyz coordinates in MNI space 0-200, 0-200, 0-142; Figure 1, top panel). Only tracts that intersected both ROIs were kept (Figure 1, middle panel). We refer to this strategy as "widely-distributed" seeding. Next, to increase the spatial consistency of output between subjects, we took the principle eigenmode of this representative LC-TEC pathway reconstruction using widely-distributed seeds, and binarized and dilated this region to obtain a mask that could be used as a more "spatially-weighted" seeding region (Figure 1, bottom panel). In this approach, seeds are still distributed throughout the brain as described above, but placement is weighted more heavily within the "spatially-weighted" mask. As before, only tracts that intersected both ROIs were kept. For both analyses, two million starting seeds were randomly distributed throughout the seed regions, and tracking was only permitted to pass through regions where the EP was at least 0.5 (this value corresponds reliably with the location of white matter). The output from spatially-weighted seeding for all subjects was used for subsequent analyses because this strategy results in more spatially consistent output across datasets.

Using each participants' tractography output, we performed a technique we call EigenMode Imaging (EMI), which involves calculating the eigensystem of the connectivity matrix constructed from the generated tracts. The resulting eigenvectors represent the spatial distribution of probability corresponding to the most likely pathways within the set of tracts, and these pathways are called eigenmodes. The eigenvector associated with the largest eigenvalue (the principal eigenvector) corresponds with the pathway with the greatest probability (the principal eigenmode). We analyzed the principal eigenmode for all datasets.

To generate masks for visualization and statistical analyses, we applied a threshold to the EMIs. The EMIs generated from tractography are automatically normalized so that the sum of all included voxels is equal to one, where higher values correspond with a higher probability. To exclude voxels with the lowest probability of belonging to the pathway, we kept only those highest value voxels whose intensities sum to 0.9. This technique ensures a level of within-subject anatomical consistency. These thresholded EMIs were binarized and used as masks to extract measures for statistical analyses. Spatial consistency of tractography output across subjects can be seen in Figure 2.

To examine effects related to distance from the LC nucleus, we took a representative LC-TEC pathway and split it into three equal segments along its posterior-anterior axis (proximal, middle, and distal to LC). The MNI152-space y-axis coordinates for each segment were as follows: proximal = 87-102; middle = 103-118; distal = 119-132 (Figure 3). Given the inter-subject consistency in tract anatomy, we registered each of these MNI-space segments into subject native-space using SYMREG (45) for extraction of connectivity measures and statistical analysis.

Statistical analysis

Statistical analyses were performed in R (version 4.1.2; https://cran.r-project.org/). All data were checked for outliers (defined as three times the interquartile range above the third quartile or below the first quartile). There were no outliers in the cognitive composites. There was one outlier p-tau measurement, so this case was excluded from analyses involving p-tau. There were no outliers in Aβ4240 or EP.

Independent samples t-tests were used to compare groups (CN vs MCI) on age, years of education, raw MMSE and DRS totals, and CSF markers of p-tau and AB42/40. Covariates included age and sex for all analyses, education for analyses with cognitive composites, and head motion for analyses with EP. Product-moment correlations assessed the relationship between LC-TEC EP with p-tau and Aβ4240. An analysis of covariance examined average LC-TEC EP as a function of group (CN vs MCI). A repeated-measures analysis of covariance was conducted to examine average LC-TEC EP as a function of group (CN vs MCI) and tract segment (proximal vs middle vs distal).

To examine associations between LC-TEC EP and cognition in the context of AD risk as measured by CSF biomarkers, multiple linear regressions were used to examine each cognitive composite (attention, executive function, verbal learning, and verbal memory) as a function of average LC-TEC EP, p-tau, and the interaction between EP and p-tau. To assess whether our results are specific to p-tau, follow-up sets of regressions were run examining the relationship between LC-TEC EP and cognition in the context of Aβ42/40.

Results

Sample characteristics

Demographic and clinical characteristics can be found in Table 1. CN and MCI participants did not differ in age or years of education. MCI participants scored lower on the MMSE ($p < 0.05$) and DRS ($p < 0.05$) compared to CN participants. Groups did not differ on levels of p-tau or Aβ42/40, though the MCI group showed the expected trends of increased p-tau and reduced Aβ42/40 compared to CN participants. Groups did not significantly differ in average head motion (95% CI = -0.13 – 0.03, $p > 0.05$).

Connectivity associations with CSF biomarkers

A product-moment correlation controlling for age and sex revealed no relationship between average LC-TEC EP and p-tau ($r(41) = 0.05$, $n = 45$, $p > 0.05$), but there was a significant, albeit weak, relationship between LC-TEC EP and Aβ42/40 ($r(42) = -0.33$, $n = 46$, $p < 0.05$) such that higher EP was associated with lower Aβ42/40 (indicative of greater cerebral amyloid pathology).

Connectivity comparisons between CN and MCI participants

An analysis of variance examining average LC-TEC EP as a function of group while controlling for age, sex, and head motion revealed a significant main effect of group ($F(1,79) = 4.16$, $p < 0.05$, $\eta 2G = 0.05$), whereby the MCI group had higher average EP (mean = 0.70 +/- 0.046) compared to CN participants (mean = 0.67 +/- 0.048). A repeated measures analysis of variance examining average LC-TEC EP with the between-subjects variable of group (CN, MCI) and the within-subjects variable of tract segment (proximal, middle, distal) while controlling for age, sex, and head motion revealed no main effect of group ($F(1,80) = 0.003$, $p > 0.05$, $\eta 2G <$

0.001). However, there was a main effect of segment ($F(1.5,119.65) = 4.54$, $p < 0.05$, $\eta 2G = 0.02$), such that distal < middle < proximal LC-TEC EP.

Connectivity associations with cognition

Tract EP and cognition relationships in the context of p-tau

Four multiple linear regressions were run predicting each cognitive composite (attention, executive functioning, verbal learning, verbal memory) from age, sex, education, head motion, average LC-TEC EP, p-tau, and the interaction between EP and p-tau. All regression results can be found in Table 2.2.

Our attention model was not statistically significant overall ($F(7,37) = 2.03$), adjusted $R^2 = 0.14$, $p > 0.05$), although there were significant main effects of EP ($\beta = 18.85$, $p < 0.01$) and p-tau ($\beta = 0.36$, $p < 0.01$) and a significant interaction between EP and p-tau ($\beta = -0.51$, $p < 0.01$), such that the relationship between EP and attention is positive among those with low p-tau but becomes more negative in those with higher levels of p-tau. To aid in interpretation of the interaction effect, a median split of p-tau was performed to graphically depict the relationship between the three variables.

Our model predicted executive functioning ($F(7,37) = 3.24$, adjusted $R^2 = 0.26$, $p < 0.01$), with main effects of EP ($\beta = 25.11$, $p < 0.001$) and p-tau ($\beta = 0.44$, $p < 0.001$) and a significant interaction between EP and p-tau ($\beta = -0.64$, $p < 0.001$), such that the relationship between EP and executive functioning is positive in those with low p-tau and becomes more negative in those with higher p-tau. To aid in interpretation of the interaction effect, a median split of p-tau was performed to graphically depict the relationship between the three variables.

Our model significantly predicted verbal learning ($F(7,37) = 7.57$, adjusted $R^2 = 0.51$, $p < 0.0001$), with main effects of sex ($\beta = 0.71$, $p < 0.01$), education ($\beta = 0.11$, $p < 0.05$), head

motion ($\beta = -1.58$, $p < 0.05$), p-tau ($\beta = 0.31$, $p < 0.05$), and the interaction between EP and p-tau ($\beta = -0.48$, $p < 0.05$), such that the relationship between EP and verbal learning becomes more negative in those with higher p-tau. To aid in interpretation of the interaction effect, a median split of p-tau was performed to graphically depict the relationship between the three variables.

Finally, our model significantly predicted verbal memory ($F(7,37) = 3.54$, adjusted $R^2 = 0.29$, $p < 0.01$), with significant main effects of sex ($\beta = 0.63$, $p < 0.05$), education ($\beta = 0.13$, $p < 0.05$), and the interaction between EP and p-tau ($\beta = -0.48$, $p < 0.05$), such that the relationship between EP and verbal memory becomes more negative among those with higher p-tau. To aid in interpretation of the interaction effect, a median split of p-tau was performed to graphically depict the relationship between the three variables.

Tract EP and cognition relationships in the context of Aβ42/40

Four multiple linear regressions were run predicting each cognitive composite (attention, executive functioning, verbal learning, verbal memory) from age, sex, education, head motion, average LC-TEC EP, CSF Aβ42/40, and the EP by Aβ42/40 interaction. All regression results can be found in Table 2.2.

Our model did not predict attention ($F(7,38) = 0.26$, adjusted $R^2 = -0.13$, $p > 0.05$), and none of the coefficients were statistically significant. Our model did not predict executive functioning ($F(7,38) = 0.54$, adjusted $R^2 = -0.08$, $p > 0.05$), and none of the coefficients were statistically significant.

Our model predicted verbal learning ($F(7,38) = 7.81$, adjusted $R^2 = 0.52$, $p < 0.0001$), with main effects of sex ($\beta = 0.68$, $p < 0.01$), education ($\beta = 0.11$, $p < 0.01$), EP ($\beta = -30.32$, $p < 0.01$), Aβ42/40 ($\beta = -195.80$, $p < 0.05$), and the interaction between EP and Aβ42/40 ($\beta = 308.90$, $p < 0.05$). The interaction was such that the relationship between EP and verbal learning

becomes more negative among those with lower levels of Aβ42/40 (indicative of greater amyloid neuropathology). To aid in interpretation of the interaction effect, a median split of Aβ42/40 was performed to graphically depict the relationship between the three variables.

Finally, our model predicted verbal memory ($F(7,38) = 3.85$, adjusted $R^2 = 0.31$, $p < 0.01$), with main effects of education ($\beta = 0.13$, $p < 0.05$), EP ($\beta = -29.71$, $p < 0.05$), and the interaction between EP and Aβ42/40 ($\beta = 323.50$ $p < 0.05$). The interaction was such that the relationship between EP and verbal memory becomes more negative among those with lower Aβ42/40. To aid in interpretation of the interaction effect, a median split of Aβ42/40 was performed to graphically depict the relationship between the three variables.

Discussion

In this study, we reconstruct an LC-TEC pathway from diffusion MRI data collected in a sample of older adults at varying degrees of risk for AD. We extract average EP (a measure of tract connectivity) within each participant's LC-TEC pathway, compare EP between CN and MCI participants, and analyze its relationship with cognition in the context of putative tau and amyloid neuropathology measured from CSF.

Surprisingly, we find that participants with MCI have higher LC-TEC EP compared to CN participants. This weak-to-medium effect was not related to tract segment but was seen only when looking at EP over the entire pathway as a whole unit. Additionally, we find that higher LC-TEC EP is associated with lower CSF Aβ42/40 (indicative of greater cerebral amyloid pathology). While this association was weak, these two findings together seem to suggest that the EP measure could be picking up on some pathologic, inflammatory, or compensatory process rather than being simply a measure of connectivity strength. Interestingly, we did not replicate our previous preliminary finding of a negative association between tract EP and p-tau (24).

When examining associations between LC-TEC EP and cognition, we see a consistent pattern whereby the relationship between EP and cognition depends upon levels of CSF markers of AD-related pathology. There is a significant negative interaction between EP and p-tau across the examined cognitive domains (attention, executive function, verbal learning, and verbal memory) such the relationship between EP and cognition becomes more negative at greater levels of tau neuropathology. When examining these relationships in the context of Aβ42/40, we see a similar pattern only with verbal learning and delayed verbal memory. Indeed, according to the residual standard errors the attention and executive functioning models were strongest when accounting for p-tau rather than Aβ42/40, and the verbal learning and memory models were strongest when accounting for Aβ42/40 rather than p-tau. These findings support the idea that tau pathogenesis in the LC relates to early deficits in attention and executive functioning, and by the time learning and memory impairments manifest, the presence of amyloid pathology becomes an important predictor.

Taken as a whole, our findings suggest that EP is more than a simple index of connectivity. Among individuals with accumulating tau and amyloid neuropathology, the relationship between EP and cognition becomes more complex and may involve other factors. This is not an isolated issue in the neuroimaging community. Generally, measures that garner widespread interpretation as indexes of "integrity" are more multifaceted. For instance, fractional anisotropy in diffusion tensor imaging is typically used as a measure of white matter "integrity", even though we know that there are multiple underlying microstructural orientation patterns and physiological processes that can result in reduced fractional anisotropy, not all of which represent poorer integrity (48). Therefore, these results both warrant further investigation in

larger samples as well as serve as a reminder to be cautious in applying such blanketed interpretations of macroscopic neuroimaging metrics.

In our case, one of the major strengths of GO-ESP and the calculation EP – the consideration of long-range structure – may also be its weakness when applied to a clinical research question. Indeed, while the nature of GO-ESP improves tractography through regions with complex underlying fiber geometry and results in measures of connectivity that are more robust to local regions of signal dropout due to crossing fibers, this may also render EP less sensitive to focal regions of truly diminished white matter microstructure. Double-pulsed field gradient dMRI may offer more sensitivity to areas of complex fiber geometry and is a promising technique in its early stages of being applied to clinical research.

Our study has limitations. First, the true anatomy of LC pathways in the human brain are not well-understood, and the pathway we present is a postulate generated from the data with as few anatomical constraints as possible while still resulting in reliable and consistent output. Notably, the only other published LC-TEC pathway to our knowledge (49) captures a different spatial trajectory based upon understanding of LC projections from rodent studies. We make no arguments about whether either of the pathways are true or false; they are different reconstructions from fundamentally different analysis algorithms, and more anatomical research in human brains is necessary to know with more certainty which brain regions contain the projections of interest. Importantly, it has been noted that the human LC is markedly more complex than that in rodents and therefore we must be careful in assuming direct translatability from these early tracing studies (50). Second, only a small subsample of our participants with diffusion MRI data had CSF measures. Lumbar punctures are invasive and uncomfortable, limiting data availability and begging the question of selection bias. Obtaining putative

pathology measures with less invasive techniques such as blood draws may improve upon this issue but will take time to implement. Related to our small sample, we were unable to include participants with AD in our analyses due to their extremely limited group size. Further, in order to maximize our MCI sample, we made the decision to group together amnestic and multi-domain non-amnestic MCI participants, though examining amnestic MCI in isolation may offer more sensitivity to early AD-related changes. We grouped the single-domain non-amnestic MCI participants with the CN participants to try to restore some sensitivity. Finally, our sample consists of predominantly educated white older adults who live in and around a relatively affluent area, which is not representative of broader demographic characteristics in the United States or even in southern California. Given our limited sample size, we believe this study offers valuable insights from an exploratory perspective to generate further research ideas and hypotheses, but we acknowledge that interpretations or generalizability of findings are limited. There is a great need to study the impacts of sociodemographic factors such as access to healthcare and education, socioeconomic status, and chronic stress (especially relevant to the LC) on AD risk and progression, and to take these factors into account in studies such as ours.

Overall, this study builds directly upon our previous work by including a broader sample of older adults at varying degrees of AD risk, measured using neuropsychological measures of cognition and CSF measures of putative tau and amyloid neuropathology. We show that LC-TEC EP relates to cognition in a manner that depends on p-tau and Aβ42/40. Specifically, we see the expected positive association between greater EP and better cognition only among those with low pathology. This work calls for future investigations of the tract connectivity-cognition relationship particularly among individuals with greater pathology, in which case other risk

factors – potentially sociodemographic factors in a more diverse sample – may benefit our understanding of early AD.

Acknowledgements

The authors thank Thomas Lesperance, M.S., at CSCI for his work on the graphical user interface and visualization of results, and Aaron Jacobson, M.A., at CFMRI for assistance in the collection of the data. We especially thank all those who participated in the study for their dedication to advancing Alzheimer's disease research. This work was supported by the National Science Foundation (NSF) Graduate Research Fellowship Program under Grant Nos. DGE-2038238 (SKS) and DGE-1650112 (AJW), and NSF grant ACI-1550405 (LRF and VLG). Any opinions, findings, and conclusions or recommendations expressed in this material are those of the author(s) and do not necessarily reflect the views of the NSF. This work was also supported by NIH awards R01AG054049 (LRF, MWB, and VLG), R01AR070830 (LRF and VLG), and R01HD088437 (LRF), and University of California MPRI award MRP17454755 (LRF and VLG).

Chapter 2, in full, is currently being prepared for submission for publication of the material. Solders, S.K.; Galinsky, V.L; Bondi, M.W.; Frank, L.R. "Tau and amyloid moderate the relationship between locus coeruleus-transentorhinal cortex equilibrium probability and cognition". The dissertation author was the primary researcher and author of this paper.

Figures

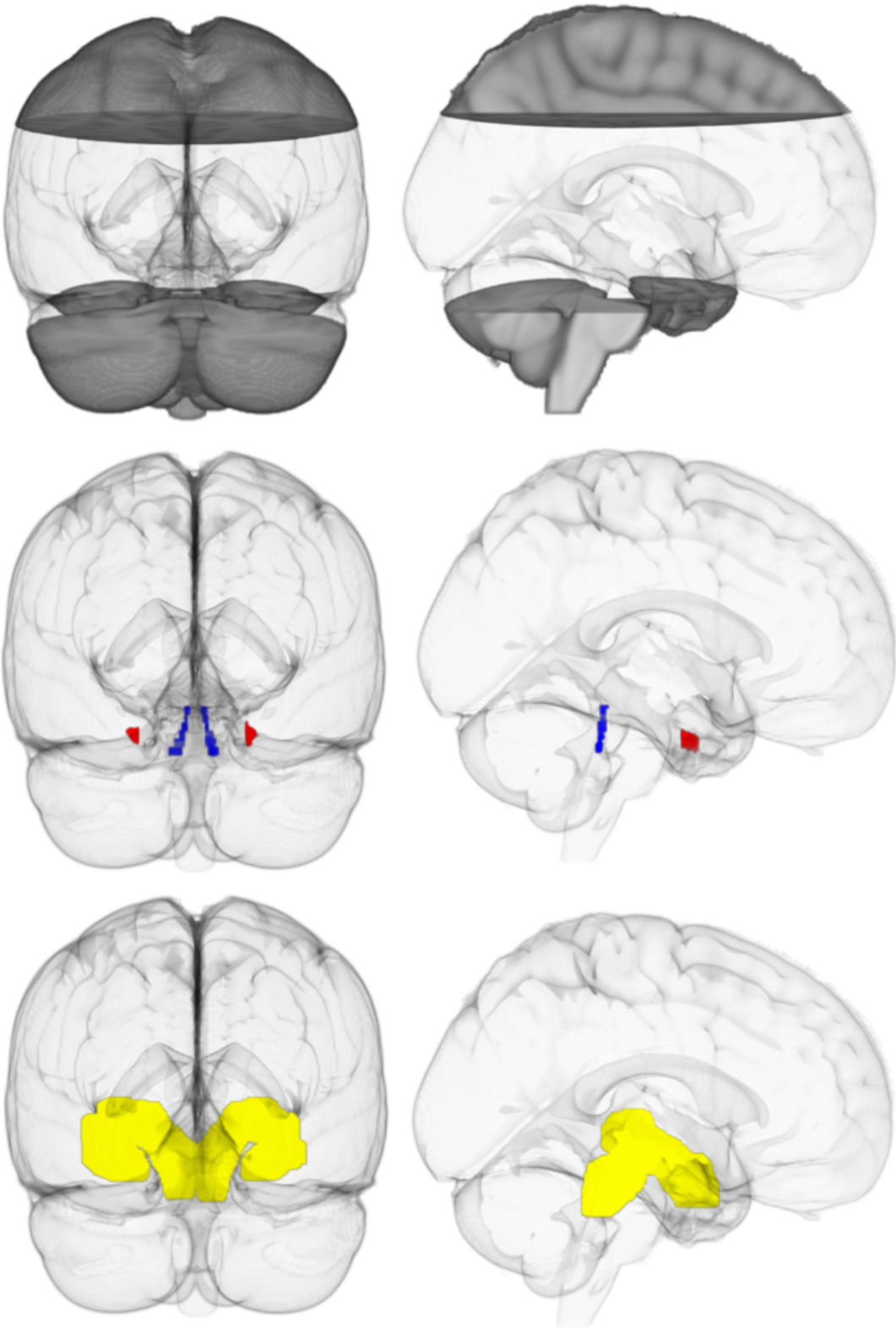

Figure 2.1: Whole-brain tract vs. eigenmode images. Left: Whole-brain tractography tract results. Right: eigenmode of connectivity matrix. Top: View from right side of brain. Middle: Mid-sagittal sections. Bottom: Coronal sections.

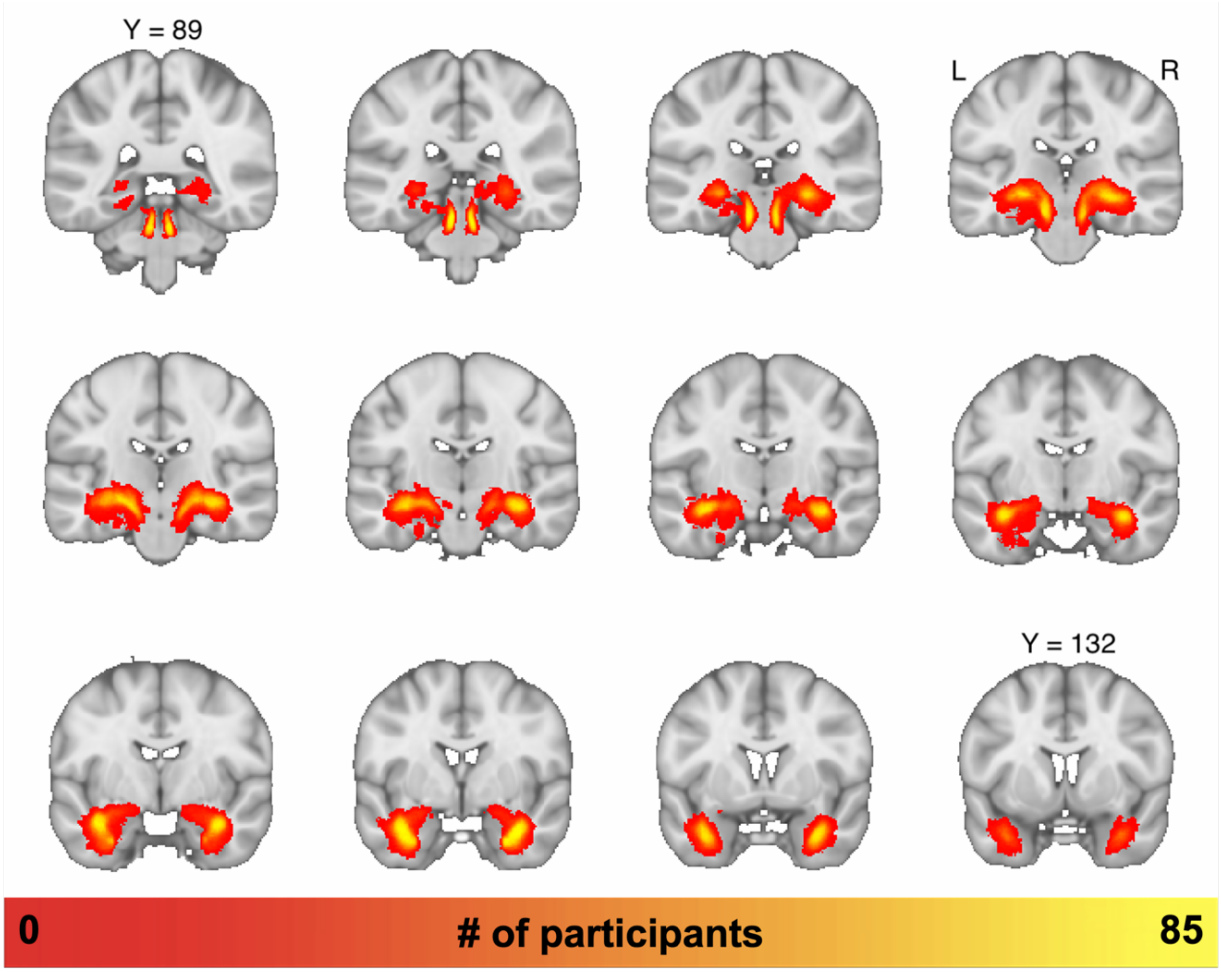

Figure 2.2: Groupwise spatial frequency map of LC-TEC pathway reconstruction. Individual participants' thresholded principle EMIs were registered to MNI space, binarized, and summed. The intensity represents the number of subjects that had output in each respective voxel.

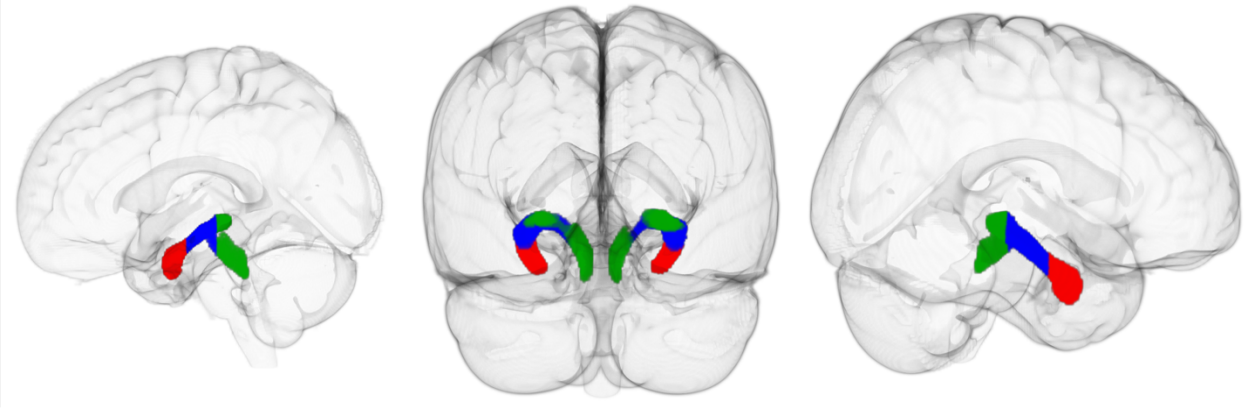

Figure 2.3: LC-TEC segments. A representative LC-TEC pathway was split into three equal segments along its posterior-anterior axis (proximal to LC, middle, and distal to LC). The MNI152-space y-axis coordinates for each segment were as follows: proximal = 87-102; middle = 103-118; distal = 119-132.

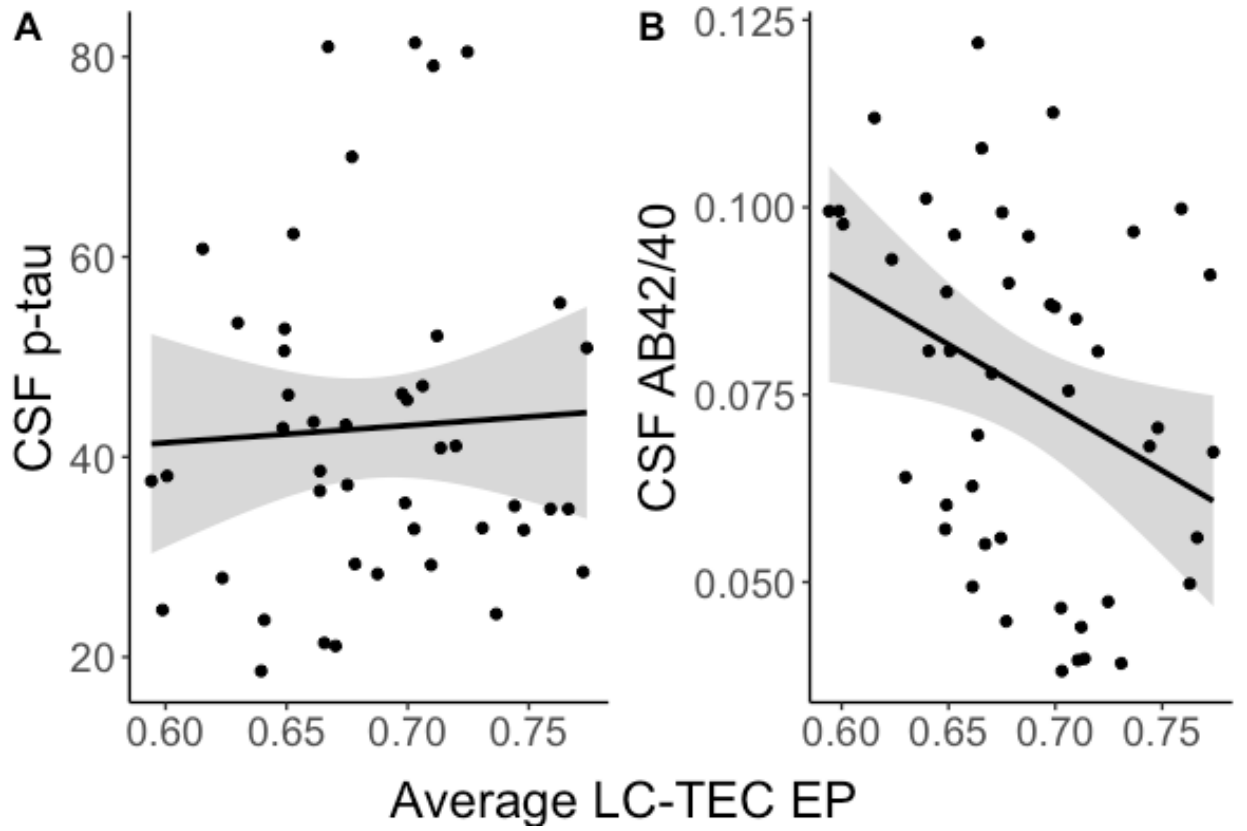

Figure 2.4: EP and CSF associations. Product-moment correlations assessed the relationship between tract EP with CSF p-tau (A) and Aβ4240 (B). The relationship between EP and Aβ4240 was significant.

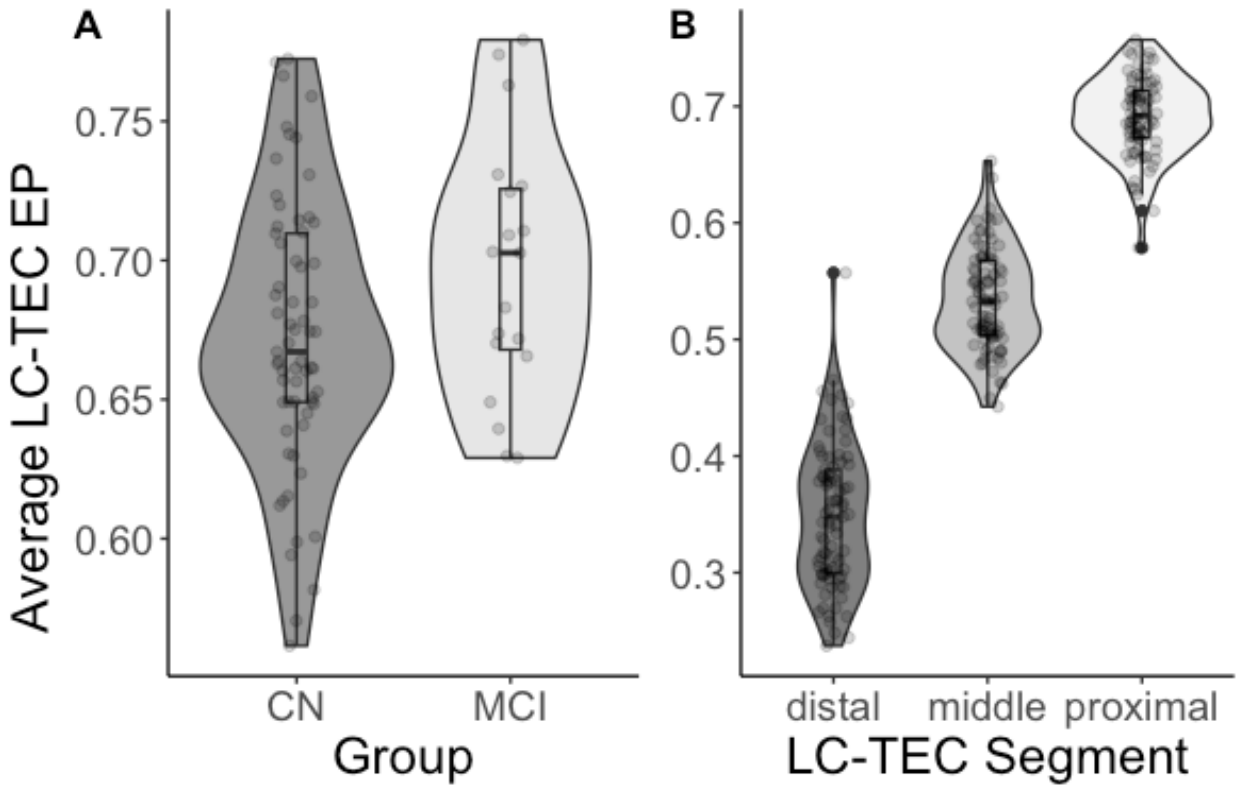

Figure 2.5: EP by group and segment. (A) An analysis of covariance examined average LC-TEC EP as a function of group (CN vs MCI) adjusting for age and sex. A repeated-measures analysis of covariance was conducted to examine average EP as a function of group (CN vs MCI) and tract segment (proximal vs middle vs distal) adjusting for age and sex. MCI participants had greater EP compared to CN participants. Tract EP was significantly higher in the proximal segment compared to middle and distal segment, and was higher in the middle segment compared to the distal segment.

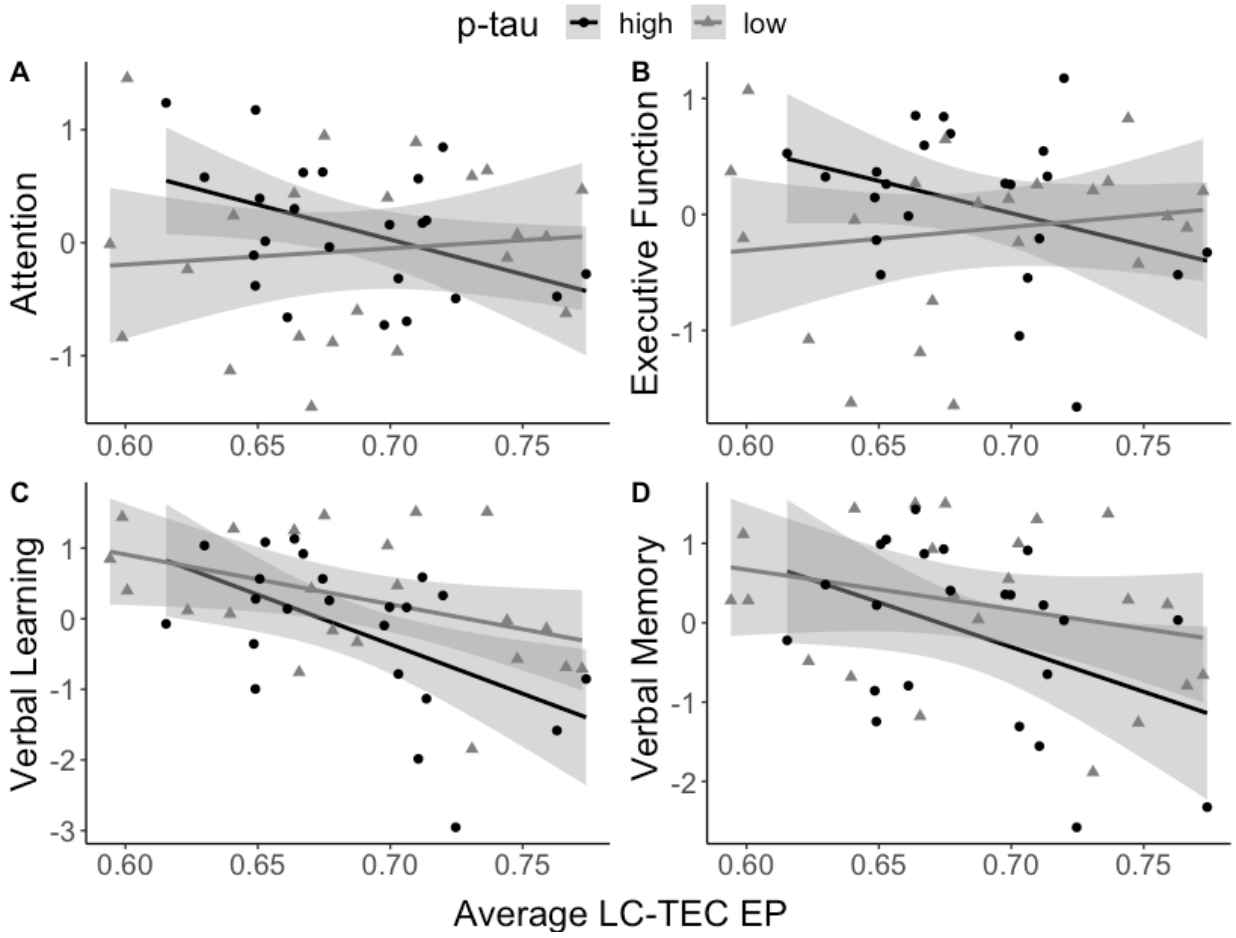

Figure 2.6: Tract EP and cognition relationships in the context of p-tau. Four multiple linear regressions were run predicting each cognitive composite (attention, executive functioning, verbal learning, verbal memory) from age, sex, education, head motion, average LC-TEC EP, CSF p-tau, and the EP by CSF p-tau interaction.

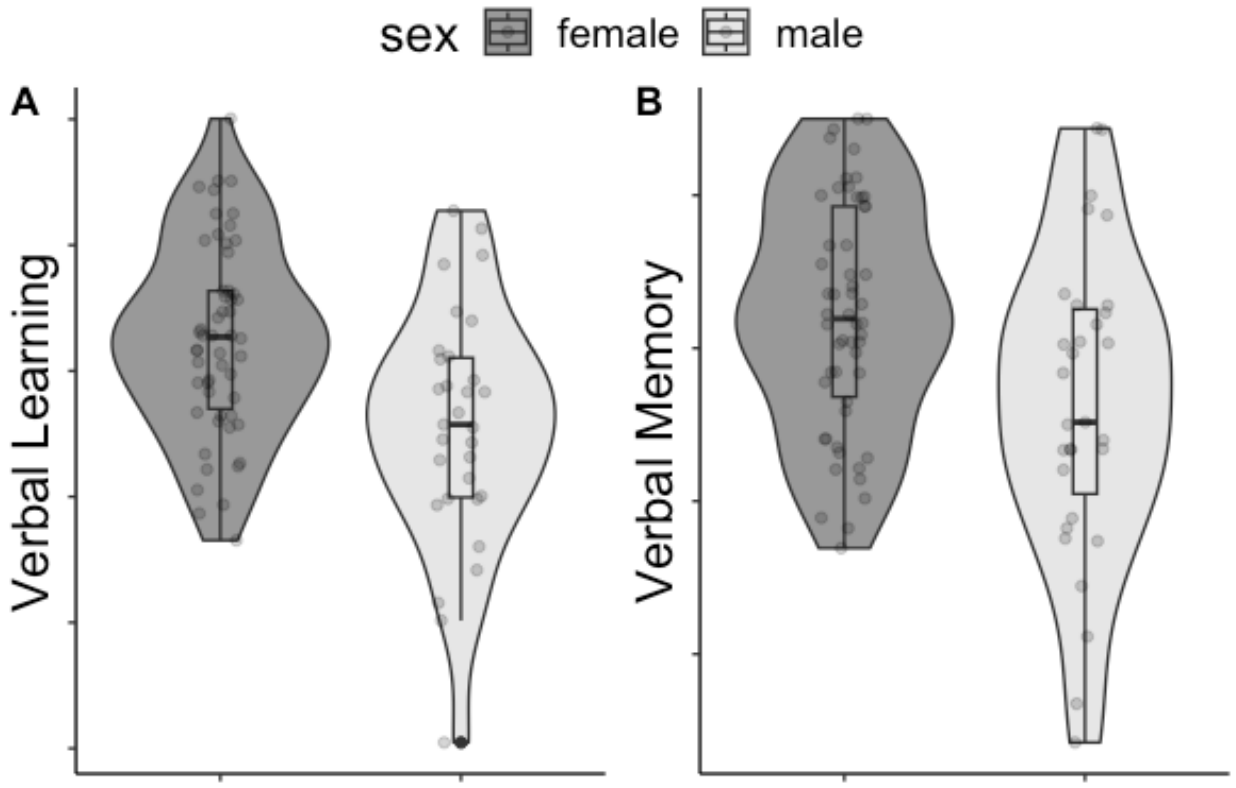

Figure 2.7: Sex differences in verbal learning and memory. Females scored higher than males on average on verbal learning (A) and memory (B).

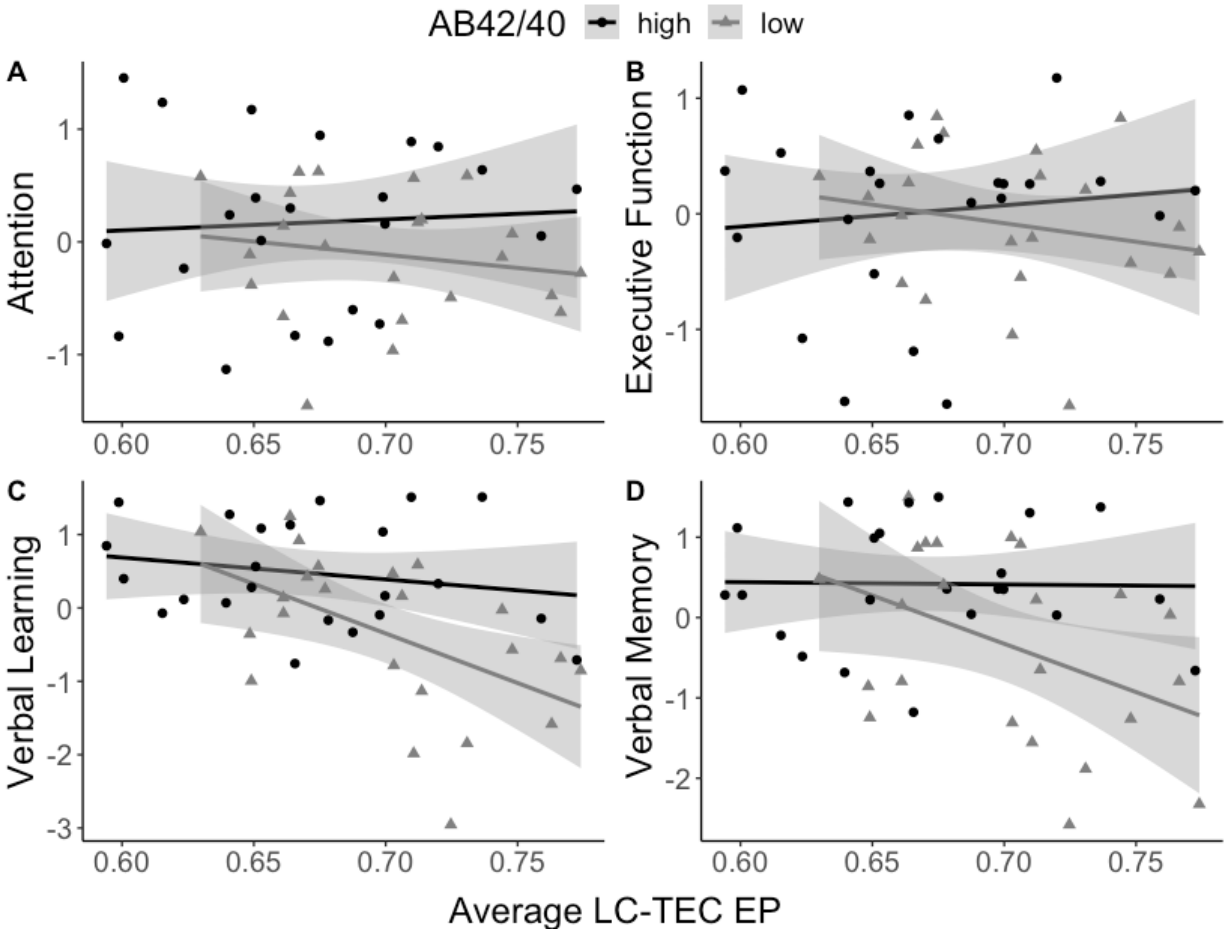

Figure 2.8: Tract EP and cognition relationships in the context of Aβ4240. Four multiple linear regressions were run predicting each cognitive composite (attention, executive functioning, verbal learning, verbal memory) from age, sex, education, head motion, average LC-TEC EP, CSF Aβ4240, and the EP by CSF Aβ4240 interaction.

Tables

Table 2.1: Sample characteristics. Demographic, cognitive, and CSF biomarker measurements.

	CN (n = 66; mean ± SD)	MCI (n = 19; mean ± SD)	p
Age (years)	74.39 ± 5.77	73.68 ± 6.92	0.69
Education (years)	16.39 ± 2.25	16.47 ± 3.29	0.92
MMSE (raw)	28.73 ± 1.52	27.53 ± 2.17	0.03
DRS (raw)	139.3 ± 3.33	136.4 ± 4.50	0.01
	n = 37	**n = 10**	**p**
CSF p-tau	43.56 ± 18.50	47.41 ± 25.72	0.67
CSF AB42/40	0.080 ± 0.021	0.061 ± 0.026	0.92
		n	
Ethnicity	4 Hispanic/Latinx	3 Hispanic/Latinx	
Race	2 Asian, 2 African American, 2 American Indian/Alaska Native, 0 Native Hawaiian/Other Pacific Islander, 58 White, 2 More than one	1 Asian, 0 African American, 1 American Indian/Alaska Native, 0 Native Hawaiian/Other Pacific Islander, 17 White, 2 more than one	

Table 2.2: Regression Results.

LC-TEC Tractography Regression Results
Attention Regression Coefficients

p-tau

	β Estimate	Std. Error	t-value	p-value
(Intercept)	-14.080	5.199	-2.708	0.010
age	0.006	0.018	0.305	0.762
sex	0.093	0.217	0.431	0.669
edu	0.023	0.036	0.640	0.526
head motion	-0.195	0.632	-0.308	0.760
LC-TEC EP	18.852	6.642	2.838	0.007
CSF p-tau	0.359	0.110	3.251	0.002
EP x CSF inter	-0.509	0.160	-3.179	0.003

Aβ42/40

	β Estimate	Std. Error	t-value	p-value
(Intercept)	1.714	7.177	0.239	0.813
age	-0.007	0.020	-0.354	0.725
sex	0.080	0.244	0.328	0.745

Table 2.2: Regression Results (continued).

edu	0.000	0.040	-0.012	0.990
head motion	-0.561	0.710	-0.789	0.435
LC-TEC EP	-1.711	10.250	-0.167	0.868
CSF Aβ42/40	-5.224	84.200	-0.062	0.951
EP x CSF inter	10.760	122.200	0.088	0.930

Executive Functioning Regression Coefficients

p-tau

	β Estimate	Std. Error	t-value	p-value
(Intercept)	-20.413	4.939	-4.133	0.000
age	0.024	0.017	1.383	0.175
sex	0.367	0.206	1.784	0.083
edu	0.067	0.034	1.972	0.056
head motion	-0.223	0.601	-0.371	0.713
LC-TEC EP	25.105	6.310	3.979	0.000
CSF p-tau	0.443	0.105	4.226	0.000
EP x CSF inter	-0.640	0.152	-4.207	0.000

Aβ42/40

	β Estimate	Std. Error	t-value	p-value
(Intercept)	0.977	7.241	0.135	0.893
age	0.009	0.021	0.414	0.682
sex	0.393	0.246	1.599	0.118
edu	0.039	0.040	0.973	0.337
head motion	-0.396	0.717	-0.553	0.584
LC-TEC EP	-3.629	10.344	-0.351	0.728
CSF Aβ42/40	-32.239	84.951	-0.380	0.706
EP x CSF inter	49.401	123.334	0.401	0.691

Verbal Learning Regression Coefficients

p-tau

	β Estimate	Std. Error	t-value	p-value
(Intercept)	-9.032	5.810	-1.554	0.129
age	0.013	0.020	0.622	0.538
sex	0.714	0.242	2.949	0.006
edu	0.107	0.040	2.675	0.011
head motion	-1.576	0.706	-2.230	0.032
LC-TEC EP	10.778	7.422	1.452	0.155
CSF p-tau	0.306	0.123	2.478	0.018
EP x CSF inter	-0.476	0.179	-2.659	0.012

Aβ42/40

Table 2.2: Regression Results (continued).

	β Estimate	Std. Error	t-value	p-value
(Intercept)	18.010	6.967	2.585	0.014
age	-0.003	0.020	-0.165	0.870
sex	0.678	0.237	2.866	0.007
edu	0.111	0.039	2.868	0.007
head motion	-0.742	0.690	-1.075	0.289
LC-TEC EP	-30.320	9.953	-3.047	0.004
CSF Aβ42/40	-195.800	81.740	-2.395	0.022
EP x CSF inter	308.900	118.700	2.603	0.013

Verbal Memory Regression Coefficients

p-tau

	β Estimate	Std. Error	t-value	p-value
(Intercept)	-11.158	7.390	-1.510	0.140
age	0.011	0.026	0.442	0.661
sex	0.632	0.308	2.054	0.047
edu	0.127	0.051	2.506	0.017
head motion	-1.195	0.899	-1.330	0.192
LC-TEC EP	13.179	9.440	1.396	0.171
CSF p-tau	0.313	0.157	1.992	0.054
EP x CSF inter	-0.481	0.228	-2.115	0.041

Aβ42/40

	β Estimate	Std. Error	t-value	p-value
(Intercept)	17.400	8.771	1.983	0.055
age	-0.004	0.025	-0.147	0.884
sex	0.577	0.298	1.936	0.060
edu	0.131	0.049	2.672	0.011
head motion	-0.464	0.868	-0.534	0.596
LC-TEC EP	-29.710	12.530	-2.371	0.023
CSF Aβ42/40	-207.500	102.900	-2.017	0.051
EP x CSF inter	323.500	149.400	2.165	0.037

References

1. International, A. s. D. (2019). *World Alzheimer's Report 2019: Attitudes to Dementia* (Alzheimer's Disease International: London, Issue.

2. Bondareff, W., Mountjoy, C., & Roth, M. (1982). Loss of neurons of origin of the adrenergic projection to cerebral cortex (nucleus locus ceruleus) in senile dementia. *Neurology*, *32*(2), 164-168. https://doi.org/https://doi.org/10.1212/wnl.32.2.164

3. Mann, D., Yates, P., & Hawkes, J. (1982). The noradrenergic system in Alzheimer and multi-infarct dementias. *Journal of Neurology Neurosurgery and Psychiatry*, *45*(2), 113-119. https://doi.org/https://doi.org/10.1136/jnnp.45.2.113

4. Tomlinson, B., Irving, D., & Blessed, G. (1981). Cell loss in the locus coeruleus in senile dementia of Alzheimer type. *Journal of the Neurological Sciences*, *49*(3), 419-428. https://doi.org/10.1016/0022-510x(81)90031-9

5. Andrés-Benito, P., Fernández-Dueñas, V., Carmona, M., Escobar, L., Torrejón-Escribano, B., Aso, E., Ciruela, F., & Ferrer, I. (2017). Locus coeruleus at asymptomatic early and middle Braak stages of neurofibrillary tangle pathology. *Neuropathology and Applied Neurobiology*, *43*(5), 373-392. https://doi.org/10.1111/nan.12386

6. Braak, H., Thal, D., Ghebremedhin, E., & Tredici, K. (2011). Stages of the pathologic process in Alzheimer disease: age categories from 1 to 100 years. *Journal of Neuropathology and Experimental Neurology*, *70*(11), 960-969. https://doi.org/10.1097/NEN.0b013e318232a379

7. Grudzien, A., Shaw, P., Weintraub, S., Bigio, E., Mash, D., & Mesulam, M. (2007). Locus coeruleus neurofibrillary degeneration in aging, mild cognitive impairment and early Alzheimer's disease. *Neurobiology of Aging*, *28*(3), 327-335. https://doi.org/10.1016/j.neurobiolaging.2006.02.007

8. Ehrenberg, A., Nguy, A., Theofilas, P., Dunlop, S., Suemoto, C., Di Lorenzo Alho, A., Leite, R., Diehl Rodriguez, R., Mejia, M., Rüb, U., Farfel, J., de Lucena Ferretti-Rebustini, R., Nascimento, C., Nitrini, R., Pasquallucci, C., Jacob-Filho, W., Miller, B., Seeley, W., Heinsen, H., & Grinberg, L. (2017). Quantifying the accretion of hyperphosphorylated tau in the locus coeruleus and dorsal raphe nucleus: the pathological building blocks of early Alzheimer's disease. *Neuropathology and Applied Neurobiology*, *43*(5), 393-408. https://doi.org/10.1111/nan.12387

9. Theofilas, P., Ehrenberg, A., Dunlop, S., Di Lorenzo Alho, A., Nguy, A., Leite, R., Rodriguez, R., Mejia, M., Suemoto, C., Ferretti-Rebustini, R., Polichiso, L., Nascimento, C., Seeley, W., Nitrini, R., Pasquallucci, C., Filho, W., Rueb, U., Neuhaus, J., Heinsen, H., & Grinberg, L. (2017). Locus coeruleus volume and cell population changes during Alzheimer's disease progression: A stereological study in human postmortem brains with potential implication for early-stage biomarker discovery. *Alzheimer's & Dementia*, *13*(3), 236-246. https://doi.org/10.1016/j.jalz.2016.06.2362

10. Assal, F., & Cummings, J. (2002). Neuropsychiatric symptoms in the dementias. *Current Opinion in Neurology*, *15*(4), 445-450. https://doi.org/10.1097/00019052-200208000-00007

11. Ehrenberg, A., Suemoto, C., França Resende, E., Petersen, C., Leite, R., Rodriguez, R., Ferretti-Rebustini, R., You, M., Oh, J., Nitrini, R., Pasquallucci, C., Jacob-Filho, W., Kramer, J., Gatchel, J., & Grinberg, L. (2018). Neuropathologic Correlates of Psychiatric Symptoms in Alzheimer's Disease. *Journal of Alzheimer's Disease*, *66*(1), 115-126. https://doi.org/10.3233/JAD-180688

12. Lanctôt, K., Amatniek, J., Ancoli-Israel, S., Arnold, S., Ballard, C., Cohen-Mansfield, J., Ismail, Z., Lyketsos, C., Miller, D., Musiek, E., Osorio, R., Rosenberg, P., Satlin, A., Steffens, D., Tariot, P., Bain, L., Carrillo, M., Hendrix, J., Jurgens, H., & Boot, B. (2017). Neuropsychiatric signs and symptoms of Alzheimer's disease: New treatment paradigms. *Alzheimer's & Dementia*, *3*(3), 440-449. https://doi.org/10.1016/j.trci.2017.07.001

13. Bell, T. R., Elman, J. A., Beck, A., Fennema-Notestine, C., Gustavson, D. E., Hagler, D. J., Jack, A. J., Lyons, M. J., Puckett, O. K., Toomey, R., Franz, C. E., & Kremen, W. S. (2022). Rostral-middle locus coeruleus integrity and subjective cognitive decline in early old age. *J Int Neuropsychol Soc*, 1-12. https://doi.org/10.1017/S1355617722000881

14. Jacobs, H. I. L., Becker, J. A., Kwong, K., Engels-Domínguez, N., Prokopiou, P. C., Papp, K. V., Properzi, M., Hampton, O. L., Uquillas, F. d. O., Sanchez, J. S., Rentz, D. M., Fakhri, G. E., Normandin, M. D., Price, J. C., Bennett, D. A., Sperling, R. A., & Johnson, K. A. (2021). In vivo and neuropathology data support locus coeruleus integrity as indicator of Alzheimer's disease pathology and cognitive decline. *Science Translational Medicine*, *13*(612), eabj2511. https://doi.org/10.1126/scitranslmed.abj2511

15. Elman, J. A., Puckett, O. K., Beck, A., Fennema-Notestine, C., Cross, L. K., Dale, A. M., Eglit, G. M. L., Eyler, L. T., Gillespie, N. A., Granholm, E. L., Gustavson, D. E., Hagler, D. J., Jr., Hatton, S. N., Hauger, R., Jak, A. J., Logue, M. W., McEvoy, L. K., McKenzie, R. E., Neale, M. C., Panizzon, M. S., Reynolds, C. A., Sanderson-Cimino, M., Toomey, R., Tu, X. M., Whitsel, N., Williams, M. E., Xian, H., Lyons, M. J., Franz, C. E., & Kremen, W. S. (2021). MRI-assessed locus coeruleus integrity is heritable and associated with multiple cognitive domains, mild cognitive impairment, and daytime dysfunction. *Alzheimers Dement*, *17*(6), 1017-1025. https://doi.org/10.1002/alz.12261

16. Liu, K. Y., Acosta-Cabronero, J., Cardenas-Blanco, A., Loane, C., Berry, A. J., Betts, M. J., Kievit, R. A., Henson, R. N., Duzel, E., Cam, C. A. N., Howard, R., & Hammerer, D. (2019). In vivo visualization of age-related differences in the locus coeruleus. *Neurobiol Aging*, *74*, 101-111. https://doi.org/10.1016/j.neurobiolaging.2018.10.014

17. Dahl, M. J., Mather, M., Düzel, S., Bodammer, N. C., Lindenberger, U., Kühn, S., & Werkle-Bergner, M. (2019). Rostral locus coeruleus integrity is associated with better memory performance in older adults. *Nature Human Behavior*, *3*(11), 1203-1214. https://doi.org/10.1038/s41562-019-0715-2

18. Betts, M. J., Cardenas-Blanco, A., Kanowski, M., Spottke, A., Teipel, S. J., Kilimann, I., Jessen, F., & Düzel, E. (2019). Locus coeruleus MRI contrast is reduced in Alzheimer's disease dementia and correlates with CSF Aβ levels. *Alzheimer's & Dementia (Amsterdam, Netherlands)*, *11*, 281-285. https://doi.org/10.1016/j.dadm.2019.02.001

19. Hämmerer, D., Callaghan, M. F., Hopkins, A., Kosciessa, J., Betts, M., Cardenas-Blanco, A., Kanowski, M., Weiskopf, N., Dayan, P., Dolan, R. J., & Düzel, E. (2018). Locus coeruleus integrity in old age is selectively related to memories linked with salient negative events. *Proceedings of the National Academy of Sciences of the United States of America*, *115*(9), 2228-2233. https://doi.org/10.1073/pnas.1712268115

20. Clewett, D. V., Lee, T.-H., Greening, S., Ponzio, A., Margalit, E., & Mather, M. (2016). Neuromelanin marks the spot: identifying a locus coeruleus biomarker of cognitive reserve in healthy aging. *Neurobiology of Aging*, *37*, 117-126. https://doi.org/10.1016/j.neurobiolaging.2015.09.019

21. Betts, M. J., Cardenas-Blanco, A., Kanowski, M., Jessen, F., & Duzel, E. (2017). In vivo MRI assessment of the human locus coeruleus along its rostrocaudal extent in young and older adults. *NeuroImage*, *163*, 150-159. https://doi.org/10.1016/j.neuroimage.2017.09.042

22. Braak, H., & Del Tredici, K. (2015). The preclinical phase of the pathological process underlying sporadic Alzheimer's disease. *Brain*, *138*(Pt 10), 2814-2833. https://doi.org/10.1093/brain/awv236

23. Braak, H., & Braak, E. (1991). Neuropathological stageing of Alzheimer-related changes. *Acta Neuropathol*, *82*(4), 239-259. https://doi.org/10.1007/BF00308809

24. Solders, S., Galinsky, V., Clark, A., Sorg, S., Weigand, A., Bondi, M., & Frank, L. (2022). Diffusion MRI tractography of the locus coeruleus-transentorhinal cortex connections using GO-ESP. *Magnetic Resonance in Medicine*, *87*(4), 1816-1831. https://doi.org/10.1002/mrm.29088

25. Galinsky, V., & Frank, L. (2015). Simultaneous multi-scale diffusion estimation and tractography guided by entropy spectrum pathways. *IEEE Transactions on Medical Imaging*, *34*(5), 1177-1193. https://doi.org/10.1109/TMI.2014.2380812

26. Petersen, R. C., Smith, G. E., Waring, S. C., Ivnik, R. J., Tangalos, E. G., & Kokmen, E. (1999). Mild cognitive impairment: clinical characterization and outcome. *Arch Neurol*, *56*(3), 303-308. https://doi.org/10.1001/archneur.56.3.303

27. Chapman, S., & Michaelson, D. (1998). Specific neurochemical derangements of brain projecting neurons in apolipoprotein E-deficient mice. *J Neurochem*, *70*, 708-714.

28. Jak, A., Bondi, M., Delano-Wood, L., Wierenga, C., Corey-Bloom, J., Salmon, D., & Delis, D. (2009). Quantification of five neuropsychological approaches to defining mild cognitive impairment. *The American Journal of Geriatric Psychiatry*, *17*(5), 368-375. https://doi.org/10.1097/JGP.0b013e31819431d5

29. Bondi, M., Edmonds, E., Jack, A., Clark, L., Delano-Wood, L., McDonald, C., Nation, D., Libon, D., Au, R., Galasko, D., & Salmon, D. (2014). Neuropsychological criteria for mild cognitive impairment improves diagnostic precision, biomarker associations, and progression rates. *Journal of Alzheimer's Disease*, *42*(1), 275-289. https://doi.org/10.3233/JAD-140276

30. Bondi, M. W., & Smith, G. E. (2014). Mild cognitive impairment: a concept and diagnostic entity in need of input from neuropsychology. *Journal of the International Neuropsychological Society*, *20*(2), 129-134. https://doi.org/10.1017/S1355617714000010

31. Clark, L. R., Delano-Wood, L., Libon, D. J., McDonald, C. R., Nation, D. A., Bangen, K. J., Jak, A. J., Au, R., Salmon, D. P., & Bondi, M. W. (2013). Are empirically-derived subtypes of mild cognitive impairment consistent with conventional subtypes? *Journal of the International Neuropsychological Society*, *19*(6), 635-645. https://doi.org/10.1017/S1355617713000313

32. Jak, A. J., Urban, S., McCauley, A., Bangen, K. J., Delano-Wood, L., Corey-Bloom, J., & Bondi, M. W. (2009). Profile of hippocampal volumes and stroke risk varies by neuropsychological definition of mild cognitive impairment. *Journal of the International Neuropsychological Society*, *15*(6), 890-897. https://doi.org/10.1017/S1355617709090638

33. Xiao, M., Xu, D., Craig, M., Pelkey, K., Chien, C., Shi, Y., Zhang, J., Resnick, S., Pletnikova, O., Salmon, D., Brewer, J., Edland, S., Wegiel, J., Tycko, B., Savonenko, A., Reeves, R., Troncoso, J., McBain, C., Galasko, D., & Worley, P. (2017). NPTX2 and cognitive dysfunction in Alzheimer's Disease. *eLife*, *6*. https://doi.org/10.7554/eLife.23798

34. Vanderstichele, H., Bibl, M., Engelborghs, S., Le Bastard, N., Lewczuk, P., Molinuevo, J., Parnetti, L., Perret-Liaudet, A., Shaw, L., Teunissen, C., Wouters, D., & Blennow, K. (2012). Standardization of preanalytical aspects of cerebrospinal fluid biomarker testing for Alzheimer's disease diagnosis: a consensus paper from the Alzheimer's Biomarkers Standardization Initiative. *Alzheimer's & Dementia*, *8*(1), 65-73. https://doi.org/10.1016/j.jalz.2011.07.004

35. Kaplow, J., Vandijck, M., Gray, J., Kanekiyo, M., Huyck, E., Traynham, C., Esquivel, R., Fagan, A., & Luthman, J. (2020). Concordance of Lumipulse cerebrospinal fluid t-tau/Aβ42 ratio with amyloid PET status. *Alzheimer's & Dementia*, *16*(1), 144-152. https://doi.org/10.1002/alz.12000

36. Lleó, A., Alcolea, D., Martínez-Lage, P., Scheltens, P., Parnetti, L., Poirier, J., Simonsen, A. H., Verbeek, M. M., Rosa-Neto, P., Slot, R. E. R., Tainta, M., Izaguirre, A., Reijs, B. L. R., Farotti, L., Tsolaki, M., Vandenbergue, R., Freund-Levi, Y., Verhey, F. R. J., Clarimón, J., Fortea, J., Frolich, L., Santana, I., Molinuevo, J. L., Lehmann, S., Visser, P. J., Teunissen, C. E., Zetterberg, H., & Blennow, K. (2019). Longitudinal cerebrospinal fluid biomarker trajectories along the Alzheimer's disease continuum in the BIOMARKAPD study. *Alzhemer's & Dementia*, *15*(6), 742-753. https://doi.org/10.1016/j.jalz.2019.01.015

37. Grundke-Iqbal, I., Iqbal, K., Tung, Y. C., Quinlan, M., Wisniewski, H. M., & Binder, L. I. (1986). Abnormal phosphorylation of the microtubule-associated protein tau (tau) in Alzheimer cytoskeletal pathology. *Proc Natl Acad Sci U S A*, *83*(13), 4913-4917. https://doi.org/10.1073/pnas.83.13.4913

38. Blennow, K., Wallin, A., Agren, H., Spenger, C., Siegfried, J., & Vanmechelen, E. (1995). Tau protein in cerebrospinal fluid: a biochemical marker for axonal degeneration in Alzheimer disease? *Mol Chem Neuropathol*, *26*(3), 231-245. https://doi.org/10.1007/BF02815140

39. Hansson, O., Lehmann, S., Otto, M., Zetterberg, H., & Lewczuk, P. (2019). Advantages and disadvantages of the use of the CSF Amyloid beta (Abeta) 42/40 ratio in the diagnosis of Alzheimer's Disease. *Alzheimers Res Ther*, *11*(1), 34. https://doi.org/10.1186/s13195-019-0485-0

40. Zahneisen, B., Aksoy, M., Maclaren, J., Wuerslin, C., & Bammer, R. (2017). Extended hybrid-space SENSE for EPI: Off-resonance and eddy current corrected joint interleaved blip-up/down reconstruction. *NeuroImage*, *153*, 97-108. https://doi.org/10.1016/j.neuroimage.2017.03.052

41. Andersson, J. L. R., Skare, S., & Ashburner, J. (2003). How to correct susceptibility distortions in spin-echo echo-planar images: application to diffusion tensor imaging. *NeuroImage*, *20*(2), 870-888. https://doi.org/10.1016/S1053-8119(03)00336-7

42. Smith, S. M., Jenkinson, M., Woolrich, M. W., Beckmann, C. F., Behrens, T. E. J., Johansen-Berg, H., Bannister, P. R., Luca, M. D., Drobnjak, I., Flitney, D. E., Niazy, R. K., Saunders, J., Vickers, J., Zhang, Y., Stefano, N. D., Brady, M., & Matthews, P. M. (2004). Advances in functional and structural MR image analysis and implementation as FSL. *NeuroImage*, *23*, S208-S219. https://doi.org/https://doi.org/10.1016/j.neuroimage.2004.07.051

43. Andersson, J. L. R., & Sotiropoulos, S. N. (2016). An integrated approach to correction for off-resonance effects and subject movement in diffusion MR imaging. *NeuroImage*, *125*, 1063-1078. https://doi.org/https://doi.org/10.1016/j.neuroimage.2015.10.019

44. Smith, S. M. (2002). Fast robust automated brain extraction. *Human Brain Mapping*, *17*(3), 143-155. https://doi.org/https://doi.org/10.1002/hbm.10062

45. Galinsky, V. L., & Frank, L. R. (2019). Symplectomorphic registration with phase space regularization by entropy spectrum pathways. *Magnetic Resonance in Medicine*, *81*(2), 1335-1352. https://doi.org/https://doi.org/10.1002/mrm.27402

46. Frank, L. R., & Galinsky, V. L. (2014). Information pathways in a disordered lattice. *Phys Rev E Stat Nonlin Soft Matter Phys*, *89*(3), 032142. https://doi.org/10.1103/PhysRevE.89.032142

47. Keren, N. I., Lozar, C. T., Harris, K. C., Morgan, P. S., & Eckert, M. A. (2009). In vivo mapping of the human locus coeruleus. *NeuroImage*, *47*(4), 1261-1267. https://doi.org/10.1016/j.neuroimage.2009.06.012

48. Jones, D. K., Knosche, T. R., & Turner, R. (2013). White matter integrity, fiber count, and other fallacies: the do's and don'ts of diffusion MRI. *NeuroImage*, *73*, 239-254. https://doi.org/10.1016/j.neuroimage.2012.06.081

49. Sun, W., Tang, Y., Qiao, Y., Ge, X., Mather, M., Ringman, J. M., Shi, Y., & for Alzheimer's Disease Neuroimaging, I. (2020). A probabilistic atlas of locus coeruleus pathways to transentorhinal cortex for connectome imaging in Alzheimer's disease. *NeuroImage*, *223*, 117301. https://doi.org/10.1016/j.neuroimage.2020.117301

50. Manger, P. R., & Eschenko, O. (2021). The Mammalian Locus Coeruleus Complex-Consistencies and Variances in Nuclear Organization. *Brain Sci*, *11*(11). https://doi.org/10.3390/brainsci11111486

3. Tau moderates the relationship between locus coeruleus MR signal and cognition

Abstract

The locus coeruleus (LC) is one of the earliest sites of tau pathogenesis in Alzheimer's disease (AD). Studies using LC-sensitive magnetic resonance imaging (MRI) have shown that AD patients have reduced relative LC signal compared to their cognitively normal peers, but findings conflict on whether changes are detectable in the mild cognitive impairment (MCI) stage. Further, little is understood about the relationship between MR LC signal and cognition in the context of AD risk as measured by cerebrospinal fluid markers of tau and amyloid. In this study, we use LC-sensitive MRI in a sample of older adults with and without MCI. We do not find a significant group difference between MCI and control participants. Further, we find that p-tau but not amyloid moderates the relationship between LC signal and cognition, whereby only those with low p-tau (indicative of lower tau neuropathology) show a positive association between LC signal and cognition. Our results support the notion that the impact of LC integrity on cognition is driven by tauopathy, but also point to a more complex relationship between LC signal and cognition whereby at greater levels of tau pathology, there are other factors contributing to the association that are unaccounted for here.

Introduction

The locus coeruleus (LC) is a small but mighty brainstem nucleus serving as the primary source of norepinephrine/noradrenaline to the brain. While the LC itself is tiny, comprising about 50,000 neurons in the adult human, it projects extensively throughout the neuraxis and displays massive arborization of individual axons, whose collaterals seem to be distributed in a modular fashion to functionally related target areas throughout the brain (see (1) for a recent review). The LC-noradrenergic system is critical for healthy neural functioning (2) and plays a central role in

shaping whole-brain neural dynamics (3) that support various cognitive functions including attention, stress responses, and learning and memory (4-6). Prior studies have shown an age-related decline in the LC-noradrenergic system associated with reduced cognition relating to episodic memory (7-9) and reduced cognitive reserve (10-12).

It's been known for decades that degeneration of neurons within the LC is a ubiquitous feature of Alzheimer's Disease (AD) (13-15), the most common form of dementia. This may account for some of the early behavioral impairments we see in AD patients involving the sleep-wake cycle, agitation, attention, appetite, anxiety, and depression (16-18). Recent histochemistry (19-21) and unbiased stereology (22,23) studies have suggested that nonfibrillar abnormal tau in the LC may be one of the earliest detectable signs of AD-like neuropathology. In particular, Chan-Palay and Asan (24) used quantitative computer recordings of tyrosine hydroxylase-immunoreactive neurons to demonstrate a rostro-caudal gradient of neuron loss in AD, whereby the rostral and middle portions of the nucleus degenerate but the caudal portion is relatively spared. This pattern has been confirmed in later postmortem reports (23,25). The LC might be vulnerable because of its high metabolic needs or proximity to 4th ventricle, exposing it to cerebrospinal fluid (CSF) toxins (12,26).

Neuroimaging advances allow us to visualize and characterize the LC in vivo using magnetic resonance imaging (MRI) (27-30), and recent studies suggest the possibility of using in vivo measurements of relative LC signal as markers for AD progression (31-35). Studies generally agree that AD patients show reduced LC signal contrast in comparison with cognitively normal (CN) older adults, but reports differ on whether changes are detectable in the mild cognitive impairment (MCI) stage (31,32,34,35). Betts et al. (31) used LC-sensitive MRI to corroborate the rostro-caudal pattern shown by Chan-Palay and Asan (24) and others (23,25),

whereby LC signal reduction in AD participants was restricted to the rostral and middle portion of the nucleus. Further, they report a negative association between LC signal and CSF amyloid but not with CSF tau. This finding is surprising in two ways: first, if LC signal is a marker of nucleus integrity, then we would expect to see a positive association whereby higher LC signal would correspond with higher CSF amyloid (indicating lower levels of amyloid being sequestered and deposited into plaques in the brain); second, if LC degeneration in early AD is a portent of tau pathogenesis, we might expect to see an association between greater LC signal and lower CSF tau (indicating lower levels of degeneration and thereby less leakage of tau out of dying neurons and into the CSF). Further, using tau and amyloid positron emission tomography, Jacobs et al. (36) showed that LC signal was associated with tau at higher levels of amyloid, suggesting a more complex relationship. There is a lack of clarity on the association between MR derived LC signal and putative measures of in vivo amyloid and tau neuropathology.

Importantly, it remains unclear how in vivo measurements of LC signal relate to cognition in the context of these AD-related CSF markers. Indeed, we are still learning how MR-derived LC signal relates to variability in cognition in healthy older adults or those in the pre-clinical phase of AD. This study aims to characterize variation in MR-assessed LC signal contrast in a sample of older adults with and without MCI. Due to the discrepant findings in terms of detectable changes in the MCI stage, we did not expect to see a meaningfully reduced signal in the MCI group compared to CN participants. Across all participants, we hypothesized that reduced LC signal contrast, particularly in the rostral and middle segments of the nucleus, would be associated with increased AD-related cognitive and biomarker (especially tau) positivity.

Methods

Participants

Participants were recruited mainly from the University of California, San Diego (UCSD) Alzheimer's Disease Research Center, which is funded by the National Institute on Aging to conduct longitudinal studies on older adults. Additional participants were recruited from the community in San Diego, California. Referrals came from participants enrolled in past studies, flyers, VA Neuropsychological Assessment Unit, and Research Match where they are screened for eligibility. This study was approved by the UCSD Institutional Review Board, and written informed consent was obtained from all participants upon enrollment.

A total of 124 participants (age range: 62-85 years, average age of 74.46 years, 58% women) were recruited, and 23 were excluded from all analyses: 1 subject was unable to receive a diagnosis due to incomplete neuropsychological data; 1 participant was unable to complete MRI scanning due to a stent that was not reported during phone screening; 1 participant had an incidental finding on MRI; 1 participant had an error in MRI acquisition that resulted in unusable data; and 8 were excluded due to excessive head motion during MRI scanning. Further, our data collection was restricted due to the COVID-19 pandemic, and we only enrolled 11 participants with AD, 2 of which were unable to complete scanning due to anxiety upon entering the scanner bore. We therefore excluded them from analyses due to lack of statistical power in such a small sample. Our final example consisted of 101 participants.

MRI acquisition and quality assessment

Scanning was performed on a 3 Tesla GE Discovery MR750 scanner at the UCSD Functional MRI Center using a 32-channel head coil (Nova Medical). Imaging parameters were: scan matrix of 512 × 512 voxels, field of view (FOV) = 220 mm × 220 mm × 24 mm (0.42972

in-plane resolution with eight 3mm-thick axial slices with no gaps), echo time (TE) = 21 msec, repetition time (TR) = 500 msec, flip angle = 125°. For each participant, we used a para-midsagittal slice of a survey scan to align the LC acquisition volume in a consistent manner. Images were acquired perpendicular to the floor of the fourth ventricle, with the third slice placed just below the inferior colliculus. The duration of the T1-FSE scan was approximately 11 min. Quality control consisted of visual inspection for image noise and movement artifacts. Eight scans were excluded due to excessive movement artifact as mentioned previously under "Participants".

Cognitive testing and diagnostic classification of MCI

Participants completed a comprehensive neuropsychological test battery including sensitive measures of memory (California Verbal Learning Test-II, WMS-R Visual Reproduction Test with delayed recall and recognition, WMS-R Logical Memory with delayed recall and recognition, Benson Complex Figure Copy), attention (WAIS-R Digit Span), language (Multilingual Naming Test, and Letter and Category Fluency Tests), problem solving and executive function (modified Wisconsin Card Sort Test, Trail-Making Test Parts A and B, Digit Symbol Substitution Test, Fluency Switching and Color-Word Interference subtests of the Delis-Kaplan Executive Functioning System [DKEFS]), constructional and visuospatial abilities (WASI-II Block Design Test, Clock Drawing Test, D-KEFS Visual Scanning), and global cognition (Mattis Dementia Rating Scale [DRS], Mini Mental State Examination [MMSE]).

We define MCI as having scores below one standard deviation of the norms on two or more tests within one or more cognitive domains (37,38). This actuarial diagnostic approach was developed to improve rigor and sensitivity and has been shown to assign MCI classifications that are less prone to false positive errors and more related to AD biomarkers (39-41).

The final sample after all exclusion criteria were applied included 77 CN older adults, 15 with amnestic MCI (9 multi-domain, 6 single-domain), 9 non-amnestic MCI (4 multi-domain, 5 single-domain). Single-domain non-amnestic MCI participants were included in the CN group due to the instability of the single-domain MCI diagnosis (37). Thus, our final groups consisted of 82 CN and 19 CI participants.

To examine associations between LC CRs and cognition, cognitive composites were created by taking the average of the z-scores for attention (Digit Symbol raw total, Digit Span forward total, Trails A seconds), executive function (Digit Span backward total, Trails B seconds, and DKEFS Color-Word Inhibition Switching seconds), verbal learning (CVLT List A 1-5 total and Logical Memory 1), and verbal memory (CVLT Long Free Recall and Logical Memory 2).

CSF biomarker assessment

A subset of our participants (after other exclusion criteria applied; n = 74 underwent lumbar punctures as part of participation in the UCSD Alzheimer's Disease Research Center with standardization of procedures, preanalytical preparation, and storage of CSF as previously described (42), and in accordance with recommended best practices (43). In brief, CSF (15–25 mL) was collected by routine lumbar puncture early in the morning after overnight fasting. Samples were processed, aliquoted into 500 µL fractions in polypropylene microtubes, snap frozen, and stored at −80°C until assayed. All samples were analyzed locally using the automated Lumipulse platform using assays developed with established monoclonal antibodies (Fujirebio Inc) (44). The majority of lumbar punctures were conducted within one year of the MRI visit (n = 26), although we included data collected within two (n = 17), three (n = 6), and four (n = 11) years of the visit given research showing the stability of CSF biomarkers over

several years (45) in an effort to maximize our sample size. Fourteen samples were excluded from analyses for being collected over 4 years from MRI scanning and cognitive testing, resulting in a final sample of 60 CSF measurements. We obtained CSF measures of Aβ40, Aβ42, total tau, and phosphorylated tau (p-tau. We used p-tau for analyses as previous research has suggested p-tau to be a more specific biomarker for AD (46) whereas total tau may be a marker of neurodegeneration in general (47). Further, we used the Aβ42/40 ratio which has been shown to perform better at identifying AD patients compared to AB42 alone (48).

LC CR calculation

To measure LC-related signal intensity, bilateral LC regions of interest (ROIs) were hand drawn on each participant's T1-FSE scan using FSLVIEW (FSL version 6.0.0, http://fsl.fmrib.ox.ac.uk/fsl/fslwiki/) (49). LC ROIs were drawn on three consecutive slices to extract signal information from the rostral, middle, and caudal divisions of the nucleus. Middle LC ROIs were marked using the methods detailed by (50). Briefly, an axial slice approximately 6-9 mm below the inferior boundary of the inferior colliculus was selected, which is itself within the range where the location of the LC is most evident on T1-FSE images (28). Within this slice, 2 LC ROIs (left and right) were drawn as a 1.29 x 1.29 mm cross centered on the voxels with the highest signal intensities in locations corresponding to the known anatomical distribution of the LC. From there, the slices above and below were used to mark the rostral and caudal ROIs, respectively, in a similar manner. Within each hemisphere, the rostral, middle, and caudal LC ROIs had to have at least one voxel touching the ROI from the adjacent slice(s). To control for inter-subject and inter-slice signal variability, for each bilateral set of LC ROIs a reference ROI was drawn in the dorsal pontine tegmentum (PT) as a 18.4 mm^2 square (10x10 voxels) placed 6 voxels above the most ventral LC ROI. This reference ROI was placed equidistantly between the

left and right LC ROIs; if there was an odd number of voxels between the two, the reference ROI was placed closer to the right LC ROI. See Figure 1 for an example of LC and PT ROI marking. LC contrast ratios (LC-CRs) were calculated as the mean LC signal intensity relative to the mean intensity within the reference PT region: LC-CR = $(LC_{intensity} - PT_{intensity}) / PT_{intensity}$. Two raters (SKS was rater 1 for all, rater 2 included ALC, RT, AJW, and JK) blinded to participant information measured LC-CRs for 85/110 scans. LC-CR interrater reliability was measured using the intraclass correlation coefficient (ICC) type 2 (two-way random effects model) in R. To increase signal to noise and reduce the number of comparisons, the average of the left and right LC-CRs was used for all analyses. Further, due to the rostro-caudal gradient aspect of our hypotheses, we averaged the rostral and middle LC CRs.

Statistical analysis

All statistical analyses were performed in R (version 4.1.2; https://cran.r-project.org/). Data were checked for extreme outliers, which were defined as three times the interquartile range above the third quartile or below the first quartile. There were three extreme outliers on CSF p-tau, so these cases were excluded from any analyses involving p-tau. There were no extreme outliers on CSF Aβ42/40, LC CRs, or any of the cognitive composites.

Product-moment correlations assessed the relationship between LC CRs and age as well as CSF measures of p-tau and Aβ42/40 while controlling for age and sex. To examine whether LC signal is related to p-tau in the context of Aβ42/40 or vice versa, we conducted linear regressions predicting one biomarker from age, sex, and the interaction between LC signal and the other biomarker. Welch's t-test was used to assess sex differences in LC CRs. A two-way mixed-measures analysis of variance was used to examine differences in LC CR as a function of group (CN, MCI) and segment (rostral-middle, caudal) while controlling for age and sex.

To examine associations between rostral-middle LC CR and cognition in the context of AD risk as measured by CSF biomarkers, multiple linear regressions were used to examine each cognitive composite (attention, executive function, verbal learning, and verbal memory) as a function of the rostral-middle average LC CR, age, sex, education, p-tau, and the interaction between LC CR and p-tau. To examine whether results are specific to putative p-tau pathology, follow-up sets of regressions were run examining the relationship between LC CR and cognition in the context of Aβ42/40. Further, to examine whether results are specific to the rostral-middle LC, follow-up regressions were run with caudal LC CR.

Results

Sample characteristics

Demographic and clinical characteristics can be found in Table 1. CN and MCI participants did not differ in age or years of education. MCI participants scored lower on the MMSE ($p < 0.05$) and DRS ($p < 0.05$) compared to CN participants. Groups did not differ on levels of p-tau or Aβ42/40, though the MCI group showed the expected trends of increased p-tau and reduced Aβ42/40 compared to CN participants.

LC CR characterization

Interrater reliability was very high for rostral (ICC = 0.98), middle (ICC = 0.91) LC-CRs, and caudal ROIs (ICC = 0.97). Given the high interrater reliability and incomplete double-rating data, measurements from rater 1 were used for subsequent analysis to ensure the most consistency in user approach.

There was no significant association between LC-CRs and age (rostral-middle: $r = -0.04$, $p > 0.05$; caudal: $r = -0.08$, $p > 0.05$), likely due to the restricted age range of the study sample. There were no significant associations between rostral-middle LC CRs and p-tau ($r = 0.17$, $p >$

0.05) or Aβ42/40 (r = 0.01, p > 0.05) or between caudal LC CRs and p-tau (r = 0.05, p > 0.05) or Aβ42/40 (r = -0.04, p > 0.05). There was no significant interaction between Aβ42/40 and rostral-middle LC signal or caudal LC signal in a linear regression predicting p-tau while accounting for age and sex, nor was there an interaction between p-tau and rostral-middle LC signal or caudal LC signal in a linear regression predicting Aβ42/40 while accounting for age and sex (p > 0.05 for all). There was no significant difference in LC-CRs between males and females (rostral-middle 95% confidence interval = -0.013, 0.009; caudal 95% confidence interval = -0.015, 0.011; p > 0.05 for both). The two-way mixed-measures analysis of variance assessing differences in LC CR as a function of group (CN, MCI) and segment (rostral-middle, caudal) controlling for age and sex revealed no effects related to group, $F(1,97) = 3.46$, $p > 0.05$, $\eta^2G = 0.03$, or segment, $F(1,97) = 0.51$, $p > 0.05$, $\eta^2G = 0.001$.

LC CR associations with cognition

LC CR and cognition relationships in the context of p-tau

Four multiple linear regressions were run predicting each cognitive composite (attention, executive functioning, verbal learning, verbal memory) from age, sex, education, p-tau, rostral-middle LC CR, and interactions between LC CR and p-tau. All regression results can be found in Table 3.2.

Our model significantly predicted attention, $F(6,50) = 3.66$, adjusted $R^2 = 0.22$, $p < 0.01$. There were significant main effects of LC CR ($\beta = 33.19$, $p < 0.001$), p-tau ($\beta = 0.04$, $p < 0.01$) and p-tau ($\beta = 0.06$, $p < 0.001$), and a negative interaction between average LC CR and p-tau ($\beta = -0.53$, $p < 0.01$) such that higher LC CR was associated with greater attention performance in those with lower p-tau (suggestive of lower neuropathology). To aid in interpretation, an analysis of simple main effects was performed by conducting a median split for p-tau and examining the

association between LC CR and attention in those with low and high p-tau (Figure 4A). Among participants with low p-tau there was a significantly positive association between rostral-middle LC CR and attention, whereas in those above the cutoff, there was no statistically significant association. A follow-up model with caudal LC CR instead of rostral-middle LC CR also predicted attention and showed a similar LC CR by p-tau interaction pattern.

Our model significantly predicted executive function, $F(6,50) = 3.31$, adjusted $R^2 = 0.20$, $p < 0.01$. There were significant main effects of LC CR ($\beta = 33.37$, $p < 0.001$), p-tau ($\beta = 0.06$, $p < 0.001$), and a negative interaction between average LC CR and p-tau ($\beta = -0.59$, $p < 0.001$) such that higher LC CR was associated with greater executive function performance in those with lower levels of p-tau. To aid in interpretation, an analysis of simple main effects was performed by conducting a median split for p-tau and examining the association between LC CR and executive functioning in those with low and high p-tau (Figure 4B). Among participants with low p-tau there was a significantly positive association between rostral-middle LC CR and executive functioning, whereas in those above the cutoff, there was no statistically significant association. A follow-up model with caudal LC CR instead of rostral-middle LC CR also predicted executive function and showed a similar LC CR by p-tau interaction pattern.

Our model significantly predicted verbal learning, $F(6,49) = 9.07$, adjusted $R^2 = 0.47$, $p < 0.0001$. There were significant main effects of sex ($\beta = 0.86$, $p < 0.0001$), education ($\beta = 0.07$, $p < 0.05$), LC CR ($\beta = 32.54$, $p< 0.01$), p-tau ($\beta = 0.05$, $p < 0.05$), and a negative interaction between LC CR and p-tau ($\beta = -0.61$, $p < 0.01$) such that higher LC CR was associated with greater verbal learning in those with lower levels of p-tau. A follow-up t-test revealed that females performed better on tests of verbal learning than males (95% confidence interval = -1.06, -0.32; $p < 0.001$; Figure 4A). To aid in interpretation of the interaction, an analysis of simple

main effects revealed no significant associations between LC CR and verbal learning after dividing participants into those with low and high p-tau using a median split (Figure 4C). A follow-up model with caudal LC CR instead of rostral-middle LC CR also predicted verbal learning and showed a similar LC CR by p-tau interaction pattern.

Finally, our model predicted verbal memory, $F(6,49) = 4.48$, adjusted $R^2 = 0.28$, $p < 0.01$. There were significant main effects of sex ($\beta = 0.60$, $p < 0.05$), LC CR ($\beta = 27.39$, $p < 0.05$), and a negative interaction between LC CR and p-tau ($\beta = -0.46$, $p < 0.05$) such higher LC CR was associated with greater verbal memory in those with lower levels of p-tau. A follow-up t-test revealed that females performed better on tests of verbal learning than males (95% confident interval = -0.89, -0.13; $p < 0.01$; Figure 4B). To aid in interpretation of the interaction, an analysis of simple main effects revealed no significant associations between LC CR and verbal memory after dividing participants into those with low and high p-tau using a median split (Figure 4D). A follow-up model with caudal LC CR instead of rostral-middle LC CR also predicted verbal memory but did not show an interaction between LC CR and p-tau.

LC CR and cognition relationships in the context of Aβ42/40

Four multiple linear regressions were run predicting each cognitive composite (attention, executive functioning, verbal learning, verbal memory) from age, sex, education, Aβ42/40, rostral-middle LC CR, and interactions between rostral-middle LC CR and Aβ42/40. All regression results can be found in Table 3.2.

Our model did not predict attention overall, $F(6,53) = 1.90$, adjusted $R^2 = 0.08$, $p > 0.05$, and there were no significant coefficients. For visual comparison with the p-tau model, the LC CR by Aβ42/40 interaction can be seen in Figure 5A. A follow-up model with caudal LC CR instead of rostral-middle LC CR did not predict attention. Our model did not predict executive

functioning overall, F(6,53) = 1.73, adjusted R^2 = 0.07, p > 0.05, and there were no significant coefficients. For visual comparison with the p-tau model, the LC CR by Aβ42/40 interaction can be seen in Figure 5B. A follow-up model with caudal LC CR instead of rostral-middle LC CR did not predict executive functioning. Our model predicted verbal learning, F(6,52) = 11.89, adjusted R^2 = 0.53, p < 0.0001. There were significant main effects of sex (β = 0.84, p < 0.0001) and education (β = 0.09, < 0.05), but no effects related to LC CR. For visual comparison with the p-tau model, the LC CR by Aβ42/40 interaction can be seen in Figure 5C. A follow-up model with caudal LC CR instead of rostral-middle LC CR also predicted verbal learning with similar effects of sex and education, with an additional main effect of LC CR. Our model predicted verbal memory, F(6,52) = 5.44, adjusted R^2 = 0.32, p < 0.001. There were significant main effects of sex (β = 0.59, p < 0.05) and education (β = 0.11, p < 0.05), but no effects related to LC CR. For visual comparison with the p-tau model, the LC CR by Aβ42/40 interaction can be seen in Figure 5D. A follow-up model with caudal LC CR instead of rostral-middle LC CR also predicted verbal memory with similar effects of sex and education.

Discussion

In this study, we aimed to clarify lingering questions from discrepant reports regarding 1) whether AD-related changes in MR-derived LC signal are detectable in the MCI stage and 2) whether LC signal is related to in vivo measures of putative tau and amyloid pathology. Further, we investigated the relationship between LC MR signal and cognition in the context of p-tau and Aβ42/40.

We did not detect a difference between the MCI and CN groups in LC signal, corroborating some previous reports (31,35) and contradicting others (32,34). Since the extant findings remain somewhat evenly split, future research should better characterize more precisely

the degree and domains of impairment necessary to detect reduced LC signal. We also did not find any significant associations between LC signal and CSF markers of amyloid and tau. To our knowledge, Betts et al. (31) is the only report directly assessing the relationship between LC signal and CSF measurements of amyloid and tau, and they report a negative association with amyloid that was difficult to explain. Thus, these relationships remain unclear. It's possible that there is no true association, our sample sizes were too low and thus we were underpowered to detect a true difference, or there are other factors we are not accounting for in examining these relationships.

In examining associations between LC signal and cognition in the context of p-tau, we found a consistent pattern whereby higher LC signal was associated with better cognition across domains (attention, executive function, verbal learning, and verbal memory) only among those with low p-tau. For attention, executive function, and verbal learning this pattern was seen in both rostral-middle LC as well as the caudal segment. However, for verbal memory, this pattern was only seen in the rostral-middle segment. Further, after performing a median split on p-tau to examine simple main effects, only those below the median showed a significant positive association with cognition when examining attention and executive function. With verbal learning and memory, there were no main effects related to LC CR after performing a median split on p-tau.

It is generally understood that the ventral-caudal LC has descending projections to the spinal cord, whereas the dorsal middle and rostral LC project to the cortex (51). Therefore, we would not expect to see the caudal LC involved in these cognitive measures. However, it has been noted that LC-sensitive scan acquisitions of anisotropic voxels may introduce partial volume effects, particularly at the rostral and caudal ends of the nucleus (52). It is possible that

our caudal (and indeed, rostral) average contained part of the middle LC as well. Therefore, assuming a perfect rostral-middle-caudal division of the LC from our scan resolution is not possible, these findings suggest that, in a sample of older adults without dementia, overall LC MR signal is more strongly related to attention, executive function, and verbal learning (dependent on p-tau). In contrast, we see effects more localized to the rostral-middle segment when examining verbal memory, which happens to be one of the earliest domains affected by AD progression (53).

When examining the associations between LC signal and cognition in the context of Aβ42/40, there were no effects related to LC signal in any models. These findings support the notion that the impact of LC integrity on cognition is driven by tauopathy. However, the interaction effects suggest a more complex relationship whereby the association changes with the degree of tau pathology. There are many reasons this could be: perhaps among those with greater tau pathology there are other factors unaccounted for that contribute to the relationship between LC signal and cognition; it's also possible that with growing pathology there are new physiological/pathological contributions to the LC MR signal that are not present or are negligible in those without pathology, raising the question of whether this measure should be thought of purely as a marker of "integrity". Indeed, an interaction effect between LC MR signal and pathology on cognition was shown by Jacobs et al. (34), whereby participants with low LC MR signal showed a negative association and those with high LC MR signal showed a positive association between neocortical amyloid (measured by positron emission tomography) and a memory composite score. Together, these findings demonstrate that pathology needs to be taken into consideration when examining the relationship between LC MR signal and cognition.

It is generally accepted that MR-derived LC signal contrast is a marker of LC integrity based off the findings of Keren et al. (54), who showed that greater LC signal contrast corresponded with areas of greater LC neuronal density. This increased signal has been thought to relate to neuromelanin content (55) as neuromelanin is found in large quantities within the LC. However, as with most MRI-derived metrics of "integrity", it isn't actually clear what precisely is contributing to the signal and thus the assumption that greater LC signal always corresponds with greater integrity is questionable. Priovoulos et al. (56) systematically examined contributions to the "neuromelanin-contrast" using a phantom and in vivo data and showed that 1) there was no relationship between neuromelanin alone and MR contrast and 2) reduced signal in the LC is likely due to a lower macromolecular pool size ratio ("more free water and/or less macromolecules"). It is important to note that larger neurons with a greater diameter and intra-cellular water pool will thus exhibit greater MR signal regardless of pathology. It is possible that changes within the nucleus due to pathology buildup or other side effects of disease progression alter the primary contribution to the signal.

Our study has limitations. First, as mentioned previously, the acquisition of anisotropic voxels may impede our ability to truly delineate the LC along its rostro-caudal axis. Second, only a small subsample of our participants with MRI data had cerebrospinal fluid measures. Lumbar punctures are invasive and uncomfortable, so we are faced with limits on data availability and must also consider the possibility of selection bias for those who choose to undergo the procedure. Obtaining putative pathology measures with less invasive techniques such as blood draws may improve upon this issue but will take time to implement. Related to our small sample, we were unable to include participants with AD in our analyses due to limited data collection during the COVID-19 pandemic. We also grouped together amnestic and multi-domain non-

amnestic MCI participants in order to maximize our MCI sample, though examining amnestic MCI in isolation may offer more sensitivity to early AD-related changes. Finally, our sample consists of predominantly white, educated older adults, which is not representative of broader demographics in the United States. This limits interpretations or generalizability of our results to a more diverse population. The impacts of sociodemographic factors such as access to healthcare and education, socioeconomic status, and chronic stress (especially relevant to the LC) on AD risk and progression are still poorly understood, and there is a critical need to expand this research. Indeed, these factors (especially stress and its intersection with other excluded identities and experiences) might help explain the more complex relationship between LC signal and cognition among those with greater tau and amyloid pathology.

In summary, we show that in a sample of older adults at varying degrees of AD risk but without outright dementia, LC MR signal does not differentiate those with and without MCI or relate to CSF measures of p-tau or Aβ42/40. We also show that among those with low p-tau, higher overall LC signal is associated with better performance on tests of attention, executive function, and verbal learning, and higher rostral-middle LC signal is associated with better performance on tests of delayed verbal memory. This work provides further support for the role of the LC and noradrenergic system in early AD and calls for future research to continue uncovering the potential for LC MR signal to aid in preclinical identification of high-risk individuals.

Acknowledgements

The authors thank Thomas Lesperance, M.S., at CSCI for his work on the graphical user interface and visualization of results, Aaron Jacobson, M.A., at CFMRI for assistance in the collection of the data, and Jasmine Kim for assistance with the LC MRI markings. We especially

thank all those who participated in the study for their dedication to advancing Alzheimer's disease research. This work was supported by the National Science Foundation (NSF) Graduate Research Fellowship Program under Grant Nos. DGE-2038238 (SKS) and DGE-1650112 (AJW), and NSF grant ACI-1550405 (LRF and VLG). Any opinions, findings, and conclusions or recommendations expressed in this material are those of the author(s) and do not necessarily reflect the views of the NSF. This work was also supported by NIH awards R01AG054049 (LRF, MWB, and VLG), R01AR070830 (LRF and VLG), and R01HD088437 (LRF), and University of California MPRI award MRP17454755 (LRF and VLG).

Chapter 3, in full, is currently being prepared for submission for publication of the material. Solders, S.K.; Weigand, A.J.; Macomber, A.; Thayer, R.E.; Granholm, E.L.; Frank, L.R.; Bondi, M.W. "Tau moderates the relationship between locus coeruleus MR signal and cognition". The dissertation author was the primary researcher and author of this paper.

Figures

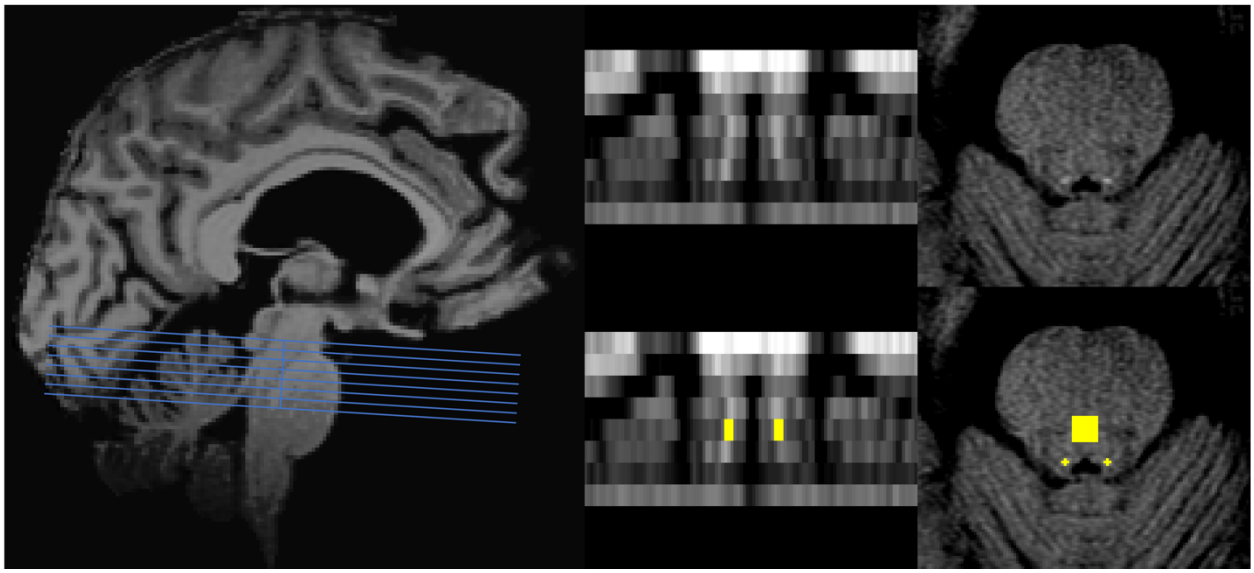

Figure 3.1: LC marking and calculation of contrast ratio. Left: Eight oblique slices acquired over brainstem perpendicular to the wall of the fourth ventricle, with the bottom of the inferior colliculus positioned between slices two and three. Middle Top: coronal view of brainstem containing the LC. Middle Bottom: Middle LC marked in yellow. Right Top: Axial view of brainstem containing middle LC. Right Bottom: Middle LC and pontine tegmentum control region marked in yellow.

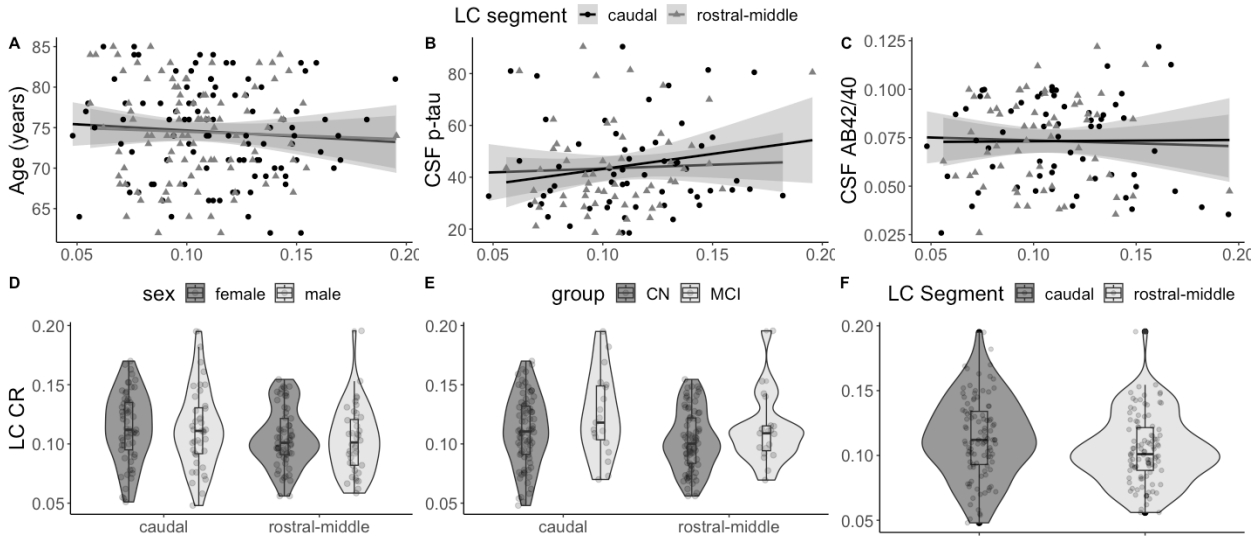

Figure 3.2: LC CR characterization. LC CR scatterplot with age (A). LC CR scatterplot with p-tau (B). LC CR scatterplot with Aβ42/40 (C). Sex differences in LC CR (D). Group (MCI vs CN) differences in LC CR (E). LC CR by segment (caudal vs rostral-middle; F).

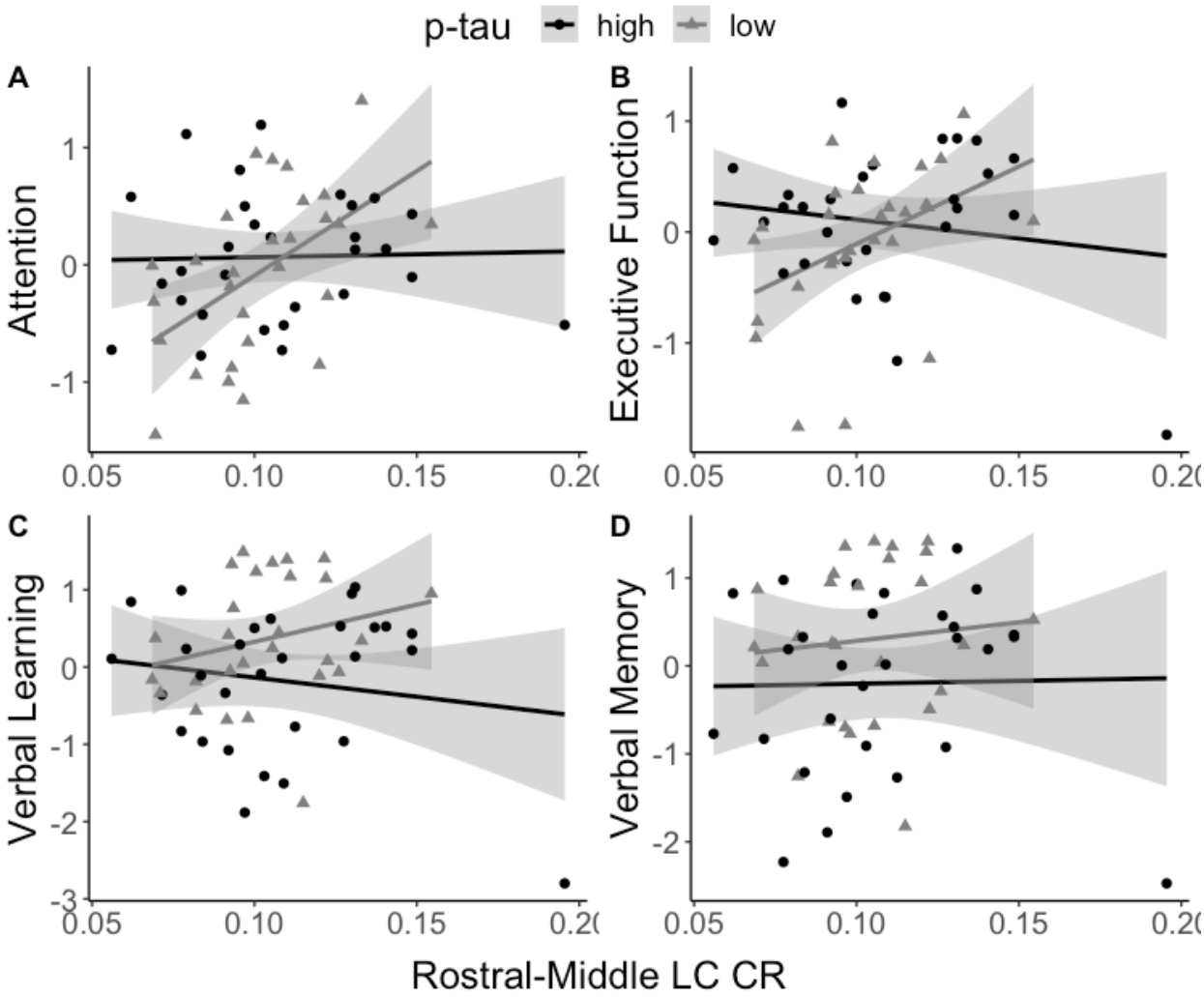

Figure 3.3: Rostral-Middle LC CR scatterplots with cognition by median split of p-tau.

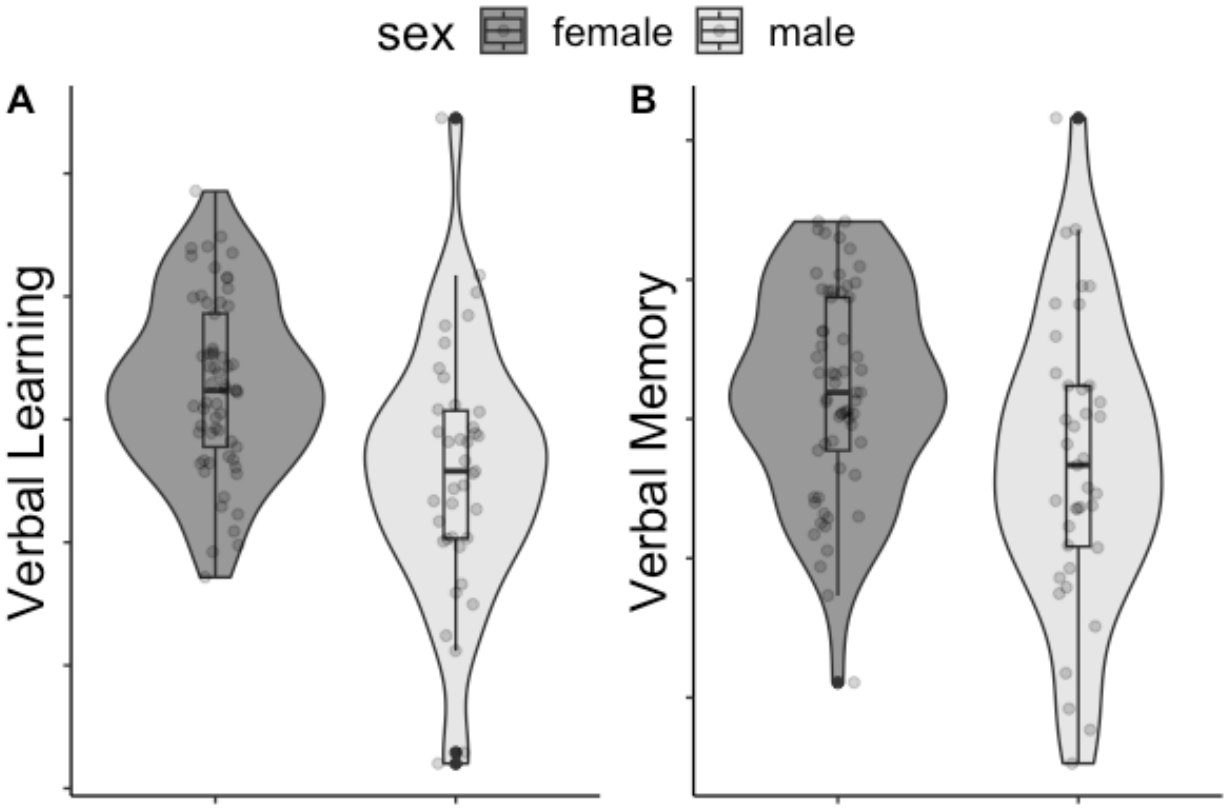

Figure 3.4: Sex differences in verbal learning.

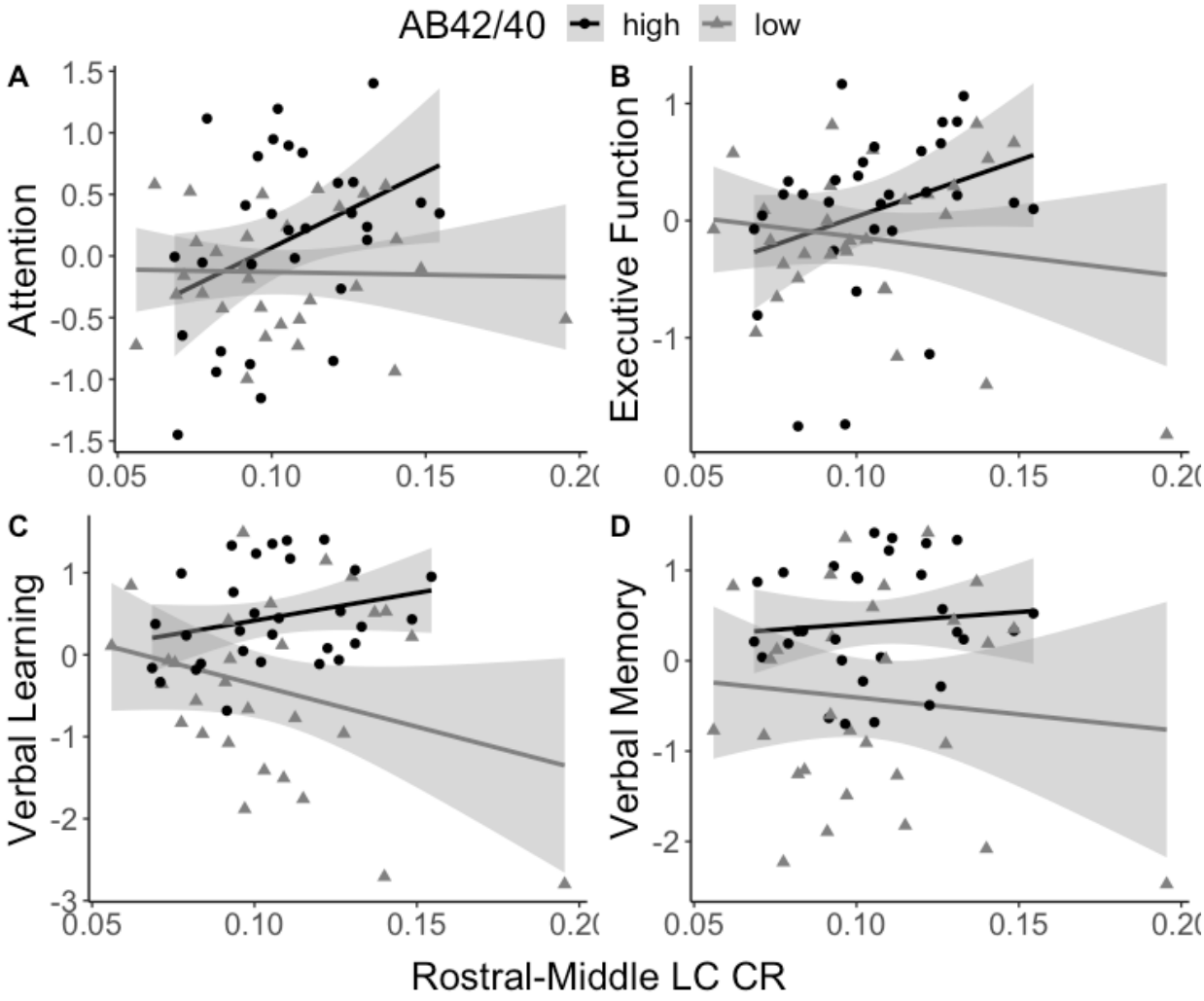

Figure 3.5: Rostral-Middle LC CR scatterplots with cognition by median split of Aβ42/40.

Tables

Table 3.1: Demographic, cognitive, and CSF biomarker measurements.

	CN (n = 82; mean ± SD)	MCI (n = 19; mean ± SD)	p
Age (years)	74.45 ± 5.57	74.47 ± 6.85	0.99
Education (years)	16.55 ± 2.32	16.47 ± 3.29	0.93
MMSE (raw)	28.87 ± 1.50	27.47 ± 2.17	0.01
DRS (raw)	139.3 ± 3.32	136.1 ± 4.66	0.01
	n = 48	**n = 9**	**p**
CSF p-tau	42.50 ± 15.35	50.30 ± 25.50	0.4
CSF AB42/40	0.077 ± 0.021	0.054 ± 0.021	0.93
		n	
Ethnicity	4 Hispanic/Latinx	3 Hispanic/Latinx	
Race	2 Asian, 2 African American, 2 American Indian/Alaska Native, 0 Native Hawaiian/Other Pacific Islander, 74 White, 2 More than one	1 Asian, 0 African American, 1 American Indian/Alaska Native, 0 Native Hawaiian/Other Pacific Islander, 17 White, 2 more than one	

Table 3.2: Regression Results.

Attention Regressions by LC CR Segment

Rostral-Middle LC CR

p-tau

	β Estimate	Std. Error	t-value	p-value
(Intercept)	-3.589	1.574	-2.280	0.027
age	-0.002	0.015	-0.123	0.903
sex	0.186	0.158	1.180	0.244
edu	0.001	0.028	0.026	0.980
rostral-middle LC-CR	33.192	8.235	4.031	0.000
CSF p-tau	0.059	0.016	3.764	0.000
LC CR x CSF inter	-0.527	0.145	-3.639	0.001

Aβ42/40

	β Estimate	Std. Error	t-value	p-value
(Intercept)	1.428	1.758	0.812	0.420
	-0.006	0.016	-0.394	0.695

Table 3.2: Regression Results (continued).

age				
sex	0.239	0.167	1.432	0.158
edu	0.006	0.031	0.182	0.856
rostral-middle LC-CR	-13.089	9.283	-1.410	0.164
CSF Aβ42/40	-23.955	14.702	-1.629	0.109
LC CR x CSF inter	255.052	130.838	1.949	0.057

Caudal LC CR

p-tau

	β Estimate	Std. Error	t-value	p-value
(Intercept)	-2.475	1.542	-1.605	0.115
age	-0.007	0.016	-0.457	0.650
sex	0.270	0.163	1.653	0.105
edu	0.011	0.029	0.372	0.712
caudal LC-CR	22.183	6.653	3.334	0.002
CSF p-tau	0.051	0.016	3.258	0.002
LC CR x CSF inter	-0.415	0.136	-3.053	0.004

Aβ42/40

	β Estimate	Std. Error	t-value	p-value
(Intercept)	1.217	1.535	0.793	0.431
age	-0.005	0.017	-0.321	0.750
sex	0.244	0.168	1.449	0.153
edu	0.005	0.031	0.159	0.874
caudal LC-CR	-10.753	6.766	-1.589	0.118
CSF Aβ42/40	-18.817	12.141	-1.550	0.127
LC CR x CSF inter	189.359	96.393	1.964	0.055

Executive Function Regressions by LC CR Segment

Rostral-Middle LC CR

p-tau

	β Estimate	Std. Error	t-value	p-value
(Intercept)	-4.387	1.688	-2.599	0.012
age	0.006	0.016	0.340	0.735
sex	0.258	0.169	1.529	0.133
edu	0.019	0.030	0.629	0.532
rostral-middle LC-CR	33.374	8.830	3.780	0.000
CSF p-tau	0.064	0.017	3.756	0.000
LC CR x CSF inter	-0.591	0.155	-3.805	0.000

Table 3.2: Regression Results (continued).

	Aβ42/40			
	β Estimate	Std. Error	t-value	p-value
(Intercept)	0.778	1.910	0.407	0.685
age	-0.003	0.018	-0.189	0.851
sex	0.316	0.181	1.746	0.087
edu	0.025	0.033	0.736	0.465
rostral-middle LC-CR	-13.967	10.088	-1.384	0.172
CSF Aβ42/40	-19.501	15.978	-1.220	0.228
LC CR x CSF inter	228.561	142.191	1.607	0.114
Caudal LC CR				
p-tau				
	β Estimate	Std. Error	t-value	p-value
(Intercept)	-4.177	1.534	-2.722	0.009
age	0.003	0.016	0.202	0.841
sex	0.360	0.163	2.213	0.032
edu	0.031	0.029	1.060	0.294
caudal LC-CR	28.565	6.622	4.314	0.000
CSF p-tau	0.067	0.016	4.259	0.000
LC CR x CSF inter	-0.583	0.135	-4.310	0.000
	Aβ42/40			
	β Estimate	Std. Error	t-value	p-value
(Intercept)	0.416	1.636	0.255	0.800
age	0.000	0.018	0.022	0.982
sex	0.320	0.179	1.782	0.081
edu	0.024	0.033	0.724	0.472
caudal LC-CR	-11.790	7.210	-1.635	0.108
CSF Aβ42/40	-17.940	12.940	-1.387	0.171
LC CR x CSF inter	194.600	102.700	1.894	0.064
Verbal Learning Function Regressions by LC CR Segment				
Rostral-Middle LC CR				
p-tau				
	β Estimate	Std. Error	t-value	p-value
(Intercept)	-3.522	1.971	-1.787	0.080
age	-0.008	0.019	-0.428	0.670
sex	0.863	0.192	4.487	0.000

Table 3.2: Regression Results (continued).

edu	0.068	0.034	1.988	0.052
rostral-middle LC-CR	32.544	10.205	3.189	0.002
CSF p-tau	0.047	0.019	2.415	0.020
LC CR x CSF inter	-0.613	0.177	-3.454	0.001
	Aβ42/40			
	β Estimate	Std. Error	t-value	p-value
(Intercept)	0.409	1.993	0.205	0.838
age	-0.023	0.018	-1.299	0.200
sex	0.841	0.186	4.516	0.000
edu	0.089	0.034	2.613	0.012
rostral-middle LC-CR	-18.996	10.385	-1.829	0.073
CSF Aβ42/40	-4.181	16.335	-0.256	0.799
LC CR x CSF inter	225.684	145.035	1.556	0.126
	Caudal LC CR			
	p-tau			
	β Estimate	Std. Error	t-value	p-value
(Intercept)	-1.049	1.858	-0.564	0.575
age	-0.014	0.019	-0.749	0.458
sex	0.966	0.198	4.884	0.000
edu	0.083	0.035	2.413	0.020
caudal LC-CR	9.408	7.928	1.187	0.241
CSF p-tau	0.021	0.019	1.103	0.275
LC CR x CSF inter	-0.341	0.162	-2.107	0.040
	Aβ42/40			
	β Estimate	Std. Error	t-value	p-value
(Intercept)	-0.211	1.608	-0.131	0.896
age	-0.019	0.017	-1.089	0.281
sex	0.859	0.176	4.870	0.000
edu	0.094	0.032	2.937	0.005
caudal LC-CR	-15.663	7.010	-2.234	0.030
CSF Aβ42/40	4.084	12.586	0.324	0.747
LC CR x CSF inter	132.685	99.793	1.330	0.189
Verbal Memory Function Regressions -by LC CR Segment				
Rostral-Middle LC CR				
	p-tau			
	β Estimate	Std. Error	t-value	p-value

Table 3.2: Regression Results (continued).

(Intercept)	-2.746	2.483	-1.106	0.274
age	-0.011	0.023	-0.483	0.631
sex	0.598	0.242	2.469	0.017
edu	0.081	0.043	1.903	0.063
rostral-middle LC-CR	27.391	12.856	2.131	0.038
CSF p-tau	0.028	0.024	1.156	0.254
LC CR x CSF inter	-0.461	0.224	-2.064	0.044
	Aβ42/40			
	β Estimate	Std. Error	t-value	p-value
(Intercept)	-0.854	2.501	-0.341	0.734
age	-0.023	0.023	-1.035	0.305
sex	0.587	0.234	2.514	0.015
edu	0.108	0.043	2.535	0.014
rostral-middle LC-CR	-8.236	13.026	-0.632	0.530
CSF Aβ42/40	7.173	20.490	0.350	0.728
LC CR x CSF inter	108.244	181.933	0.595	0.554
	Caudal LC CR			
	p-tau			
	β Estimate	Std. Error	t-value	p-value
(Intercept)	-0.431	2.270	-0.190	0.850
age	-0.019	0.023	-0.826	0.413
sex	0.681	0.242	2.817	0.007
edu	0.092	0.042	2.177	0.034
caudal LC-CR	7.714	9.687	0.796	0.430
CSF p-tau	0.014	0.023	0.601	0.551
LC CR x CSF inter	-0.297	0.198	-1.502	0.139
	Aβ42/40			
	β Estimate	Std. Error	t-value	p-value
(Intercept)	-0.488	2.058	-0.237	0.814
age	-0.022	0.022	-1.007	0.319
sex	0.607	0.227	2.677	0.010
edu	0.106	0.041	2.608	0.012
caudal LC-CR	-11.462	9.009	-1.272	0.209
CSF Aβ42/40	9.226	16.185	0.570	0.571
LC CR x CSF inter	81.168	127.869	0.635	0.528

References

1. Poe, G. R., Foote, S., Eschenko, O., Johansen, J. P., Bouret, S., Aston-Jones, G., Harley, C. W., Manahan-Vaughan, D., Weinshenker, D., Valentino, R., Berridge, C., Chandler, D. J., Waterhouse, B., & Sara, S. J. (2020). Locus coeruleus: a new look at the blue spot. *Nature Reviews Neuroscience*, *21*, 644-659. https://doi.org/https://doi.org/10.1038/s41583-020-0360-9

2. Benarroch, E. E. (2009). The locus ceruleus norepinephrine system: functional organization and potential clinical significance. *Neurology*, *73*(20), 1699-1704. https://doi.org/10.1212/WNL.0b013e3181c2937c

3. Wainstein, G., Müller, E. J., Taylor, N., Munn, B., & Shine, J. M. (2022). The role of the locus coeruleus in shaping adaptive cortical melodies. *Trends in Cognitive Sciences*, *26*(6), 527-538. https://doi.org/10.1016/j.tics.2022.03.006

4. Berridge, C., & Waterhouse, B. (2003). The locus coeruleus-noradrenergic system: modulation of behavioral state and state-dependent cognitive processes. *Brain Research Reviews*, *42*(1), 33-84. https://doi.org/10.1016/s0165-0173(03)00143-7

5. Aston-Jones, G., & Waterhouse, B. (2016). Locus coeruleus: From global projection system to adaptive regulation of behavior. *Brain Research*, *1645*, 75-78. https://doi.org/10.1016/j.brainres.2016.03.001

6. Sara, S. J. (2009). The locus coeruleus and noradrenergic modulation of cognition. *Nature Reviews Neuroscience*, *10*(3), 211-223. https://doi.org/10.1038/nrn2573

7. Hämmerer, D., Callaghan, M. F., Hopkins, A., Kosciessa, J., Betts, M., Cardenas-Blanco, A., Kanowski, M., Weiskopf, N., Dayan, P., Dolan, R. J., & Düzel, E. (2018). Locus coeruleus integrity in old age is selectively related to memories linked with salient negative events. *Proceedings of the National Academy of Sciences of the United States of America*, *115*(9), 2228-2233. https://doi.org/10.1073/pnas.1712268115

8. Jacobs, H. I. L., Wiese, S., Ven, V. v. d., Gronenschild, E. H. B. M., Verhey, F. R. J., & Matthews, P. M. (2015). Relevance of parahippocampal-locus coeruleus connectivity to memory in early dementia. *Neurobiology of Aging*, *36*(2), 618-626. https://doi.org/10.1016/j.neurobiolaging.2014.10.041

9. Dahl, M. J., Mather, M., Düzel, S., Bodammer, N. C., Lindenberger, U., Kühn, S., & Werkle-Bergner, M. (2019). Rostral locus coeruleus integrity is associated with better memory performance in older adults. *Nature Human Behavior*, *3*(11), 1203-1214. https://doi.org/10.1038/s41562-019-0715-2

10. Robertson, I. H. (2013). A noradrenergic theory of cognitive reserve: implications for Alzheimer's disease. *Neurobiology of Aging*, *34*(1), 298-308. https://doi.org/10.1016/j.neurobiolaging.2012.05.019

11. Wilson, R. S., Nag, S., Boyle, P. A., Hizel, L. P., Yu, L., Buchman, A. S., Schneider, J. A., & Bennett, D. A. (2013). Neural reserve, neuronal density in the locus ceruleus, and cognitive decline. *Neurology*, *80*(13), 1202-1208. https://doi.org/10.1212/WNL.0b013e3182897103

12. Mather, M., & Harley, C. W. (2016). The Locus Coeruleus: Essential for Maintaining Cognitive Function and the Aging Brain. *Trends in Cognitive Sciences*, *20*(3), 214-226. https://doi.org/10.1016/j.tics.2016.01.001

13. Tomlinson, B. E., Irving, D., & Blessed, G. (1981). Cell loss in the locus coeruleus in senile dementia of Alzheimer type. *Journal of the Neurological Sciences*, *49*(3), 419-428. https://doi.org/10.1016/0022-510x(81)90031-9

14. Bondareff, W., Mountjoy, C. Q., & Roth, M. (1982). Loss of neurons of origin of the adrenergic projection to cerebral cortex (nucleus locus ceruleus) in senile dementia. *Neurology*, *32*(2), 164-168. https://doi.org/10.1212/wnl.32.2.164

15. Mann, D. M., Yates, P. O., & Hawkes, J. (1982). The noradrenergic system in Alzheimer and multi-infarct dementias. *Journal of Neurology Neurosurgery and Psychiatry*, *45*(2), 113-119. https://doi.org/10.1136/jnnp.45.2.113

16. Assal, F., & Cummings, J. L. (2002). Neuropsychiatric symptoms in the dementias. *Current Opinion in Neurology*, *15*(4), 445-450. https://doi.org/10.1097/00019052-200208000-00007

17. Lanctôt, K. L., Amatniek, J., Ancoli-Israel, S., Arnold, S. E., Ballard, C., Cohen-Mansfield, J., Ismail, Z., Lyketsos, C., Miller, D. S., Musiek, E., Osorio, R. S., Rosenberg, P. B., Satlin, A., Steffens, D., Tariot, P., Bain, L. J., Carrillo, M. C., Hendrix, J. A., Jurgens, H., & Boot, B. (2017). Neuropsychiatric signs and symptoms of Alzheimer's disease: New treatment paradigms. *Alzheimer's & dementia (New York, N.Y.)*, *3*(3), 440-449. https://doi.org/10.1016/j.trci.2017.07.001

18. Ehrenberg, A. J., Suemoto, C. K., Resende, E. d. P. F., Petersen, C., Leite, R. E. P., Rodriguez, R. D., Ferretti-Rebustini, R. E. d. L., You, M., Oh, J., Nitrini, R., Pasqualucci, C. A., Jacob-Filho, W., Kramer, J. H., Gatchel, J. R., & Grinberg, L. T. (2018). Neuropathologic Correlates of Psychiatric Symptoms in Alzheimer's Disease. *Journal of Alzheimer's Disease*, *66*(1), 115-126. https://doi.org/10.3233/JAD-180688

19. Grudzien, A., Shaw, P., Weintraub, S., Bigio, E., Mash, D. C., & Mesulam, M. M. (2007). Locus coeruleus neurofibrillary degeneration in aging, mild cognitive impairment and early Alzheimer's disease. *Neurobiology of Aging*, *28*(3), 327-335. https://doi.org/10.1016/j.neurobiolaging.2006.02.007

20. Braak, H., Thal, D. R., Ghebremedhin, E., & Tredici, K. D. (2011). Stages of the pathologic process in Alzheimer disease: age categories from 1 to 100 years. *Journal of Neuropathology and Experimental Neurology*, *70*(11), 960-969. https://doi.org/10.1097/NEN.0b013e318232a379

21. Andrés-Benito, P., Fernández-Dueñas, V., Carmona, M., Escobar, L. A., Torrejón-Escribano, B., Aso, E., Ciruela, F., & Ferrer, I. (2017). Locus coeruleus at asymptomatic early and middle Braak stages of neurofibrillary tangle pathology. *Neuropathology and Applied Neurobiology*, *43*(5), 373-392. https://doi.org/10.1111/nan.12386

22. Ehrenberg, A. J., Nguy, A. K., Theofilas, P., Dunlop, S., Suemoto, C. K., Alho, A. T. D. L., Leite, R. P., Rodriguez, R. D., Mejia, M. B., Rüb, U., Farfel, J. M., Ferretti-Rebustini, R. E. d. L., Nascimento, C. F., Nitrini, R., Pasquallucci, C. A., Jacob-Filho, W., Miller, B., Seeley, W. W., Heinsen, H., & Grinberg, L. T. (2017). Quantifying the accretion of hyperphosphorylated tau in the locus coeruleus and dorsal raphe nucleus: the pathological building blocks of early Alzheimer's disease. *Neuropathology and Applied Neurobiology*, *43*(5), 393-408. https://doi.org/10.1111/nan.12387

23. Theofilas, P., Ehrenberg, A. J., Dunlop, S., Alho, A. T. D. L., Nguy, A., Leite, R. E. P., Rodriguez, R. D., Mejia, M. B., Suemoto, C. K., Ferretti-Rebustini, R. E. D. L., Polichiso, L., Nascimento, C. F., Seeley, W. W., Nitrini, R., Pasqualucci, C. A., Filho, W. J., Rueb, U., Neuhaus, J., Heinsen, H., & Grinberg, L. T. (2017). Locus coeruleus volume and cell population changes during Alzheimer's disease progression: A stereological study in human postmortem brains with potential implication for early-stage biomarker discovery. *Alzheimer's & Dementia*, *13*(3), 236-246. https://doi.org/10.1016/j.jalz.2016.06.2362

24. Chan-Palay, V., & Asan, E. (1989). Alterations in catecholamine neurons of the locus coeruleus in senile dementia of the Alzheimer type and in Parkinson's disease with and without dementia and depression. *The Journal of Comparative Neurology*, *287*(3), 373-392. https://doi.org/10.1002/cne.902870308

25. German, D. C., Manaye, K. F., 3rd, C. L. W., Woodward, D. J., McIntire, D. D., Smith, W. K., Kalaria, R. N., & Mann, D. M. (1992). Disease-specific patterns of locus coeruleus cell loss. *Annals of Neurology*, *32*(5), 667-676. https://doi.org/10.1002/ana.410320510

26. Weinshenker, D. (2018). Long Road to Ruin: Noradrenergic Dysfunction in Neurodegenerative Disease. *Trends in Neurosciences*, *41*(4), 211-223. https://doi.org/10.1016/j.tins.2018.01.010

27. Sasaki, M., Shibata, E., Tohyama, K., Takahashi, J., Otsuka, K., Tsuchiya, K., Takahashi, S., Ehara, S., Terayama, Y., & Sakai, A. (2006). Neuromelanin magnetic resonance imaging of locus ceruleus and substantia nigra in Parkinson's disease. *Neuroreport*, *17*(11), 1215-1218. https://doi.org/10.1097/01.wnr.0000227984.84927.a7

28. Shibata, E., Sasaki, M., Tohyama, K., Kanbara, Y., Otsuka, K., Ehara, S., & Sakai, A. (2006). Age-related changes in locus ceruleus on neuromelanin magnetic resonance imaging at 3 Tesla. *Magnetic Resonance in Medical Sciences*, *5*(4), 197-200. https://doi.org/10.2463/mrms.5.197

29. Keren, N. I., Lozar, C. T., Harris, K. C., Morgan, P. S., & Eckert, M. A. (2009). In vivo mapping of the human locus coeruleus. *NeuroImage*, *47*(4), 1261-1267. https://doi.org/10.1016/j.neuroimage.2009.06.012

30. Priovoulos, N., Jacobs, H. I. L., Ivanov, D., Uludağ, K., Verhey, F. R. J., & Poser, B. A. (2018). High-resolution in vivo imaging of human locus coeruleus by magnetization transfer MRI at 3T and 7T. *NeuroImage*, *168*, 427-436. https://doi.org/10.1016/j.neuroimage.2017.07.045

31. Betts, M. J., Cardenas-Blanco, A., Kanowski, M., Spottke, A., Teipel, S. J., Kilimann, I., Jessen, F., & Düzel, E. (2019). Locus coeruleus MRI contrast is reduced in Alzheimer's disease dementia and correlates with CSF Aβ levels. *Alzheimer's & Dementia (Amsterdam, Netherlands)*, *11*, 281-285. https://doi.org/10.1016/j.dadm.2019.02.001

32. Takahashi, J., Shibata, T., Sasaki, M., Kudo, M., Yanezawa, H., Obara, S., Kudo, K., Ito, K., Yamashita, F., & Terayama, Y. (2015). Detection of changes in the locus coeruleus in patients with mild cognitive impairment and Alzheimer's disease: high-resolution fast spin-echo T1-weighted imaging. *Geriatrics & Gerontology International*, *15*(3), 334-340. https://doi.org/10.1111/ggi.12280

33. Olivieri, P., Lagarde, J., Lehericy, S., Valabrègue, R., Michel, A., Macé, P., Caillé, F., Gervais, P., Bottlaender, M., & Sarazin, M. (2019). Early alteration of the locus coeruleus in phenotypic variants of Alzheimer's disease. *Annals of Clinical and Translatoinal Neurology*, *6*(7), 1345-1351. https://doi.org/10.1002/acn3.50818

34. Jacobs, H. I. L., Becker, J. A., Kwong, K., Engels-Domínguez, N., Prokopiou, P. C., Papp, K. V., Properzi, M., Hampton, O. L., Uquillas, F. d. O., Sanchez, J. S., Rentz, D. M., Fakhri, G. E.,

Normandin, M. D., Price, J. C., Bennett, D. A., Sperling, R. A., & Johnson, K. A. (2021). In vivo and neuropathology data support locus coeruleus integrity as indicator of Alzheimer's disease pathology and cognitive decline. *Science Translational Medicine*, *13*(612), eabj2511. https://doi.org/10.1126/scitranslmed.abj2511

35. Li, M., Liu, S., Zhu, H., Guo, Z., Zhi, Y., Liu, R., Jiang, Z., Liang, X., Hu, H., & Zhu, J. (2022). Decreased locus coeruleus signal associated with Alzheimer's disease based on neuromelanin-sensitive magnetic resonance imaging technique. *Frontiers in Neuroscience*, *16*, 1014485. https://doi.org/10.3389/fnins.2022.1014485

36. Jacobs, H., Becker, A., Kwong, K., D'Oleire Uquillas, F., Sperling, R., & Johnson, K. (2018). Locus coeruleus signal intensity is associated with entorhinal tau pathology at higher levels of amyloid burden [Conference Abstract]. *Alzheimer's & Dementia*, *14*, P509-510.

37. Jak, A., Bondi, M., Delano-Wood, L., Wierenga, C., Corey-Bloom, J., Salmon, D., & Delis, D. (2009). Quantification of five neuropsychological approaches to defining mild cognitive impairment. *The American Journal of Geriatric Psychiatry*, *17*(5), 368-375. https://doi.org/10.1097/JGP.0b013e31819431d5

38. Bondi, M., Edmonds, E., Jack, A., Clark, L., Delano-Wood, L., McDonald, C., Nation, D., Libon, D., Au, R., Galasko, D., & Salmon, D. (2014). Neuropsychological criteria for mild cognitive impairment improves diagnostic precision, biomarker associations, and progression rates. *Journal of Alzheimer's Disease*, *42*(1), 275-289. https://doi.org/10.3233/JAD-140276

39. Bondi, M. W., & Smith, G. E. (2014). Mild cognitive impairment: a concept and diagnostic entity in need of input from neuropsychology. *Journal of the International Neuropsychological Society*, *20*(2), 129-134. https://doi.org/10.1017/S1355617714000010

40. Clark, L. R., Delano-Wood, L., Libon, D. J., McDonald, C. R., Nation, D. A., Bangen, K. J., Jak, A. J., Au, R., Salmon, D. P., & Bondi, M. W. (2013). Are empirically-derived subtypes of mild cognitive impairment consistent with conventional subtypes? *Journal of the International Neuropsychological Society*, *19*(6), 635-645. https://doi.org/10.1017/S1355617713000313

41. Jak, A. J., Urban, S., McCauley, A., Bangen, K. J., Delano-Wood, L., Corey-Bloom, J., & Bondi, M. W. (2009). Profile of hippocampal volumes and stroke risk varies by neuropsychological definition of mild cognitive impairment. *Journal of the International Neuropsychological Society*, *15*(6), 890-897. https://doi.org/10.1017/S1355617709090638

42. Xiao, M.-F., Xu, D., Craig, M. T., Pelkey, K. A., Chien, C.-C., Shi, Y., Zhang, J., Resnick, S., Pletnikova, O., Salmon, D., Brewer, J., Edland, S., Wegiel, J., Tycko, B., Savonenko, A., Reeves, R. H., Troncoso, J. C., McBain, C. J., Galasko, D., & Worley, P. F. (2017). NPTX2 and

cognitive dysfunction in Alzheimer's Disease. *eLife*, *6*, e23798. https://doi.org/10.7554/eLife.23798

43. Vanderstichele, H., Bibl, M., Engelborghs, S., Bastard, N. L., Lewczuk, P., Molinuevo, J. L., Parnetti, L., Perret-Liaudet, A., Shaw, L. M., Teunissen, C., Wouters, D., & Blennow, K. (2012). Standardization of preanalytical aspects of cerebrospinal fluid biomarker testing for Alzheimer's disease diagnosis: a consensus paper from the Alzheimer's Biomarkers Standardization Initiative. *Alzheimer's & Dementia*, *8*(1), 65-73. https://doi.org/10.1016/j.jalz.2011.07.004

44. Kaplow, J., Vandijck, M., Gray, J., Kanekiyo, M., Huyck, E., Traynham, C. J., Esquivel, R., Fagan, A. M., & Luthman, J. (2020). Concordance of Lumipulse cerebrospinal fluid t-tau/Aβ42 ratio with amyloid PET status. *Alzheimer's & Dementia*, *16*(1), 144-152. https://doi.org/10.1002/alz.12000

45. Lleó, A., Alcolea, D., Martínez-Lage, P., Scheltens, P., Parnetti, L., Poirier, J., Simonsen, A. H., Verbeek, M. M., Rosa-Neto, P., Slot, R. E. R., Tainta, M., Izaguirre, A., Reijs, B. L. R., Farotti, L., Tsolaki, M., Vandenbergue, R., Freund-Levi, Y., Verhey, F. R. J., Clarimón, J., Fortea, J., Frolich, L., Santana, I., Molinuevo, J. L., Lehmann, S., Visser, P. J., Teunissen, C. E., Zetterberg, H., & Blennow, K. (2019). Longitudinal cerebrospinal fluid biomarker trajectories along the Alzheimer's disease continuum in the BIOMARKAPD study. *Alzheimer's & Dementia*, *15*(6), 742-753. https://doi.org/10.1016/j.jalz.2019.01.015

46. Grundke-Iqbal, I., Iqbal, K., Tung, Y. C., Quinlan, M., Wisniewski, H. M., & Binder, L. I. (1986). Abnormal phosphorylation of the microtubule-associated protein tau (tau) in Alzheimer cytoskeletal pathology. *Proc Natl Acad Sci U S A*, *83*(13), 4913-4917. https://doi.org/10.1073/pnas.83.13.4913

47. Blennow, K., Wallin, A., Agren, H., Spenger, C., Siegfried, J., & Vanmechelen, E. (1995). Tau protein in cerebrospinal fluid: a biochemical marker for axonal degeneration in Alzheimer disease? *Mol Chem Neuropathol*, *26*(3), 231-245. https://doi.org/10.1007/BF02815140

48. Hansson, O., Lehmann, S., Otto, M., Zetterberg, H., & Lewczuk, P. (2019). Advantages and disadvantages of the use of the CSF Amyloid beta (Abeta) 42/40 ratio in the diagnosis of Alzheimer's Disease. *Alzheimers Res Ther*, *11*(1), 34. https://doi.org/10.1186/s13195-019-0485-0

49. Smith, S. M., Jenkinson, M., Woolrich, M. W., Beckmann, C. F., Behrens, T. E., Johansen-Berg, H., Bannister, P. R., De Luca, M., Drobnjak, I., Flitney, D. E., Niazy, R. K., Saunders, J., Vickers, J., Zhang, Y., De Stefano, N., Brady, J. M., & Matthews, P. M. (2004). Advances in functional and structural MR image analysis and implementation as FSL. *NeuroImage*, *23 Suppl 1*, S208-219. https://doi.org/10.1016/j.neuroimage.2004.07.051

50. Clewett, D. V., Lee, T.-H., Greening, S., Ponzio, A., Margalit, E., & Mather, M. (2016). Neuromelanin marks the spot: identifying a locus coeruleus biomarker of cognitive reserve in healthy aging. *Neurobiology of Aging*, *37*, 117-126. https://doi.org/10.1016/j.neurobiolaging.2015.09.019

51. Aston-Jones, G. (2004). CHAPTER 11 - Locus Coeruleus, A5 and A7 Noradrenergic Cell Groups. In G. Paxinos (Ed.), *The Rat Nervous System* (3rd ed., pp. 259-294). Academic Press. https://doi.org/https://doi.org/10.1016/B978-012547638-6/50012-2

52. Liu, K. Y., Marijatta, F., Hämmerer, D., Acosta-Cabronero, J., Düzel, E., & Howard, R. J. (2017). Magnetic resonance imaging of the human locus coeruleus: A systematic review. *Neuroscience and Biobehavioral Reviews*, *83*, 325-355. https://doi.org/10.1016/j.neubiorev.2017.10.023

53. Salmon, D. P., & Bondi, M. W. (1999). Neuropsychology of Alzheimer Disease. In K. R. Terry RD, Bick KL, Sisodia SS (Ed.), *Alzheimer disease* (2nd ed., pp. 39-56). Lippincott Williams & Wilkins.

54. Keren, N. I., Taheri, S., Vazey, E. M., Morgan, P. S., Granholm, A.-C. E., Aston-Jones, G. S., & Eckert, M. A. (2015). Histologic validation of locus coeruleus MRI contrast in post-mortem tissue. *NeuroImage*, *113*, 235-245. https://doi.org/10.1016/j.neuroimage.2015.03.020

55. Cassidy, C. M., Zucca, F. A., Girgis, R. R., Baker, S. C., Weinstein, J. J., Sharp, M. E., Bellei, C., Valmadre, A., Vanegas, N., Kegeles, L. S., Brucato, G., Kang, U. J., Sulzer, D., Zecca, L., Abi-Dargham, A., & Horga, G. (2019). Neuromelanin-sensitive MRI as a noninvasive proxy measure of dopamine function in the human brain. *Proceedings of the National Academy of Sciences of the United States of America*, *116*(11), 5108-5117. https://doi.org/10.1073/pnas.1807983116

56. Priovoulos, N., Boxel, S. C. J. v., Jacobs, H. I. L., Poser, B. A., Uludag, K., Verhey, F. R. J., & Ivanov, D. (2020). Unraveling the contributions to the neuromelanin-MRI contrast. *Brain Structure & Function*, *225*(9), 2757-2774. https://doi.org/10.1007/s00429-020-02153-z